THE USE OF SEMICONDUCTOR DETECTORS FOR SHORT NUCLEAR HALF-LIFE MEASUREMENTS

R.J.BISHOP

A thesis submitted in part fulfilment

of the requirements for a C.N.A.A. Ph.D. degree

School of Physics

Kingston Polytechnic

1973

To my wife

Eraine

ABSTRACT

A study is made of the use of pairs of semiconductor detectors operated in coincidence for short nuclear half-life measurements. The factors affecting the energy resolution obtainable from such detectors is discussed. The pulse shapes delivered by surface barrier and lithium drifted planar detectors is considered with regard to their effect on the time resolution. The problems associated with deriving a timing signal are also discussed. A delayed coincidence system is set up and the apparatus described. The performance of a Ge(Li) - surface barrier system is investigated and the half-lives of the 59.6 keV state in Np-237 and the 86.5 keV state in Pa-233 remeasured to be (68.5 ± 0.4) ns and (37.7 ± 0.2) ns respectively. A similar investigation is also undertaken using a pair of Si(Li) beta particle detectors. The results obtained and the limitations of the present approach are critically discussed.

CONTENTS

APPENDICES

1. INTRODUCTION

The experimental measurement of the half-lives of excited nuclear states provides valuable information which may be used to verify the predictions of nuclear models through comparison of experimentally and theoretically derived transition probabilities. Various experimental techniques are available for extracting the half-life depending on its magnitude and the energies of the radiations involved (SCHWARZSCHILD and WARBURTON 1968).

A technique which has been in use for many years, and which was used in this work, is the delayed coincidence method. This method involves determining the time of formation and decay of the excited state under consideration by detecting the radiation populating and depopulating that state. One of the first uses of the technique was by JACOBSEN (1934) who made use of two moving iron oscillographs. More conventional measuring instruments were introduced in 1943 with the use of pairs of Geiger counters (JACOBSEN and SIGURGEIRSSON 1943). These enabled a resolving time of 75 μs to be achieved. Major progress in the field was made with the introduction of the scintillation counter in the early 1950s following the first application of the photomultiplier tube to the detection of the light flashes by Curran and Baker in 1944. Another important contributory factor was the discovery of fast organic

scintillators such as anthracene and stilbene which enabled much shorter resolving times to be attained (< 1 ns) and hence allowed the measurement of considerably shorter half-lives. Further, though not nearly so dramatic progress in reducing the lower limit on half-lives measurable with the scintillation counter has been maintained to the present time through improvements in photomultipliers, scintillators and the associated electronics and this has helped to maintain this device as the most widely used detector for delayed coincidence measurements.

A possible rival to the scintillation counter for delayed coincidence measurements is the semiconductor detector. Such detectors offer a fast response and an energy resolution at least an order of magnitude better than that obtainable from the scintillation counter (unless combined with some form of magnetic spectrometer). Studies had been made on the effects of nuclear radiation on crystals in the 1930s but it was not until 1949 (MACKAY 1949) that a semiconductor detector basically similar to those in use today was developed. It was a reverse biased germanium point contact diode and was used to detect alpha particles. In the following decade many P-N junction and surface barrier detectors were constructed using both silicon and germanium and their characteristics investigated (ORMAN et al 1950, MACKAY 1951, MAYER and GOSSICK 1956, DAVIS 1958, MAYER 1959, McKENZIE and BROMLEY 1959). The first

lithium drifted detector was constructed in 1960 (PELL 1960) and pioneered the way to the development of large volume silicon and germanium detectors. The latter devices have now replaced the scintillation counter in many applications. During the past decade steady progress has been made in improving the energy resolution and efficiency (for gamma rays) obtainable from semiconductor detector systems.

In view of the fast response and excellent energy resolution obtainable from semiconductor detectors it appeared that a study of the feasability of their use in delayed coincidence measurements would be valuable. This work sets out to investigate this possibility when using pairs of semiconductor detectors operated in coincidence to determine short nuclear half-lives.

2. THE SEMICONDUCTOR DETECTOR

2.1. INTRODUCTION

Semiconductor nuclear radiation detectors have come into widespread use in recent years for detection and high resolution spectroscopy of both directly and indirectly ionising radiation. These detectors may be regarded as the solid state analogue of the gaseous ionisation chamber. The incident radiation is wholly or only partially absorbed in the detector material (a semiconductor) with the consequent release of electron-hole pairs. These charge carriers are collected by an applied electric field across the counter. The amplitude of the resulting output signal, whether in pulse or current form, is proportional to the energy deposited in the detector by the incident radiation whilst the temporal position of the signal is related to the time of arrival of the incident radiation.

Initially detectors were made in the form of homogeneous conduction counters but these devices had very poor energy resolution and have found little or no use as spectrometers. Three main classes of semiconductor detector are currently produced, namely, P-N junction, surface barrier and lithium drifted types. The fabrication technique and principle of operation of these detector types are discussed fully in the literature (for example BERTOLINI and COCHE 1968).

Silicon and germanium are the only two semiconducting materials currently being used for high resolution detectors. This is, in part, a result of the large amount of research and development work already carried out on these materials by the electronics industry which has led to the production of silicon and germanium crystals with purities several orders of magnitude better than crystals of other materials. Further, the energy band gap in silicon and germanium is small and the carrier mobility in these materials is high.

Germanium detectors are particularily suitable for use with gamma rays on account of the comparitively high atomic number of germanium whilst silicon detectors are generally used for the detection of charged particles such as electrons, protons, alpha particles etc and also for the detection of low energy X-rays. Germanium detectors have the advantage of a higher density and therefore higher stopping power for charged particles than those made from silicon but have the large disadvantage that they must be operated at low temperatures (77 ^{o}K) if good resolution is required.

The main advantage of these devices over other similar detectors lies in their high energy resolution. This is the result of the low energy, about 3 eV, required to produce an ion pair. This may be compared with about 30 eV for a gaseous

ionisation chamber and 300 eV for a scintillation counter (Na(Tl)). Other advantageous properties are short output risetimes, high detector material density and good linearity.

2.2. DETECTOR ENERGY RESOLUTION

In this section such factors as incomplete charge collection, statistics of charge production, detector and amplifier noise, variations in charge collection times and window thickness are briefly considered with regard to their effect on the energy resolution obtainable from semiconductor detectors.

2.2.1. Charge Collection

An ionising particle losing all its energy E in the detector depletion region will create E/w electron-hole pairs, where w is the average energy to create a pair. If η is the charge collection efficiency then the charge Q collected on the electrodes is

$$Q = Ee\eta/w \qquad (2.2.1.)$$

where e is the charge on the electron. The corresponding voltage pulse has amplitude v given by

$$v = Ee\eta/wC$$

where C is the capacitance of the detector. Assuming η and w to be independent of the energy E, then the output pulse amplitude v

is directly proportional to E. This linear relationship has been verified by a large number of experiments over a wide range of energies for both particles and photons (WILLIAMS 1964 for example).

Trapping and recombination are the two important processes responsible for inefficient charge collection (η less than 1) both usually occurring because of defects and or impurities in the semiconductor crystal.

Trapping, applying to both holes and electrons, involves the holding of a charge carrier at a trapping centre (crystal imperfection). The carrier may be subsequently released by thermal excitation. If the trapping is short term (trapping time less than collection time of carrier) then the carrier, after its release will again contribute to the output signal, but if the trapping time is long compared with the clipping time used in the subsequent electronics, then the released carriers will not contribute. Trapping is particularly important in detectors having large depletion depths because of the long path taken by the carrier before collection. Further, operating the detector at low temperatures may increase trapping since the carriers are released from the traps by thermal excitation.

In recombination an impurity centre captures first one charge carrier and then a second carrier of opposite sign before the first is released so that both are annihilated and no longer contribute to the output signal. Recombination is thus most important at the

beginning of the charge collection process when carriers of both signs exist in close proximity after their creation by the incident radiation. This is particularly true for heavily ionising incident radiations (eg alpha particles) where the initial density of released electrons and holes is very high.

Important consequences of incomplete charge collection are output pulses of diminished amplitude, large dependence of output pulse amplitude on applied reverse bias and loss of resolution due to non-uniform charge collection. Both trapping and recombination effects can be reduced by increasing the applied electric field strength but not beyond the point where the leakage current becomes significant.

2.2.2. Statistics of Charge Production

The upper limit for the resolution of semiconductor detectors is set by fluctuations in the number of electron-hole pairs produced by incident ionising radiation of a given energy.

If N is the number of electron-hole pairs created when a quantity of energy E is deposited in the detector by an incident charged particle or photon, then there would be no fluctuations in N for a mono-energetic incident beam of radiation provided all the absorbed energy were converted into ionisation. But if the probability of an ionising event is small compared with alternative ways of dissipating the energy, such as heating of the crystal lattice, then

the fluctuations in N would follow a Poisson distribution with r.m.s. fluctuation $\sqrt{N}$ and full width at half maximum (f.w.h.m.) of $2.35\sqrt{N}$. In silicon, for example, the band gap is about 1.1 eV whereas the average energy (w) to create an electron-hole pair is about 3.6 eV. Thus silicon (and germanium also) falls between the above two extremes.

The observed f.w.h.m. is given by

$$2.35\sqrt{FN} = 2.35\sqrt{F\,\frac{E}{w}}$$

or in terms of energy

$$2.35\sqrt{FEw} \quad \text{eV}$$

where F is the Fano factor. This factor was introduced by FANO (1947) in a study of the statistics of ion pair formation in gaseous detectors. Theoretical calculations of F for silicon and germanium have been performed by ALKHAZOV (1967) and VAN ROOSBROECK (1965). Experimentally determined values of F for silicon have yielded values less than 0.2 for electrons and between 0.1 and 0.5 for heavy charged particles. In germanium values less than 0.1 for gamma rays have been obtained. Figure 2.2.(a) gives the peak broadening due to electronic collisions in silicon and germanium as a function of energy for different values of the Fano factor (after BERTOLINI and COCHE 1968).

When considering heavy charged particles (e.g. alpha particles) an additional contribution to the fluctuation in N may result from nuclear collisions. This is an alternative energy loss mechanism to ionisation and becomes important near the end of the range of the

particle. It has been estimated (LINDHARD and NIELSON 1962) that nuclear collisions contribute about 6 keV to the f.w.h.m. for 6 MeV alpha particles. The corresponding figure calculated for electronic stopping using the above formula is 6 keV for 6 MeV alpha particles stopped in a silicon detector assuming F is 0.3. Thus the calculated f.w.h.m. is 8.4 keV for electronic and nuclear stopping combined.

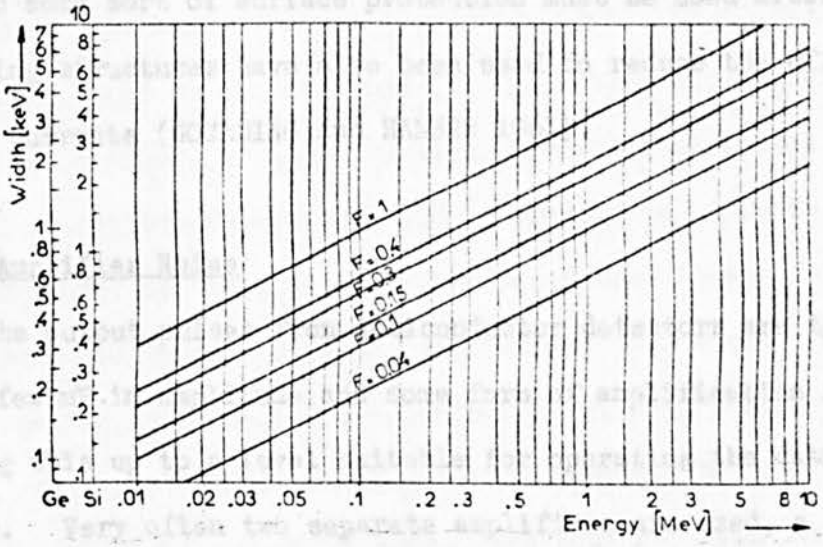

Figure 2.2.(a) Peak broadening due to electronic collisions in silicon and germanium, as a function of energy for different values of the Fano factor (BERTOLINI & COCHE 1968).

2.2.3. Detector Noise

This noise source arises from fluctuations in the detector leakage current (the current flowing between the detector electrodes when reverse biased). Such noise will be superimposed upon the wanted signal from the detector, producing a spread in output pulse

amplitude and hence loss of resolution.

The total leakage current is a combination of bulk leakage current, arising from the thermal generation of electron-hole pairs in the depletion region, and surface leakage current. Bulk leakage currents can be greatly reduced by cooling the detector, this being essential for germanium detectors. To achieve low surface leakage currents some sort of surface protection must be used after manufacture. Guard ring structures have also been used to reduce the effect of these surface currents (GOULDING and HANSEN 1961).

2.2.4. Amplifier Noise

The output pulses from semiconductor detectors are typically only a few mV in amplitude and some form of amplification is necessary to bring this up to a level suitable for operating the data analysing systems. Very often two separate amplifiers are used, a pre-amplifier in close proximity to the detector and a main amplifier located with the other electronics.

Any noise source within the associated electronics used with these detectors will have the effect of degrading the information contained in the detector output signals. The most important noise sources are those which arise in the pre-amplifier, especially those appearing in the first stages as there exists the possibility of such noise receiving the full amplification of the electronic system.

Thus the energy resolution obtainable from a semiconductor detector spectrometer system depends critically on the design of the pre-amplifier. Present day pre-amplifiers make use of field effect transistors (F.E.T.) in the first stage (or stages), these devices having a considerably better noise performance than bi-polar transistors or valves. The F.E.T. is often cooled to reduce its noise contribution. Because the capacitance of semiconductor detectors changes with applied reverse bias, charge sensitive pre-amplifiers are normally used as the amplitude of the output signal from these is, to a good degree of approximation, proportional to the charge injected at the input terminals and independent of detector capacitance. The noise level of the pre-amplifier does depend though on the input capacitance and increases as the capacitance increases. Thus detectors with large depletion depths are preferred for high resolution spectroscopy. Many pre-amplifier designs have appeared in the literature (see e.g. BERTOLINI and COCHE 1968), the best of these having equivalent noise line widths of $\approx$ 200 eV at room temperature and noise slopes of about 30 eV per pF (KERN and McKENZIE 1970).

The main amplifier is included in the system not only to give some additional gain but also to provide some form of shaping of the signal pulses. This pulse shaping is used to improve the signal to noise ratio and to reduce the possibility of pulse pile-up, simple systems making use of single R.C. integration and differentiation networks with time constants of a few μs. The noise contribution

of the main amplifier and subsequent electronics can usually be considered to be negligible.

2.2.5. Charge Collection Time Variations

With detectors having large sensitive depths, such as the lithium drifted types, the variations in charge carrier collection times causes a spread in output pulse rise-times (Section 2.3.4.). After these pulses have been passed through the shaping networks in the main amplifier a spread in pulse height will be observed. With amplifier time constants greater than about five times the carrier collection times this spread is usually negligible.

2.2.6. Detector Window Thickness

Before incident radiation can enter the sensitive volume of the detector it must pass through an insensitive region which constitutes an entry window. Fluctuations in the energy lost by the radiation in this window contributes to a loss of resolution, but it is only significant for heavy charged particles. For example, a 6 MeV alpha particle passing through a gold window of thickness $2X10^{-8}$ m would suffer an energy loss of about 8 keV, the window contributing about 3 keV fwhm to the overall resolution (ENGELKEMEIR 1967).

2.3. DETECTOR TIME RESOLUTION

2.3.1. Introduction

The output signal from a semiconductor radiation detector not only provides information on the energy of the incident radiation but also on the time of occurrence of the event which produced it, for example, the formation or decay of an excited nuclear state. For good timing it is essential to know under what conditions semiconductor detectors deliver fast risetime pulses with minimum pulse shape jitter (variations in shape from one pulse to another for a given situation).

The interaction of incident radiation with the detector produces electron-hole pairs in a time of the order of 10^{-11} s. The initial distribution of these charge carriers within the detector will depend on the energy and nature of the radiation. The positive and negative charges produced in the sensitive region of the detector will separate and each carrier will move towards its relevant electrode under the action of the applied electric field, the carrier inducing a current in the external circuit until it is collected. The collection time will depend on the initial position of the carrier relative to the collecting electrode and the carrier velocity, the latter being a function of the electric field and carrier mobility provided the carrier saturation velocity has not been reached.

The inherent timing resolution of semiconductor detectors is very high. Narrow depletion depth detectors and photomultipliers

used with fast organic scintillators have approximately the same charge collection times (of the order of ns). Therefore, because of the low average energy to produce an electron-hole pair in a semiconductor detector (3 eV compared with about 2000 eV to obtain a single photoelectron from the photomultiplier cathode), these detectors should have a timing resolution about $\sqrt{2000/3}$ times better than a scintillation counter (BELL 1965). Unfortunately the output signals from the semiconductor detector are small in amplitude and some form of amplification is usually necessary to bring the signals up to a level which will satisfactorily operate the subsequent electronics. At the present time the noise introduced by these amplifiers is far too high to enable the full timing potential of semiconductor detectors to be realised. Further, large sensitive depth detectors which are necessary for efficient detection of gamma rays have somewhat long and variable charge collection times (Section 2.3.4.).

Many publications have appeared dealing with the subject of charge collection times and time resolution in semiconductor detectors. Examples of review articles are those by QUARANTA et al (1969) and BERTOLINI and COCHE (1968), both providing extensive references. Recent articles have concentrated on the timing performance obtainable from germanium detectors. BENGTSON and MOSZYNSKI (1972) investigated timing with a 0.25 cc planar Ge(Li) detector used in conjunction with a plastic scintillator and obtained a prompt curve with a slope of 130 ps for 511 keV

annihilation radiation. The work of MIRNE and GIFFERT (1970) discussed the influence of several parameters related to the detector and the electronics (compensated thickness, noise etc.) on the timing performance. RYGE and BORCHERS (1971) studied timing with coaxial Ge(Li) detectors whilst CHO and LLACER (1972) showed that the recently developed uncompensated high purity germanium coaxial detectors possess better timing characteristics than coaxial Ge(Li) detectors. This is as a result of the fixed space charge in the depletion region yielding a much more uniform field than the 1/r variation found in Ge(Li) devices.

In the following sections an analysis is made, based on the published literature, of the pulse shapes obtained from surface barrier and planar P-I-N detectors, the two detector types used in this work. The current pulse shape resulting from the production of a single electron-hole pair in the detector sensitive region is determined and then the pulse shape (current and voltage) at the preamplifier input is calculated from a knowledge of the detector and preamplifier input stage equivalent circuit.

In view of the many parameters which can affect the pulse shape some simplifying assumptions are made, namely, the mobility is field independent, trapping and recombination are negligible and the plasma time (QUARANTA et al 1969) is zero. Further, when considering the many electron-hole pairs created by incident

radiation it is assumed that these are produced in a plane parallel with and adjacent to the junction plane.

2.3.2. Current Pulse Shape due to the Collection of a Single Electron-Hole Pair

(i) Surface barrier detector

In the schematic diagram of a surface barrier detector shown in Figure 2.3.2.(a), the motion of a single electron-hole pair in the electric field is considered. The magnitude of the field strength E at a distance x from the junction can be found

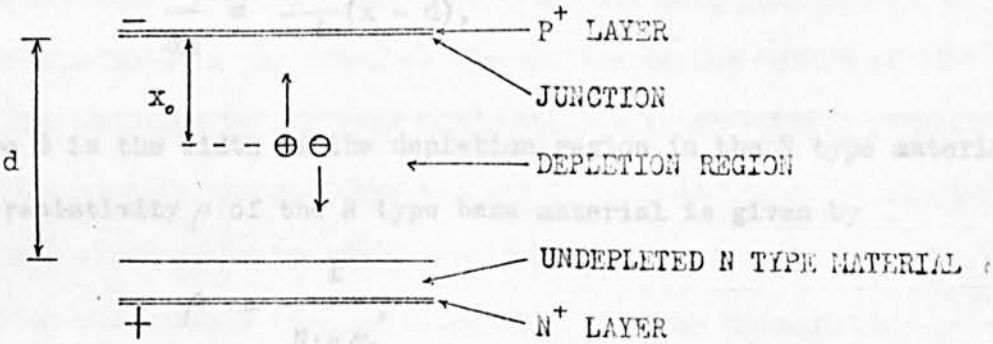

Figure 2.3.2.(a) Schematic diagram of a surface barrier detector.

by applying Poisson's equation. Assuming the potential changes only in the direction perpendicular to the junction, then

$$\frac{d^2V}{dx^2} = -\frac{\rho'}{\epsilon}$$

where ρ' is the charge density of the volume element considered and ϵ is the permittivity of the material. For completely ionised donors in N type material $\rho' = e(N_d + p - n)$, where N_d is the donor concentration and p and n are the hole and electron

densities respectively. Assuming p and n are negligible compared with N_d in the depletion region, then

$$\frac{d^2 V}{dx^2} = -\frac{eN_d}{\epsilon} .$$

Integrating gives

$$\frac{dV}{dx} = -\frac{eN_d}{\epsilon}(x - d),$$

where d is the width of the depletion region in the N type material. The resistivity ρ of the N type base material is given by

$$\rho = \frac{1}{N_d e \mu_n},$$

where μ_n is the mobility of the electrons. Therefore

$$\frac{dV}{dx} = \frac{d - x}{\rho \epsilon \mu_n} .$$

Putting $\rho\epsilon = \tau$, the dielectric relaxation time, and since $E = -dV/dx$,

$$E(x) = -\frac{d - x}{\tau \mu_n} . \qquad (2.3.1.)$$

Thus the field strength E is a linear function of the distance x from the junction. The drift velocity of the holes under the field is given by

$$\frac{dx}{dt} = \mu_p E = -\frac{d - x}{\tau} \cdot \frac{\mu_p}{\mu_n} .$$

Integrating gives

$$x_p(t) = d - (d - x_o)e^{t\mu_p/\tau\mu_n}, \qquad (2.3.2.)$$

where x_o is the initial position of the hole ($t = 0$). The current induced in the external circuit due to the motion of the hole can be found by applying Ramo's theorem (RAMO 1939). The validity of this theorem when applied to semiconductor detectors having a fixed space charge in the depletion region (as in P-N junction and surface barrier detectors) has been demonstrated by CAVALLERI et al (1971). In the situation considered here this theorem can be written $\delta Q = e\delta x/d$, where δQ is the charge flowing in the external circuit when a charge e moves a distance δx perpendicular to the collecting electrodes, the spacing between the electrodes being d. The corresponding current i is given by

$$i = \frac{dQ}{dt} = \frac{ev}{d} = \frac{e\mu E}{d}.$$

Substituting for E and x from equations 2.3.1. and 2.3.2. gives

$$i_p(t) = \frac{e\ \mu_p}{d\tau\mu_n}(d - x_o)e^{t\mu_p/\tau\mu_n}. \qquad (2.3.3.)$$

By a similar argument to that given above for the hole, the position of the electron at time t is given by

$$x_n(t) = d - (d - x_o)e^{-t/\tau} , \qquad (2.3.4.)$$

The contribution to the current from the electron is then

$$i_n(t) = \frac{e}{d\tau}(d - x_o)e^{-t/\tau} . \qquad (2.3.5.)$$

The electron , moving into a region of decreasing field, is collected (x = d) only when t approaches ∞ (equation 2.3.4.). Thus there is no finite collection time for electrons, but the electron collection time may be characterised by the time constant τ, which is also the dielectric relaxation time. Since the hole moves towards a region of increasing field it does have a finite collection time t_p found by putting x = 0 in equation 2.3.2. . Thus

$$t_p = \frac{\tau \mu_n}{\mu_p} \log_e \frac{d}{d - x_o} . \qquad (2.3.6.)$$

Figure 2.3.2.(b) shows a rough plot of equations 2.3.3. and 2.3.5. for a silicon detector at room temperature ($\mu_n \simeq 3\mu_p$). The initial position of the electron-hole pair was taken to be midway between the electrodes ($x_o = d/2$). As can be seen, the resultant current waveform has a risetime which is equal to zero (when considering the large number of electron-hole pairs produced by the incident radiation, the risetime of the current pulse

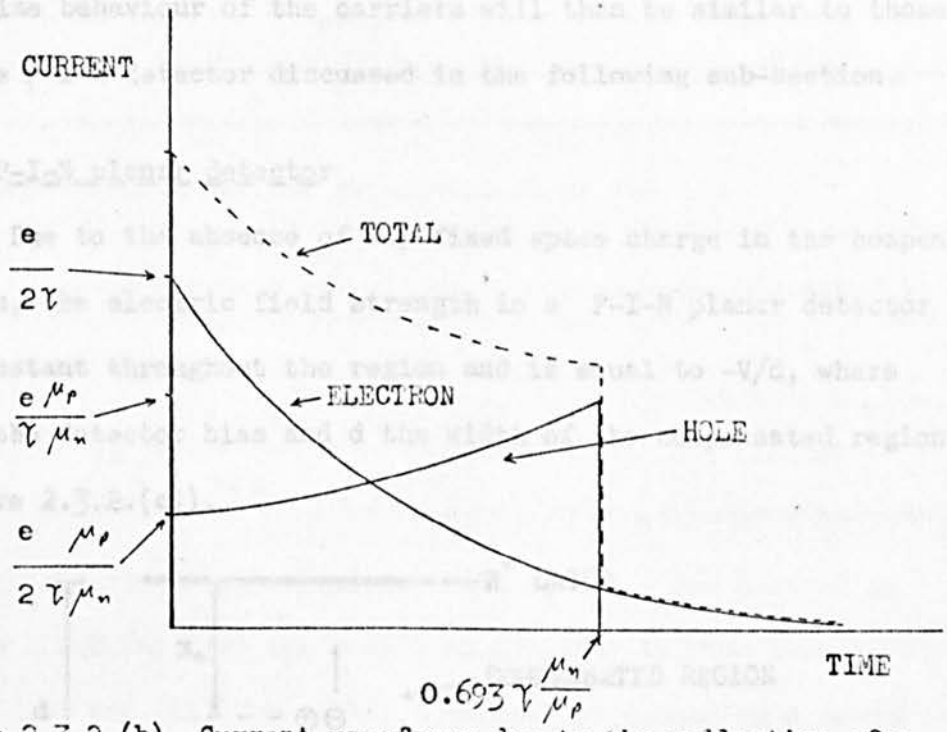

Figure 2.3.2.(b) Current waveforms due to the collection of a single electron-hole pair in a silicon surface barrier detector at room temperature.

will be limited by the time taken for the radiation to produce these carriers, a time of about 10^{-11} s). Following the collection of the holes the current decreases with the time constant τ. Since $\tau = \rho\epsilon$, this time constant in a silicon detector is approximately equal to $10^{-12}\rho$ s when ρ is expressed in Ω cm. Thus it can be seen that the resistivity ρ of the base material should be as small as possible in order to maximise the current pulse amplitude and at the same time minimise the pulse duration.

If a sufficiently high bias voltage is applied, the electric

field may become uniform throughout the detector sensitive volume. The time behaviour of the carriers will then be similar to those in the P-I-N detector discussed in the following sub-section.

(ii) P-I-N planar detector

Due to the absence of any fixed space charge in the compensated region, the electric field strength in a P-I-N planar detector is constant throughout the region and is equal to -V/d, where V is the detector bias and d the width of the compensated region (Figure 2.3.2.(c)).

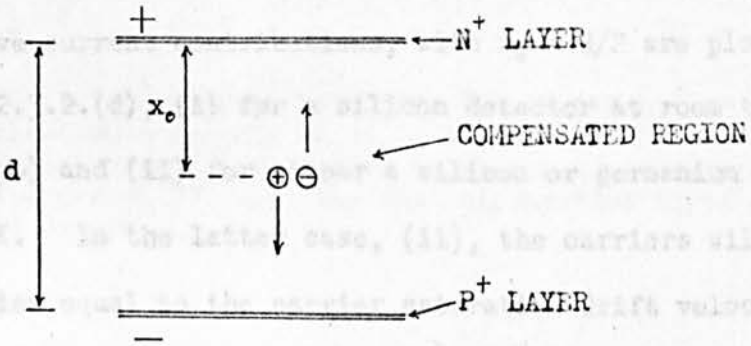

Figure 2.3.2.(c) Schematic diagram of a P-I-N detector.

Applying Ramo's theorem to this situation gives the current contributions from the electron and the hole as

$$i_n(t) = \frac{e\mu_n V}{d^2} \qquad \text{(electron)}$$

and

$$i_p(t) = \frac{e\mu_p V}{d^2} \qquad \text{(hole)}$$

The corresponding carrier collection times are

$$t_n = \frac{x_o}{\mu_n E} = \frac{x_o d}{\mu_n V} \qquad \text{(electron)}$$

and

$$t_p = \frac{d - x_o}{\mu_p E} = \frac{(d - x_o)d}{\mu_p V} \qquad \text{(hole)}$$

The above current contributions, with $x_o = d/2$ are plotted in Figure 2.3.2.(d), (i) for a silicon detector at room temperature ($\mu_n \simeq 3\mu_p$) and (ii) for either a silicon or germanium detector at 77 °K. In the latter case, (ii), the carriers will have velocities equal to the carrier saturation drift velocity v_s, which is approximately equal to 10^7 cms^{-1} in both silicon and germanium. Carrier collection times will therefore be about 10 ns per mm of carrier collection path. For a silicon detector at room temperature it will be seen that due to the higher mobility of the electron compared with the hole, the electron current duration is about one third the hole current duration Thus for short range particles (range small compared with the width of the compensated region) it would be advantageous to inject these through the P^+ layer.

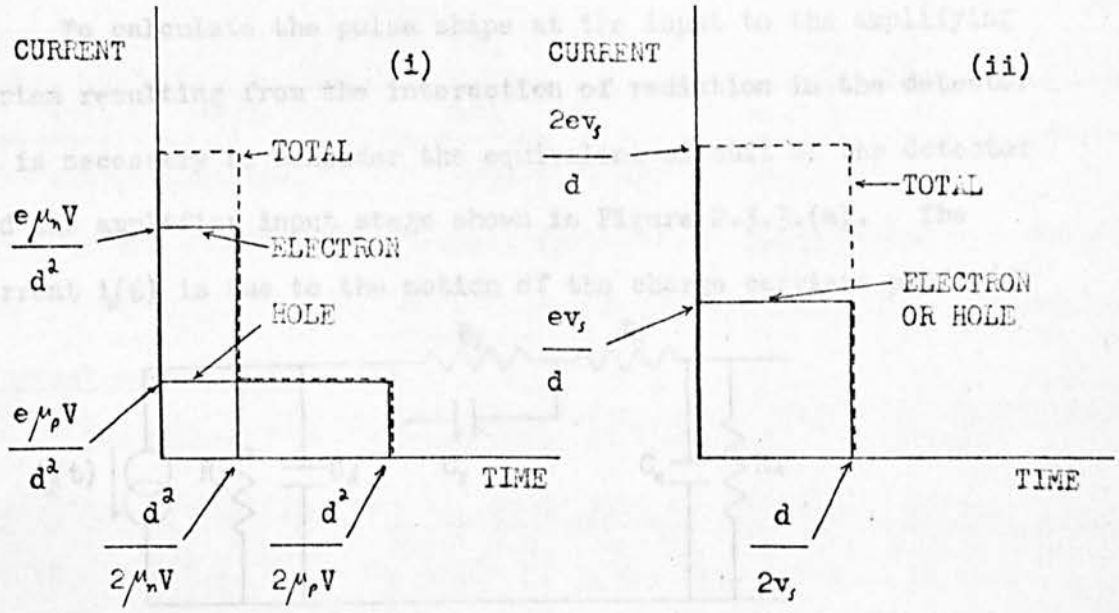

Figure 2.3.2.(d) Current waveforms due to the collection of a single electron-hole pair in (i) a silicon P-I-N detector at room temperature and (ii) either a silicon or germanium planar P-I-N detector at 77 °K. The initial position x_o of the electron-hole pair is d/2.

2.3.3. Pulse Shapes at the Input of the Amplifying System

To calculate the pulse shape at the input to the amplifying system resulting from the interaction of radiation in the detector it is necessary to consider the equivalent circuit of the detector and the amplifier input stage shown in Figure 2.3.3.(a). The current $i_d(t)$ is due to the motion of the charge carriers produced

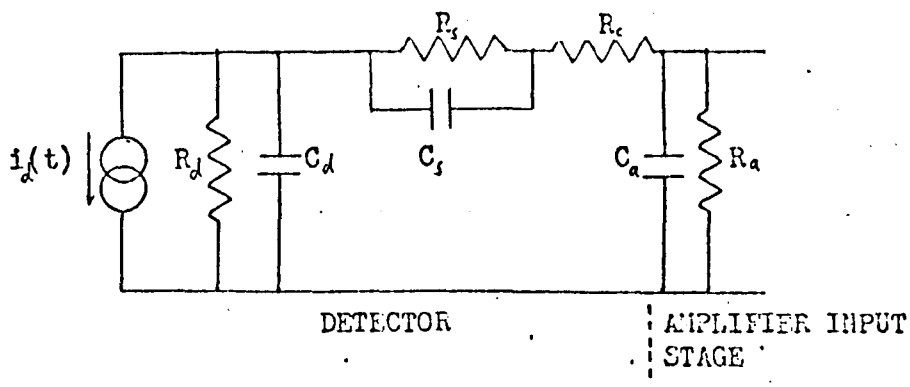

Figure 2.3.3.(a) Detector and amplifier input stage equivalent circuit.

in the detector depletion region by incident radiation, R_d and C_d are the resistance and capacitance respectively of the depletion region, R_s and C_s represent the resistance and capacitance respectively of the undepleted (or uncompensated for a lithium drifted detector) material and R_c the contact resistance. Usually R_d has a very high value (at least $10^8\Omega$) and will therefore be considered to act as an open circuit. A further simplification can be made if the contact resistance R_c is assumed negligible. The amplifier input stage is represented by its input capacitance C_a and input resistance R_a, the magnitudes of these depending on the preamplifier

type:-

	C_a	R_a
voltage sensitive	small (pF)	high (10's MΩ)
charge sensitive	large (10's nF)	high (10's MΩ)
current sensitive	small (pF)	small (10'sΩ).

Current pulse shape

The shape of the current pulse at the input of a current sensitive preamplifier can be found using the equivalent circuit of Figure 2.3.3.(b). The value of R_a has been taken to be zero.

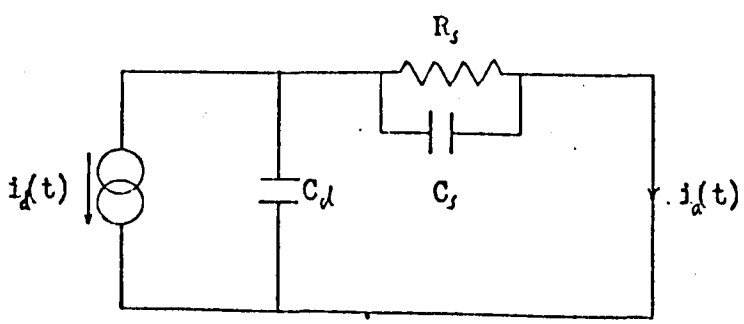

Figure 2.3.3.(b) Equivalent circuit used to determine the current pulse shape.

The Laplace transform of the transfer function of the network is

$$\frac{i_a(p)}{i_d(p)} = \frac{1 + R_s C_s p}{1 + p(R_s C_s + R_s C_d)} = \frac{1 + \tau p}{1 + p(\tau + R_s C_d)} \qquad (2.3.7.)$$

where $\tau = R_s C_s$.

For a junction detector where the incident radiation deposites its energy close to the junction, essentially only one type of carrier will contribute to $i_d(t)$ and hence from equation 2.3.5.

$$i_d(t) = \frac{Q}{\tau} e^{-t/\tau} \qquad (2.3.8.)$$

where Q is given by equation 2.2.1. The Laplace transform of this is

$$i_d(p) = \frac{Q}{1 + \tau p} \qquad (2.3.9.)$$

Hence the Laplace transform of the current pulse at the amplifier input is

$$i_a(p) = \frac{Q \quad (1 + \tau p)}{(1 + \tau p)\ (1 + p(\tau + R_s C_d)}$$

The inverse transform of this gives

$$i_a(t) = \frac{Q}{\tau + R_s C_d} \quad e^{-t/(\tau + R_s C_d)}$$

which can be written

$$i_a(t) = \frac{Q}{\tau'} e^{-t/\tau'}$$

where $\tau' = \tau + R_s C_d$. Thus the expression for $i_a(t)$ has the same form as equation 2.3.8. and electron waveforms similar to those in Figure 2.3.2.(b) will be obtained, but with the longer time constant τ'. For a fully depleted detector ($R_s = 0$) the time constant reverts to τ.

A similar treatment can be used to derive the current pulse shape at the amplifier input when radiation is incident on a P-I-N detector. For simplicity only the current contribution from the carriers which cross the whole compensated region will be considered. From Section 2.3.2. these contribute a current

$$i_d(t) = \frac{Q}{t_c}$$

where t_c is the time taken for the relevant carriers to cross the entire compensated region. The Laplace transform of $i_d(t)$, in the time interval $0 \leq t \leq t_c$ (since $i_d(t) = 0$ when $t > t_c$), is

$$i_d(p) = \frac{Q}{t_c p}(1 - e^{-pt_c}) \qquad (2.3.10.)$$

Hence from equation 2.3.7. the Laplace transform of the current pulse at the amplifier input becomes

$$i_a(p) = \frac{Q}{t_c p}\frac{(1 - e^{-pt_c})(1 + \tau p)}{(1 + p(\tau + R_s C_d))}$$

The inverse transform of this gives

$$i_a(t) = \frac{Q}{t_c}\left[1 - (1 - \tau/\tau')e^{-t/\tau'} - H(t - t_c)(1 - (1 - \tau/\tau')e^{-(t - t_c)/\tau'})\right]$$

which in the interval $0 \leq t \leq t_c$ becomes

$$i_a(t) = \frac{Q}{t_c}(1 - \frac{\tau' - \tau}{\tau'} e^{-t/\tau'})$$

or

$$i_a(t) = \frac{Q}{t_c}\left(1 - \frac{R_s C_d}{\gamma + R_s C_d} e^{-t/(\gamma + R_s C_d)}\right)$$

The initial amplitude (t = 0) of the current pulse at the amplifier input is therefore reduced by the factor $\gamma/(\gamma + R_s C_d)$ compared with the detector current pulse amplitude at the same time. For good timing a detector with no uncompensated material ($R_s = 0$) should be used as then $i_a(t) = Q/t_c$ giving a rectangular pulse as in Figure 2.3.2.(d). This further implies that t_c should be small ie. the use of a shallow compensated region and a high detector bias voltage (provided the saturation carrier velocity has not been reached). The former may be satisfactory for charged particles but would cause greatly reduced efficiency for detection of gamma rays.

Voltage pulse shape

The shape of the voltage pulse at the input of a voltage or charge sensitive preamplifier can be found using the equivalent circuit of Figure 2.3.3.(c). The value of R_a has been taken to

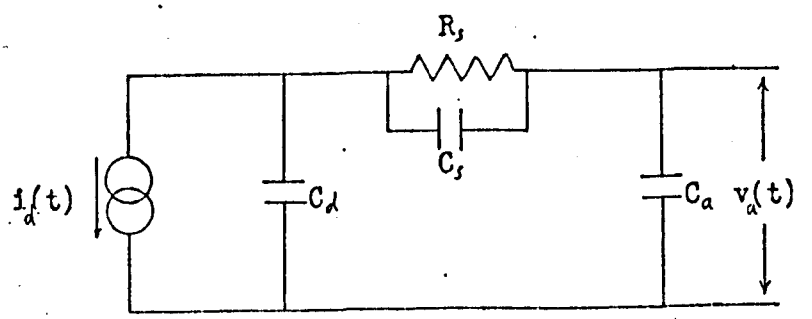

Figure 2.3.3.(c) Equivalent circuit used to determine the voltage pulse shape.

be infinitely large. The Laplace transform of the transfer function of the network is

$$\frac{v_a(p)}{i_d(p)} = \frac{pC_s R_s + 1}{p((pC_s R_s + 1)(C_a + C_d) + pR_s C_d C_a)}$$

$$= \frac{1 + \tau p}{p((1 + \tau p)(C_a + C_d) + pR_s C_d C_a)} \qquad (2.3.11.)$$

Hence from equation 2.3.9. the Laplace transform of the voltage pulse at the amplifier input for a junction detector operating under the stated conditions becomes

$$v_a(p) = \frac{Q}{p((1 + \tau p)(C_a + C_d) + pR_s C_d C_a)}$$

The inverse transform of this gives

$$v_a(t) = \frac{Q}{C_a + C_d}\left(1 - e^{-(C_a + C_d)t/(\tau(C_a + C_d) + R_s C_d C_a)}\right)$$

or

$$v_a(t) = \frac{Q}{C_a + C_d}\left(1 - e^{-t/\tau''}\right) \qquad (2.3.12.)$$

where $\tau'' = \tau + R_s C_d C_a/(C_a + C_d)$. The risetime of the pulse is thus governed by the time constant τ''. For a totally depleted detector ($R_s = 0$) this time constant will equal τ, the time constant associated with the collection of carriers in the detector. For a detector which is not totally depleted the term $R_s C_d C_a/(C_a + C_d)$ could be much larger than τ, especially for high capacitance detectors.

In such a case the observed pulse risetime at the amplifier input could easily be an order of magnitude greater than the carrier collection time constant.

For a N-I-P detector with $i_d(p)$ given by equation 2.3.10. and $v_a(p)/i_d(p)$ by equation 2.3.11., the Laplace transform of the voltage pulse at the amplifier input becomes

$$v_a(p) = \frac{Q(1 + \tau p)\ (1 - e^{-t_c p})}{t_c p^2((1 + \tau p)(C_a + C_d) + pR_s C_d C_a)}$$

The inverse transform in the time interval $0 \leqslant t \leqslant t_c$ is then

$$v_a(t) = \frac{Q}{t_c(C_a + C_d)}\left(t - \frac{R_s C_d C_a}{C_a + C_d}(1 - e^{-t/\tau''})\right) \qquad (2.3.13.)$$

where τ'' is again given by $\tau'' = \tau + R_s C_d C_a/(C_a + C_d)$. For a detector with no uncompensated material ($R_s = 0$) the voltage pulse rises linearly with time. The rate of rise depends on t_c and hence on the carrier velocity.

When considering charge sensitive preamplifiers, the amplifier input capacitance C_a will, in general, be much larger than C_d. The value of C_a is given by $C_a = AC_f$, where the open loop gain, A, of the amplifier is assumed large. C_f is the feedback capacitance used. Equations 2.3.12. and 2.3.13. respectively then become

$$v_a(t) = \frac{Q}{AC_f}(1 - e^{-t/\tau'''})$$

and

$$v_a(t) = \frac{Q}{AC_f t_c}\left(t - R_s C_d\left(1 - e^{-t/\tau'''}\right)\right),$$

where $\tau''' = \tau + R_s C_d$. Thus τ''' (charge sensitive amplifier) is greater than τ'' (voltage sensitive amplifier), the difference depending on the relative magnitude of C_d and C_a of the voltage amplifier. For detectors with $R_s = 0$, $\tau''' = \tau'' = \tau$.

2.3.4. Charge Pulse Shape due to the Interaction of Gamma Rays in a Planar Germanium P-I-N Detector

When examining gamma rays in the approximate energy range of 100 keV to 1 MeV they may be considered to produce a uniform distribution of events throughout the detector volume. This is because in this range the gamma rays have a low probability of interacting with the germanium, lower energy radiation would be preferentially absorbed in the region close to the detector entry window producing a non-uniform event distribution. Since the range of a 1 MeV electron is 0.8 mm in germanium, the ionisation produced by gamma rays up to 1 MeV is essentially localised at a point for detectors having a sensitive thickness which is large compared with this figure.

For a germanium detector operating at 77 °K, where the drift velocity of the electrons and holes are equal and assuming there are no dead layers in the detector, the charge waveforms shown in Figure 2.3.4.(a) will be obtained under the conditions of the

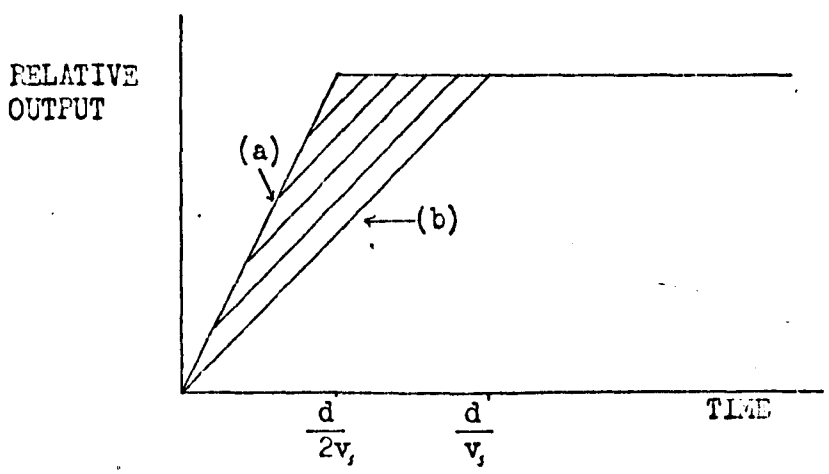

Figure 2.3.4.(a) Charge pulse shapes due to the interaction of gamma rays in a germanium P-I-N detector at 77 °K.

above paragraph. The width of the sensitive region is d and v_s is the carrier saturation velocity. The fastest charge pulse, waveform (a), is obtained when the ionising event occurs in the middle of the detector sensitive region whilst, for those events produced adjacent to either the P^+ or N^+ contact, waveform (b), where only one type of carrier contributes to the signal, the pulse risetime is twice as long. Further, since there is an equal probability of an event occurring at any position between these two extremes, the range of pulse shapes between (a) and (b) will be obtained with equal probability. For non-ideal detectors with regions of poorly compensated material much slower risetime pulses will be obtained due to the non-uniformity of the electric field throughout the detector volume (MOSZYNSKI and BENGTSON 1972).

3. THE DELAYED COINCIDENCE TECHNIQUE

3.1. THE TECHNIQUE

The delayed coincidence method can be used to measure excited nuclear state half-lives in the approximate range of 10^{-3} s to 10^{-11} s. It involves the detection of radiations populating and depopulating the state under measurement. In this work these radiations are alphas and betas (populating radiation) and gammas, X-rays and internal conversion electrons (depopulating radiation) and they are detected by semiconductor detectors. X-rays emitted on rearrangement of atomic electrons as a result of de-excitation by internal conversion have here been included under the category of depopulating radiations.

The amplitude of the output signals from the detectors provides information on the energy of the incident radiation and enables the desired excited state to be selected (energy resolution permitting), whilst the use of a suitable timing discriminator associated with each detector (Section 3.2.) produces standard shape timing signals. The pair of time signals corresponding to populating and depopulating of the level are then fed to some form of time-to-amplitude converter which converts the time difference between these two signals into a pulse whose amplitude is proportional to this difference. Since a distribution of time differences occurs when considering the many nuclei in the same excited state in the source, the output of the time-to-amplitude converter can

be fed to a standard multi-channel analyser which will then store and display the resulting time spectrum. This distribution may then be related to the excited state half-life. By suitable gating, the multi-channel analyser can be arranged to operate only when the populating and depopulating radiations have the desired energies.

When a delayed coincidence system is viewing an excited state having a very short half-life, where the populating and depopulating radiations can be considered to be emitted simultaneously, the resulting time distribution shows the intrinsic time resolution of the system. This distribution, known as the prompt spectrum or curve, can be characterised by its full width at half maximum height, fwhm, (analogous to the characterisation of energy resolution) and by the slope of the tail of the curve often expressed as an apparent half-life. The shape of the prompt curve is a result of the fluctuations occurring in the processes of detection and analysis (Sections 2.3. and 3.2. respectively).

Several methods of obtaining the half-life from a delayed coincidence curve are possible depending on the relation of the half-life to the properties of a prompt spectrum taken under the same conditions and resulting from prompt radiations of exactly similar type and energy to the delayed radiations. When the half-life is more than about 30% larger than the slope of the prompt curve then the slope method of analysis can be used

(NEWTON 1950). If only one half-life $T_{\frac{1}{2}}$ is involved the slope of the delayed curve is $\lambda = 0.693/T_{\frac{1}{2}}$ where λ is the total de-excitation probability of the excited state. For life-times shorter than this the method of higher moments has to be used (BAY 1950, NEWTON 1950, BELL et al 1952, WEAVER and BELL 1960).

3.2. DERIVATION OF THE TIMING SIGNAL

To obtain simultaneously an energy and a timing signal from a semiconductor detector some form of signal pick-off circuit must be used. It is important that such an arrangement should not appreciably degrade either the energy or the time resolution of the system. Some possible arrangements which have been used are shown in Figure 3.2.(a). Arrangements c) and d)

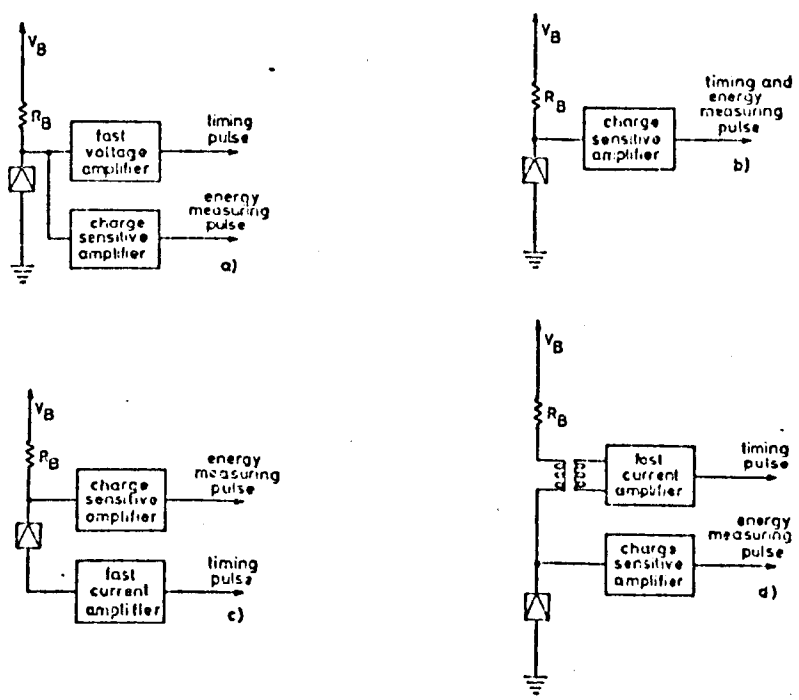

Figure 3.2.(a) Some possible arrangements for obtaining simultaneously an energy and a timing signal from a semiconductor detector (QUARANTA et al 1969).

make use of the current pulse from the detector and use separate energy and timing amplifiers, as does (a), whilst in (b) the energy and timing signals are obtained from the output of a single charge

sensitive amplifier. The use of dual amplifiers has the advantage that the energy amplifier can be a narrow band low noise type and the timing amplifier wide band. Full advantage can then be made of the fast response and good energy resolution of the detector. A single amplifier cannot be designed for simultaneous optimum low noise and fast response. However, with c) and d) the charge sensitive amplifier cannot be assumed to act as a high value capacitance to earth for the detector current pulses as these pulses normally have risetimes shorter than the amplifier closed loop risetime. Thus only a fraction of the available detector current is fed into the current amplifiers. This problem can be overcome if capacitance is added in parallel with the charge sensitive amplifier input, but this results in a deterioration of the energy resolution. A similar effect occurs with arrangement a) except that the fed-back capacitance of the charge sensitive amplifier appears in parallel with the input of the voltage amplifier, thus reducing the amplitude of the voltage signal there. A partial remedy is to connect the charge sensitive amplifier to the detector through a small value resistor or better still to parallel the resistor with a small inductor, thus delaying the signal fed to the charge sensitive amplifier and at the same time virtually removing the noise added to the system by the resistor (SHERMAN et al 1968). A further limitation to the use of arrangements c) and d) is that for planar lithium

drifted detectors the current pulse amplitude depends not only on the energy deposited in the detector by the incident radiation but also on the charge carrier collection time (Section 2.3.2.(ii)). Thus it is impossible to use detectors having thick compensated regions with low energy radiations when fast current amplifiers are employed as the wanted signals would be swamped by the amplifier noise. Arrangement b) is most commonly used in such cases.

The leading edge of the timing signal from the pick-off circuitry defines the time of occurrence of the detected event. It is necessary to feed this signal to some form of discriminator which will produce standard shape (of given amplitude, risetime and duration) timing output signals suitable for operating the time-to-amplitude converter. It is important that these standard signals should be accurately related to the time of occurrence of the initiating event. Inaccuracies of time derivation are caused basically by two factors, namely walk and jitter. Walk is the variation in the time of occurrence of the standard timing

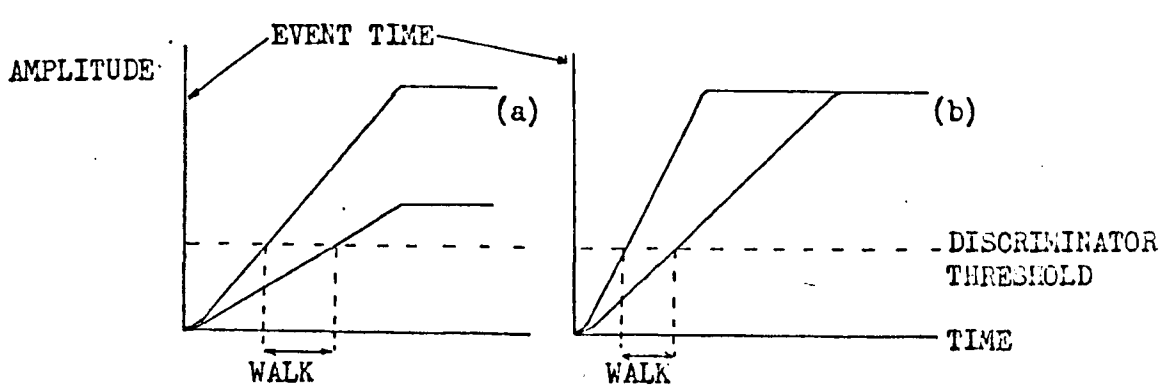

Figure 3.2.(b) Walk produced by variations in a) the amplitude and b) the risetime of the input signal.

signals, relative to the initiating event, produced by variations in the amplitude and risetime of the input signal. This is illustated in Figure 3.2.(b). Jitter (Figure 3.2.(c)) is a source of timing error introduced by statistical fluctuations in the noise present on the signal at the input to the discriminator. This noise may be produced in the detector, the pick-off circuitry or the input stage of the discriminator. In practice, with semiconductor detectors, the dominant noise source is the amplifier

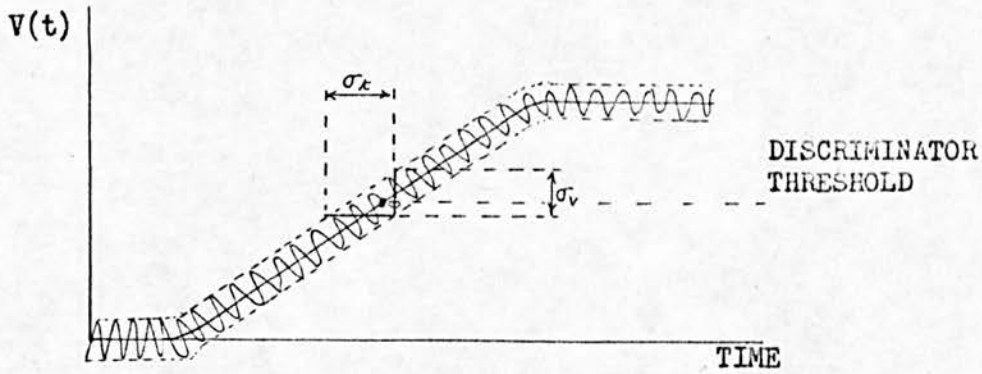

Figure 3.2.(c) Time jitter due to noise.

used in the pick-off arrangement. From consideration of Figure 3.2.(c) a good approximation to the time resolution due to jitter is $\sigma_t = \sigma_v/(dV/dt)$, where σ_t is the time standard deviation, σ_v the r.m.s. voltage noise at the discriminator input and dV/dt the slope of the signal at the triggering point. This shows that the best resolution is obtained with the smallest ratio of noise to slope at the triggering point. When considering

the effect on σ_t of the amplifier used to feed the discriminator it is seen that it should have as wide a bandwidth as possible in order to minimise σ_t, since σ_V is proportional to amplifier gain and the square root of amplifier bandwidth whilst dV/dt is directly proportional to both gain and bandwidth.

Some of the most commonly used methods of deriving the standard timing signals will now be briefly discussed with regard to their use with semiconductor detectors.

Leading edge timing

A single discriminator is used with a fixed threshold level. Figure 3.2.(b) shows that for input pulses with a wide dynamic amplitude range and or a range of risetimes, walk could be severe resulting in serious deterioration of the time resolution. The walk can be minimised by setting the discriminator threshold level as low as the noise will allow (no spurious triggering), but then noise jitter may become dominant. Leading edge triggering has the advantage of simplicity and gives good results when used with a narrow dynamic range of pulse heights together with detectors producing pulses of constant risetime.

Constant fraction timing

The walk resulting from handling pulses with a wide dynamic range of pulse heights but constant risetimes can be virtually eliminated if the leading edge discriminator can be arranged to trigger at a constant fraction of the maximum amplitude of

the input pulse regardless of what this amplitude may be (GEDCKE and McDONALD 1967, MAIER and SPERR 1970). The actual triggering fraction can be selected to give optimum time resolution.

Amplitude and risetime compensated timing

The ARC method of timing (CHASE 1968) was introduced to attempt to overcome the problem of obtaining good time resolution with semiconductor detectors which produce variable pulse shapes, such as from Ge(Li) devices. It is a slightly modified arrangement of the constant fraction trigger and provided the slope of the input pulse does not change early in its rise to maximum amplitude, compensation of risetime variations is achieved.

Pulse shape selection

When using Ge(Li) detectors a strong tailing is very often observed on the late side of timing spectra and the use of sophisticated timing discriminators, such as the ARC type above, only partially reduces it. The pulse shape selection method (MOSZYŃSKI and BENGTSON 1970, 1972) selects only those pulses having a given range of risetimes by the use of two discriminators and a time-to-amplitude converter. One discriminator has a low threshold and generates the start pulse for the time-to-amplitude converter, the other discriminator has a higher threshold but below that equivalent to the energy being studied and provides the time-to-amplitude stop pulse. The resulting time distribution of pulses can be analysed by a single channel analyser, the

output of which is applied to the slow coincidence unit (Section 3.3.) of the timing system. In this way the slow rising pulses from the detector (Section 2.3.4.) may be rejected, giving a time spectrum with a late slope which is exponential over several decades and faster by about an order of magnitude compared with using the methods discussed above (BENGTSON and MOSZYŃSKI 1972).

3.3. THE PRESENT MEASUREMENT SYSTEM

The choice of apparatus for the present study of the use of semiconductor detectors for short nuclear half-life measurements was arrived at by consideration of the factors outlined in this and the previous chapter. The choice was also partly dictated by the apparatus already available and the finances allocated to research in the Physics Department which initially were small but improved during the course of the work.

Block diagrams of the two measurement systems used are shown in Figures 3.3.(a) and 3.3.(b). In both cases the standard timing signals were obtained by the use of leading edge triggering with no compensation for amplitude and risetime dependent walk. The more sophisticated timing techniques (Section 3.2.) were developed several years after this work commenced.

Considering Figure 3.3.(a), the signals from the two detectors D_1 and D_2 were amplified by fast charge sensitive preamplifiers each having separate timing and energy outputs. The energy signals were coupled to a pair of shaping amplifiers and thence to single channel analysers which selected the energies of interest. The outputs from the two single channel analysers were fed to a slow coincidence unit which opened the gate on the multi-channel analyser when the detector pulses corresponded to the desired energies. The timing output signals from the charge sensitive preamplifiers were passed to two identical leading edge discriminators

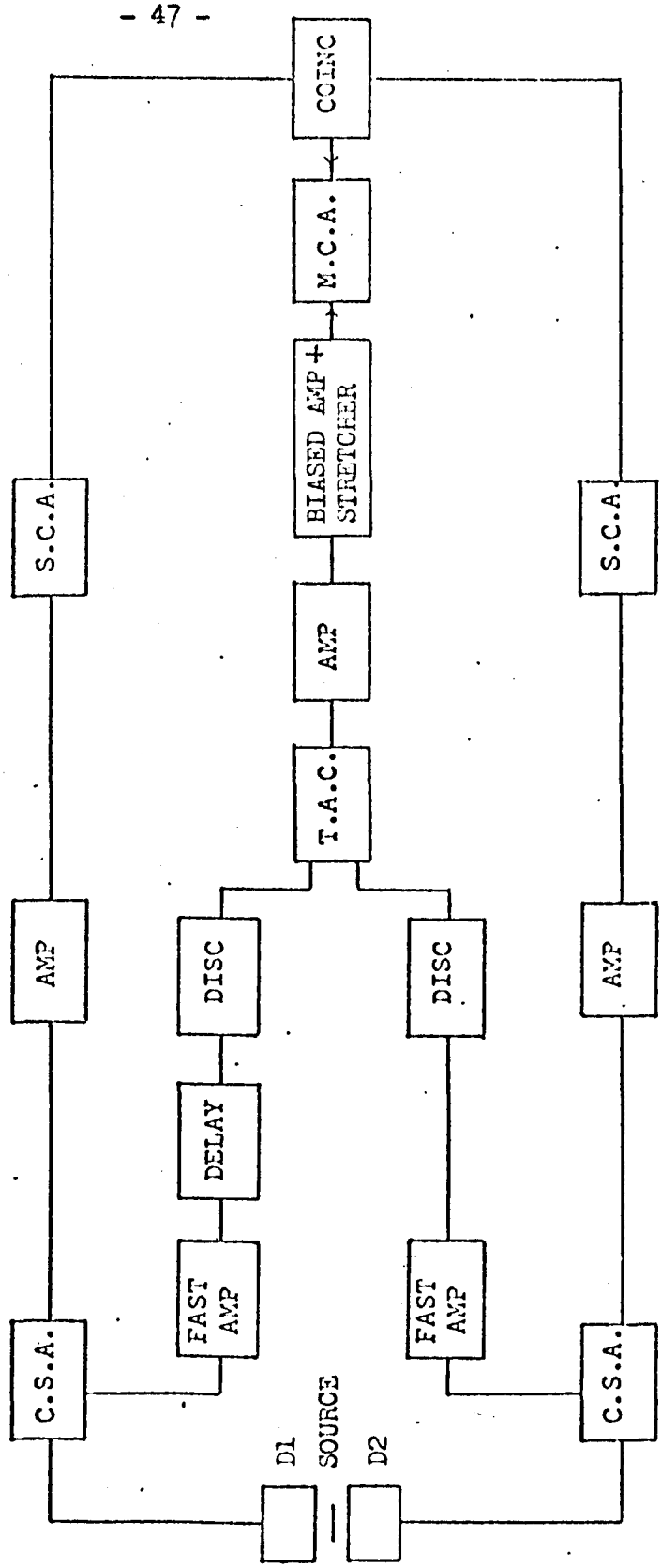

Figure 3.3.(a) Block diagram of one of the measurement systems.

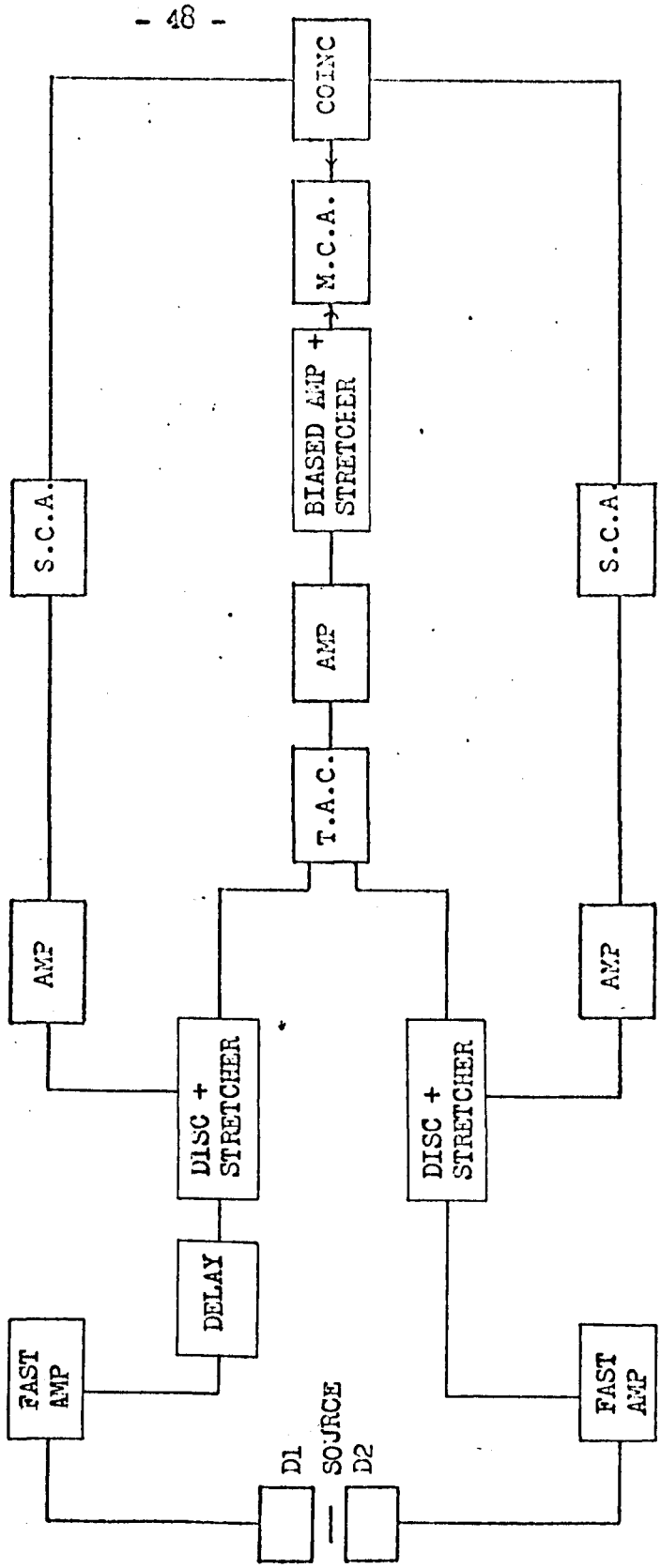

Figure 3.3.(b) Block diagram of the second measurement system.

the outputs of which were fed to a time-to-amplitude converter. The time-to-amplitude converter output pulses were amplified and stretched before being applied to the ADC input on the multi-channel analyser. The stretcher was used to ensure that these pulses overlapped in time with the gate pulses (the fast and slow channels had different delays). In the later work variations in delay of the slow channel with pulse height (energy) were kept to a minimum as the output signals from the single channel analysers were accurately timed to the cross-over point of the doubly differentiated pulses from the shaping amplifiers. The biased amplifier could be used to expand a selected region of the resulting time spectrum. The fast channel handling the depopulating radiation (referred to in this work as the "start" channel, the other fast channel being the "stop" channel) incorporated a delay prior to the discriminator to ensure satisfactory operation of the time-to-amplitude converter. The other system used (Figure 3.3.(b)) was very similar to that of Figure 3.3.(a) except that fast current amplifiers replaced the charge sensitive ones and the energy signal was obtained from the output of fast pulse stretchers. The discriminators used were identical in the two systems. The delay inserted in the start channel was also used for calibration purposes.

4. THE APPARATUS

4.1. INTRODUCTION

In this chapter the principle items of apparatus used during the course of this research programme are described. Outline operating principles are given, together with circuit and or block diagrams where appropriate, only for those electronic units which the author had to personnally construct. With the standard commercially available nuclear electronic units used, only their performance specifications, as quoted by the manufacturer, are given.

4.2. THE SEMICONDUCTOR DETECTORS

Use was made of four different semiconductor detectors, namely one Ge(Li), two Si(Li) and one surface barrier type.

The 3 cc active volume, 5 mm sensitive depth Ge(Li) detector (detector number 42 T) had a planar configuration and was manufactured by Nuclear Enterprises Ltd. It was housed by the manufacturer in the liquid nitrogen cryostat system shown in Figure 4.3.(a) such that the front face of the detector was 4 mm from the end face of the aluminium can. The makers quoted capacitance for the detector was 10 pF at an operating voltage of 800 V.

The two Si(Li) detectors were model numbers SL 50 - 1 (3 star) and 50 - 1.0 - 35 and were manufactured by 20th Century Electronics

Ltd and Simtec Ltd respectively. The 20th Century detector had an active area of 50 mm^2, a sensitive depth of 0.5 mm and an entry window thickness of 0.3 μm. Figures for the Simtec detector were 50 mm^2 active area, 1.0 mm sensitive depth and 0.2 μm thick entry window. Both detectors had recommended operating voltages in the range 100 V to 200 V.

The silicon surface barrier detector manufactured by Mullard Ltd was type PPY 51 - 100/sq. It had an active area of 25 mm^2 and a depletion depth of 0.1 mm. The recommended operating voltage was 15 V and the total detector capacitance at this voltage was 50 pF. The entry window consisted of 40 μgcm^{-2} of gold.

4.3. THE DETECTOR CRYOSTAT SYSTEMS

The use of the Ge(Li) detector necessitated the construction of a liquid nitrogen cryostat system in which the detector could be housed. This was because the detector had to be operated at a low temperature in order to reduce the leakage current to an acceptable value and had in any case to be stored at a low temperature to prevent the deterioration of the detectors performance through the lithium drifting back out. A conventional design was used (Figure 4.3.(a)), the cryostat being made from stainless steel with the exception of the aluminium cap surrounding the detector. The end face of this cap was thinned

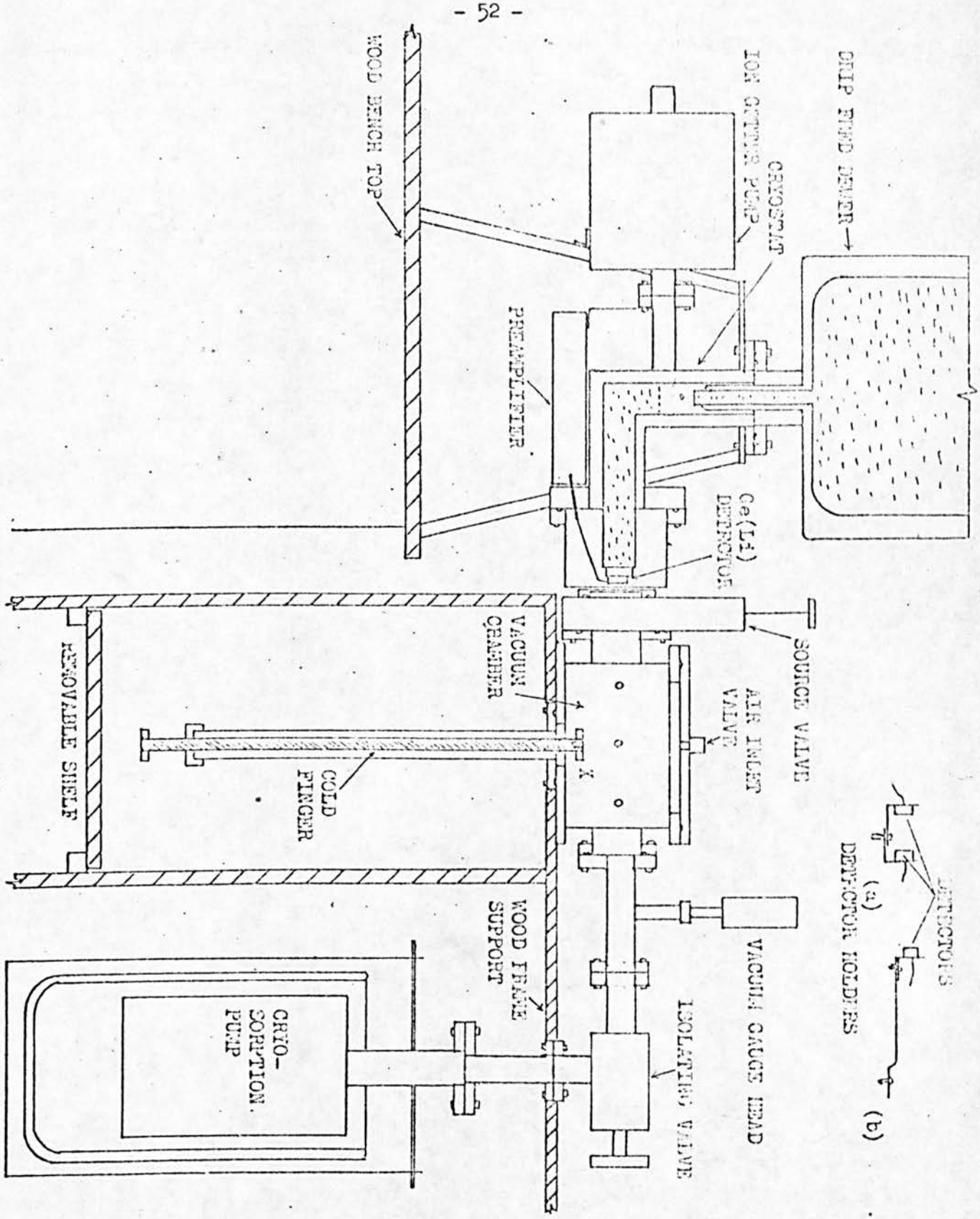

Figure 4.3.(a) The cryostat systems used with the detectors.

to present a 1 mm thick radiation window to the detector. To prevent contamination of the detector and rapid loss of liquid nitrogen the system was evacuated to a pressure below 10^{-9} mm Hg by use of an 8 litre per second ion getter pump. This pump was powered by a 5 kV D.C. supply. Five electrical feedthroughs provided the coupling between the front end of the preamplifier housed inside the aluminium cap and the remainder of the preamplifier. The liquid nitrogen dewar had a capacity of 10 litres and was topped up every four days approximately.

A second cryostat system was required for use with the two Si(Li) detectors and a cross-sectional view of it is shown in Figure 4.3.(a). The circular vacuum chamber with removable lid was made from brass and could be evacuated to below 10^{-3} mm Hg using the attached cryosorption pump. Detector holder (a) housing the two Si(Li) detectors or holder (b) with the surface barrier detector could be mounted on the small platform X fixed to a solid copper rod. This rod was surrounded by molecular sieve material and the whole was enclosed by a thin walled stainless steel tube. The lower part of this arrangement could be immersed in a dewar of liquid nitrogen, the copper rod then acting as a cold finger and the sieve material serving to maintain the vacuum, the larger cryosorption pump being isolated from the system. A source valve was attached to the vacuum chamber to enable sources to be changed without loss of

vacuum in the chamber. This facility was only suitable for use when the Ge(Li) detector was used with the surface barrier detector.

4.4. THE NON-STANDARD NUCLEAR ELECTRONIC UNITS

4.4.1. The Fast Charge Sensitive Preamplifiers

The fast, low noise, charge sensitive preamplifier used with the semiconductor detectors other than the Ge(Li) detector was similar to the design of SHERMAN and RODDICK (1970). The preamplifier was capable of delivering a fast output signal suitable for timing whilst simultaneously producing a low noise signal for amplitude measurements. Figure 4.4.(a) shows

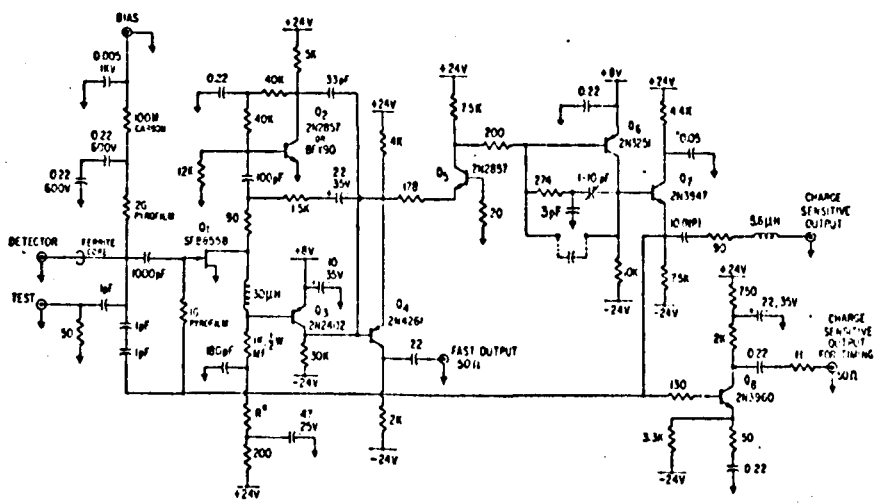

Figure 4.4.(a) Circuit diagram of the fast charge sensitive preamplifiers. (SHERMAN & RODDICK 1970).

the circuit diagram of the preamplifiers. A single field effect transistor Q_1 was used in the input stage followed by a fast amplifier comprising Q_{2-4}. Two second stage transistors were used to allow the low and high frequency components of the signal to take separate paths. A single fast transistor here would have generated increased low frequency noise. A fast voltage sensitive output (pulse risetime 2 ns) was available from Q_4. Transistors Q_5 and Q_6 formed common base and common emitter stages respectively, the added capacitance between base and collector of Q_6 limiting the high frequency performance of that stage. The emitter follower Q_7 provided the energy charge sensitive output and the output transistor Q_8 the timing charge sensitive output (pulse risetime 5 ns).

Two amplifiers of this type were required and were built on laminate panels having copper cladding on one face which acted as a ground plane. The two trimmer capacitors associated with Q_6 were adjusted to give optimum pulse risetime with minimum overshoot for a given detector. The value of the resistor R^* was 390 Ω, giving a Q_1 drain current of approximately 10 mA. The value of this resistor was found to be not very critical.

4.4.2. The Fast Amplifiers

A slightly modified version of the fast pulse amplifier designed by RUSH (1964) was used. The original supply voltages were lowered to reduce the risk of the amplifier oscillating when connected to a signal source and also to improve the signal to noise ratio. A further improvement in the amplifier noise performance was obtained by omitting the first common base amplifier in the input stage. This was possible as this input stage, when used, was always fed from a current source. These two changes reduced the equivalent input noise by approximately a factor of two compared with the original design. A further reduction was attempted by substituting low noise transistors for those in the input stage but this produced no measurable change. The circuit diagram of the modified five stage amplifier is shown in Figure 4.4.(b). Each of the five stages, with the

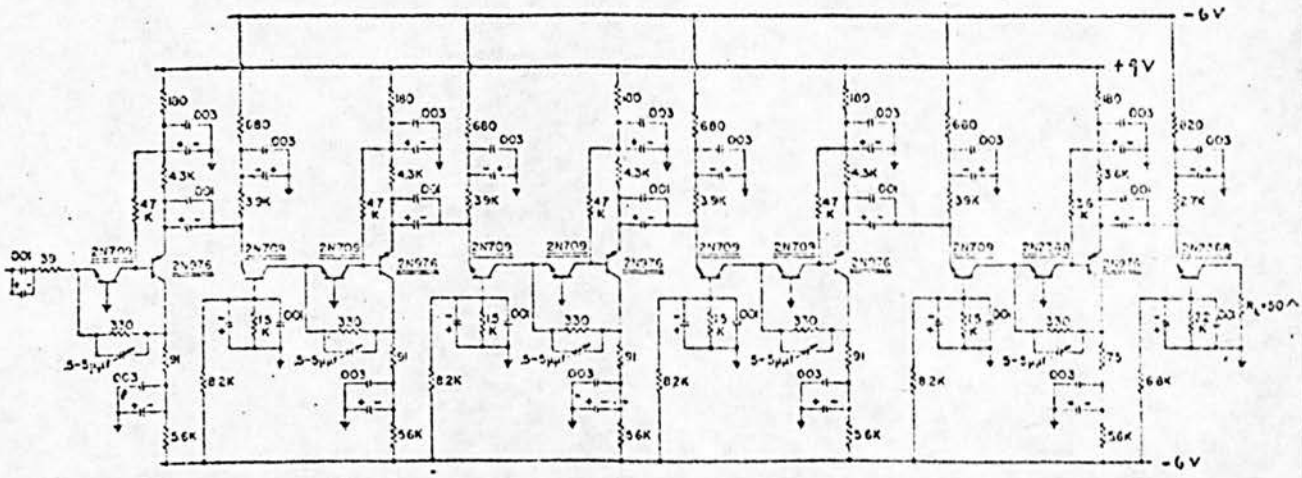

Figure 4.4.(b) Circuit diagram of the fast amplifiers (RUSH 1964).

exception of the first, consisted of a fed-back pair plus an isolating common base amplifier.

The two amplifiers required were built on laminate panels having ground planes and were housed in two separate aluminium cases. Considerable attention was given to the problem of earthing the amplifiers to their cases to ensure low noise operation. The completed amplifiers had current gains close to 550 and risetimes of approximately 3 ns.

4.4.3. The Fast Discriminators and Pulse Stretchers

Two fast discriminators were required to operate between the fast amplifiers and the time-to-amplitude converter and also to form part of the circuitry of the two fast pulse stretchers. The circuit diagram of the combined fast discriminator and fast pulse stretcher is shown in Figure 4.4.(c). The pulse stretcher part of the circuit was similar to the design of WEDDIGEN and HAASE (1965). Transistors T_1 (2N1141) and T_2 (2N706A) formed a common input amplifier to both the discriminator and the stretcher whilst T_3 (2N708) was a common base stage offering a high source impedance to the tunnel diode 1N2941. The 30 μH inductor forming part of the diode load determined the "on" time of the diode and thus the width of the pulse applied to the common emitter stage T_4 (2N976). This pulse had a width of 0.5 μs. The output from the emitter

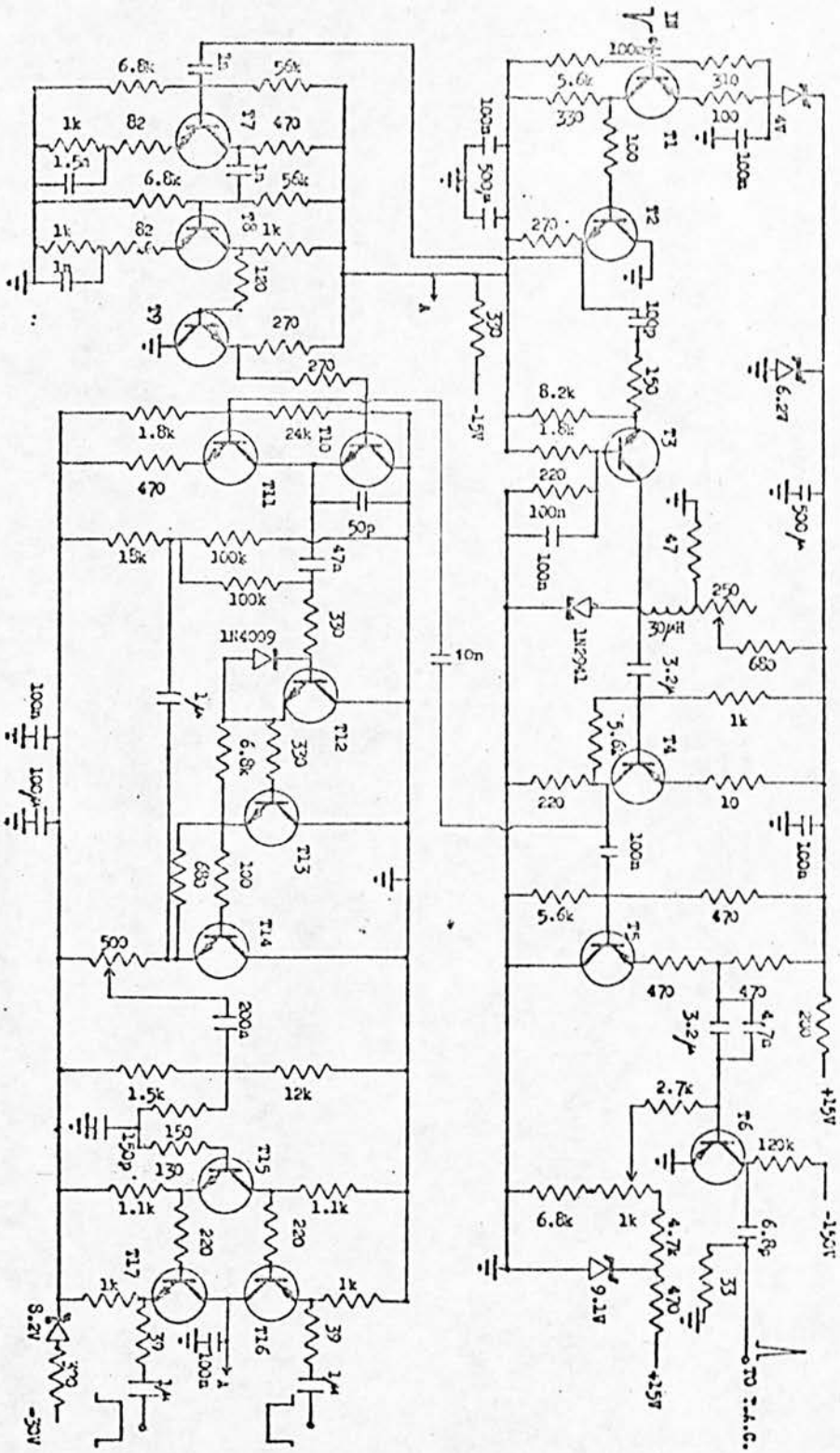

Figure 4.4.(c) Circuit diagram of the fast discriminator and pulse stretcher.

follower T_5 (AF121) was fed to the avalanche transistor T_6 (ASZ 23) which acted as a pulse shaper producing a positive output pulse of 8 ns duration, less than 2 ns risetime and 0.6 V amplitude. The 250 Ω and 1 kΩ potentiometers associated with the tunnel diode and avalanche transistor stages respectively were used to set up these stages for monostable operation.

The output from T_2 was also taken to the two stage amplifier comprising T_7 and T_8 (both OC170), with an emitter follower T_9 (2N706) at the output. The addition of these stages to the original design was found necessary in order that the stretcher should be able to operate on input pulses with amplitudes in the mV range. Transistor T_{10} (MM1711) was an emitter follower whilst T_{11} (2N709) acted as a constant current source. During the risetime of the input pulse the tunnel diode was triggered and the output from T_4 switched off T_{11}. Transistor T_{10} continued conducting, discharging the 50 pF capacitor, until the input pulse reached its maximum amplitude when T_{10} also switched off. The potential difference across the 50 pF capacitor had then decreased by the peak pulse amplitude. Due to the high input impedance (about 4 MΩ) of the bootstrapped compound emitter follower stage T_{12} - T_{14} (all MM1711) the charge on the capacitor remained unchanged until the tunnel diode returned to the "off" state (after 0.5 μs) and T_4 conducted again charging the capacitor. Transistors

T_{15} - T_{17} (MM1711, 2N1307 and 2N1306 respectively) formed the output stage enabling both positive and negative output signals to be obtained.

The two combined fast discriminators and fast pulse stretchers were constructed on laminate panels with ground planes. They were housed, together with the time-to-amplitude converter, in a triple width Harwell 2000 series module. The interior walls of the module were lined with 8 mm thick expanded polystyrene to lessen the effects of sudden room temperature changes. In the original design a heating element was provided in the module, controlled by a temperature sensing device, in an attempt to stabilize the interior temperature. This was abandoned though when it was found that the interior temperature rose to approximately 42 ^{o}C due to the heat produced by the electronic circuits and remained within ± 1 ^{o}C of this figure during the course of an experimental run. A small electric fan incorporated inside the module was used to try to keep a uniform air temperature throughout the unit.

4.4.4. The Time-to-amplitude Converter

The time-to-amplitude converter used was based on the design of WEISBERG (1965), the circuit diagram of which is shown in Figure 4.4.(d). The five tunnel diodes used were type 1N3858 and were biased in the monostable mode of operation. Transistors Q_{1-7} (2N1143) served to isolate the various tunnel diode stages from each other. Tunnel diode TD_1 produced a very

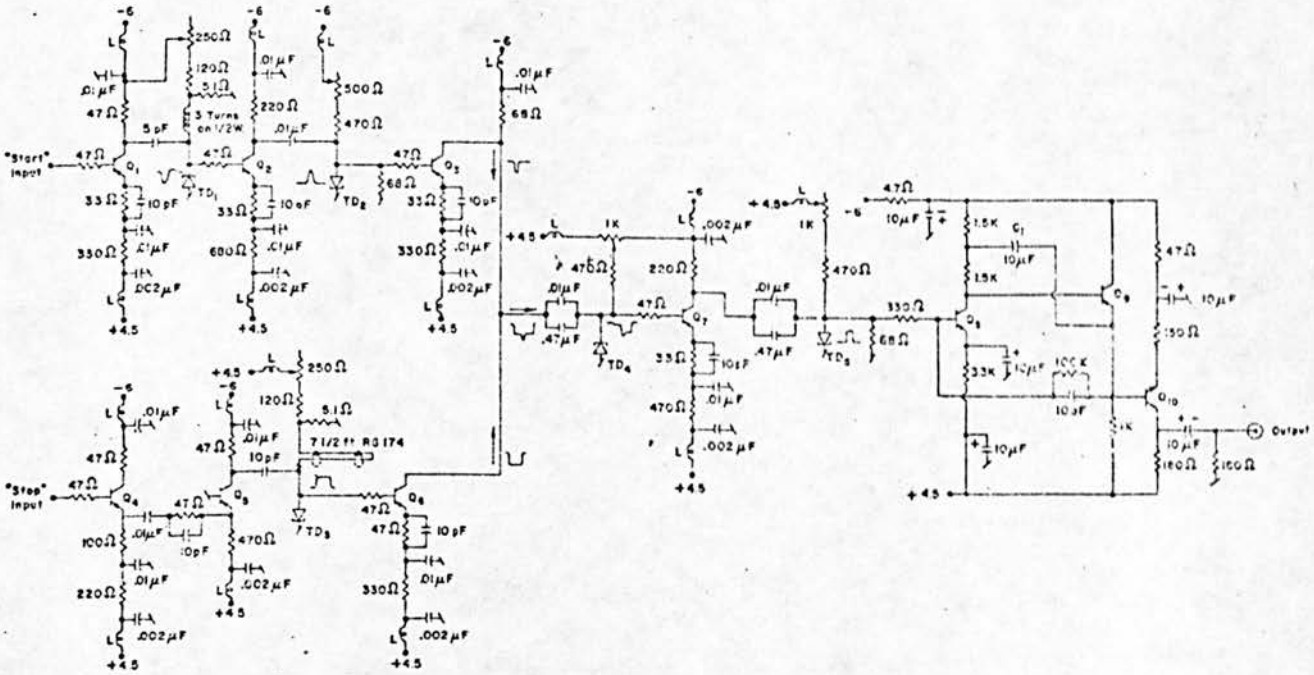

Figure 4.4.(d) Circuit diagram of the time-to-amplitude converter (WEISBERG 1965).

narrow pulse approximately 2.5 ns wide (Figure 4.4.(e)) when triggered into operation by a "start" input pulse. Additional shaping was provided by TD_2. The arrival of the "stop" input

pulse triggered TD_3 which produced a comparitively wide flat-topped pulse. The width of this pulse was determined by the length of shorted delay line used and was approximately 25 ns in the original design. The "narrow" and "wide" pulses were added together, after being fed through Q_3 and Q_6 respectively, and applied to TD_4. This tunnel diode was biased such that

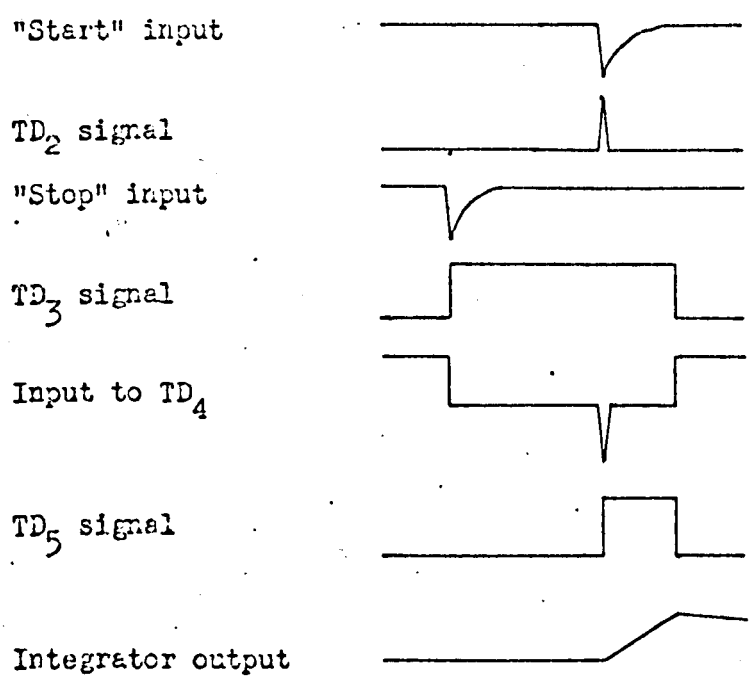

Figure 4.4.(e) Time-to-amplitude converter waveforms.

it was triggered to the "on" state only when the "narrow" and "wide" pulses occurred simultaneously in time but would not revert to the "off" state until the "wide" pulse had ended. The length of time TD_4 was in the "on" state, and hence the

duration of the output pulse from it, was thus linearly related to the time separation between the initial "start" and "stop" pulses. The possibility of singles feedthrough producing a spurious component to the output signals was eliminated by use of TD_5. The output from TD_5 was fed to an integrator consisting of the operational amplifier Q_{8-9} (2N2400) with capacitive feedback. The amplitude of the output pulse from this stage was proportional to the width of the input pulse from TD_5 and hence to the time separation between the "start" and "stop" pulses. The output stage transistor was type 2N585.

The converter was constructed on a laminate panel having a ground plane. Metal oxide resistors were used throughout in view of their excellent stability and the decoupling capacitors used were low inductance types. All wiring was kept as short as possible to minimise loss of high frequency performance.

To set up the correct bias currents through the five tunnel diodes the waveforms at the diodes were monitored using a high input impedance 100 MHz oscilloscope whilst the appropriate bias potentiometer was adjusted. TD_1 followed by TD_2 and TD_3 were set up first, their bias currents being adjusted such that they triggered decisively when an input signal was present but were well below the point of triggering spuriously when an input signal was absent. The bias for TD_4 and TD_5 was set

so they would only trigger when the narrow and wide pulses overlapped in time. Provided the circuit component values were left unchanged it was found that these five bias settings were stable throughout the course of the research work described here.

The range of the converter described above was about 25 ns which was adequate for measurements of half-lives of the order of nanoseconds. As part of the research programme involved measuring half-lives considerably longer than this it was necessary to extend the range of the original converter. This was achieved by substituting a 60 m long delay line (coaxial cable type RG174) for the existing one. To handle the longer pulse widths in the circuit larger decoupling capacitors were used in the emitters of Q_6 and Q_7 (0.22 μF paralleled with the existing 0.01 μF and 50 μF from the junction of the 470 Ω and 33 Ω resistors in Q_7 emitter to chassis) and in the collector of Q_7 (0.1 μF paralleled with the existing 0.002 μF). In addition the series resistor in the input of the integrator was increased from 330 Ω to 8.5 kΩ to prevent the integrator from overloading. These modifications increased the converter range to approximately 600 ns with no detriment to the original units performance.

4.4.5. The Time-to-amplitude Converter Calibrator

A simple electronic unit was designed and constructed using TTL integrated circuits enabling rapid calibration of the time scale of the time-to-amplitude converter (BISHOP 1973). The principle of operation of the unit was similar to that used in the design of BAKER et al (1968). A block diagram of the calibrator unit together with idealised waveforms is shown in Figure 4.4.(f). The start and stop pulses were both accurately

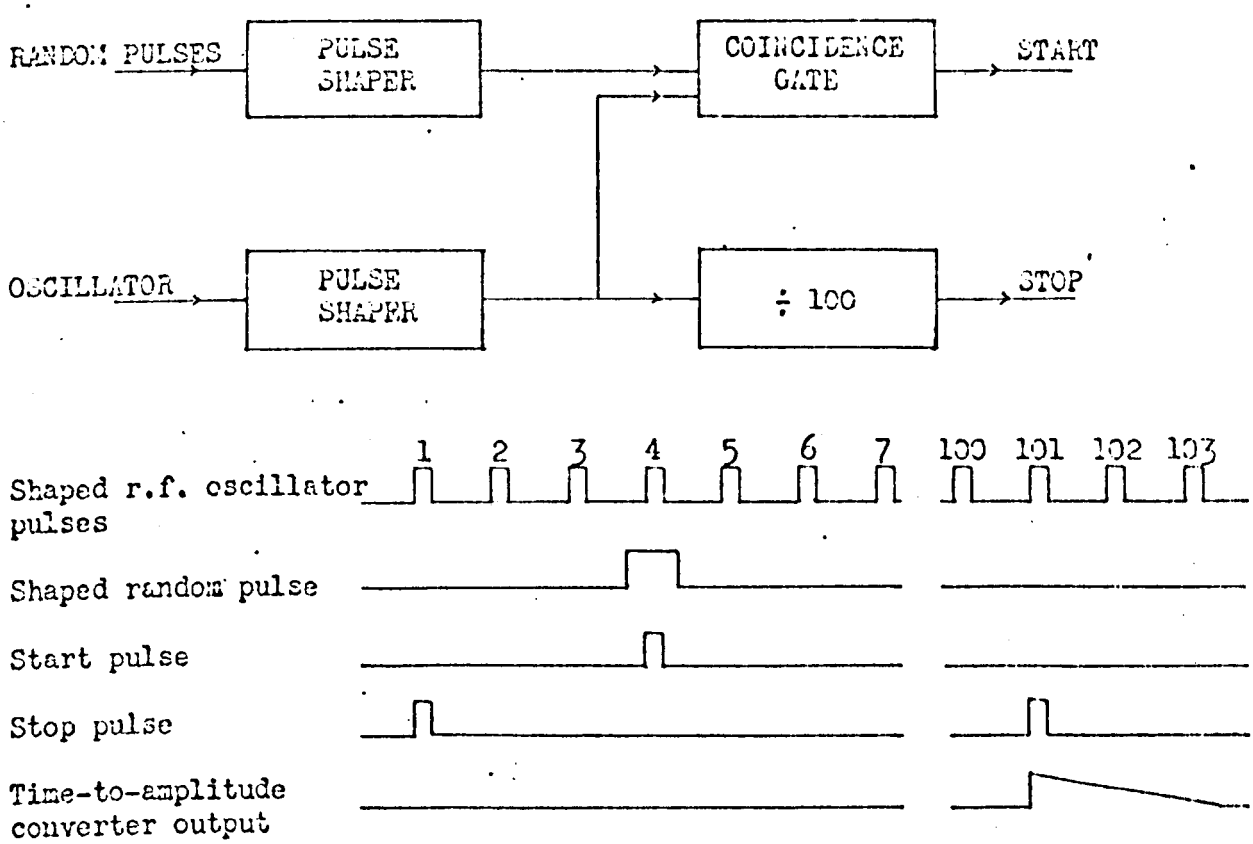

Figure 4.4.(f) Block diagram of the time-to-amplitude converter calibrator together with idealised calibrator waveforms.

phased to the r.f. oscillator pulses and as the oscillator pulses were scaled down by a factor of 100 to provide the stop pulses there existed 100 possible time intervals between start and stop pulses. No fixed phase relation existed between the oscillator pulses and the random input pulses and thus these time intervals occurred with equal probability. The resulting calibration spectrum consisted of up to 100 peaks (depending on the time-to-amplitude converter range) of equal intensity separated in time by the oscillator period. Figure 4.4.(g) shows the schematic circuit diagram of the device. Pulses

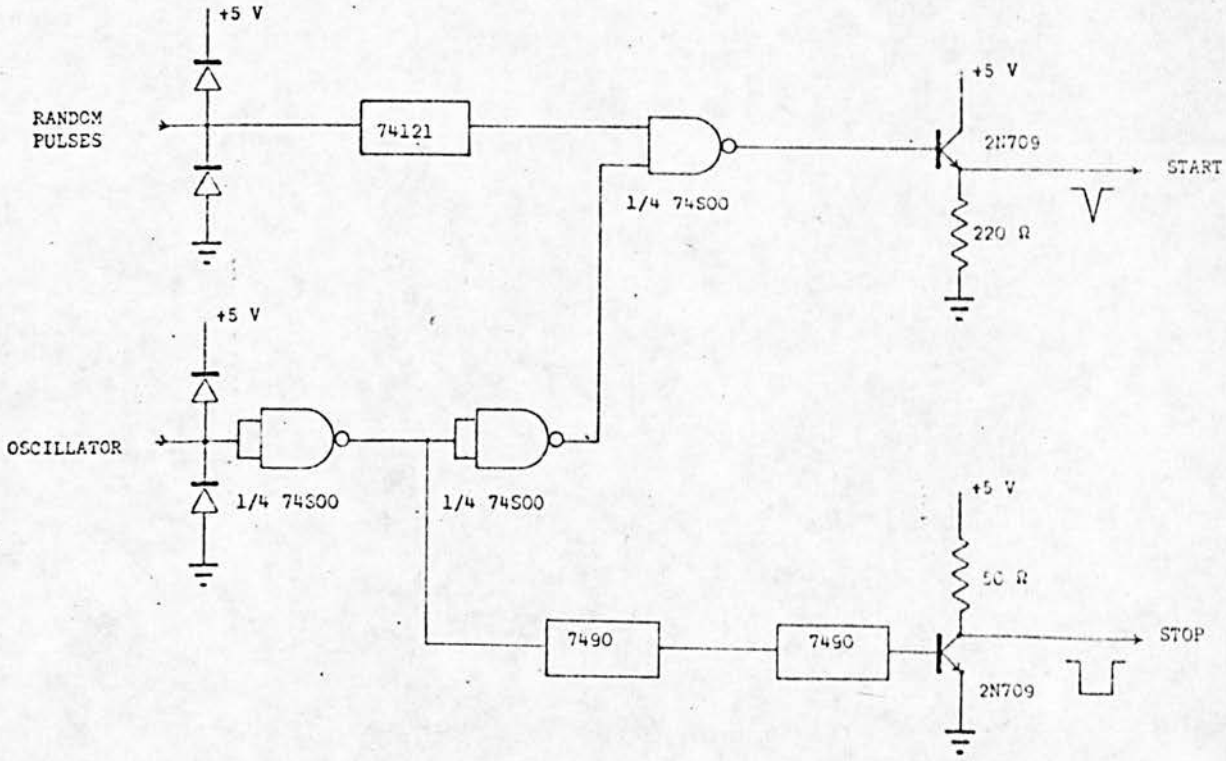

Figure 4.4.(g) Circuit diagram of the time-to-amplitude converter calibrator.

randomly distributed in time relative to the oscillator pulses were obtained initially from the output of a radiation detector but later a pulse generator was used. These pulses were shaped by the 74121 monostable before being applied to the 74S00 coincidence gate. The monostable was set to produce pulses having a width approximately 20% less than the oscillator period. Oscillator pulses shaped by the two 74S00 gates were applied to the other input of the coincidence gate. The output from this gate provided the start pulses. Stop pulses were obtained by scaling down the oscillator frequency by a factor of 100 using a pair of 7490 decade counters. Speed limitations in the discriminators associated with the time-to-amplitude converter forced the use of such a large scaling factor.

4.4.6. The Coincidence Unit

The double coincidence unit was designed around a Rossi type circuit and was constructed in a single width Harwell 2000 series module. Valves were chosen as the active devices as the unit had to deliver a comparatively large output signal (about 30 V) to ensure correct operation of the gate on the multichannel analyser. Figure 4.4.(h) shows the circuit diagram of the unit. Valves V_1 and V_2 were normally conducting and their anode voltages were low. If a negative signal was applied to the control grid of either V_1 or V_2 so as to cut

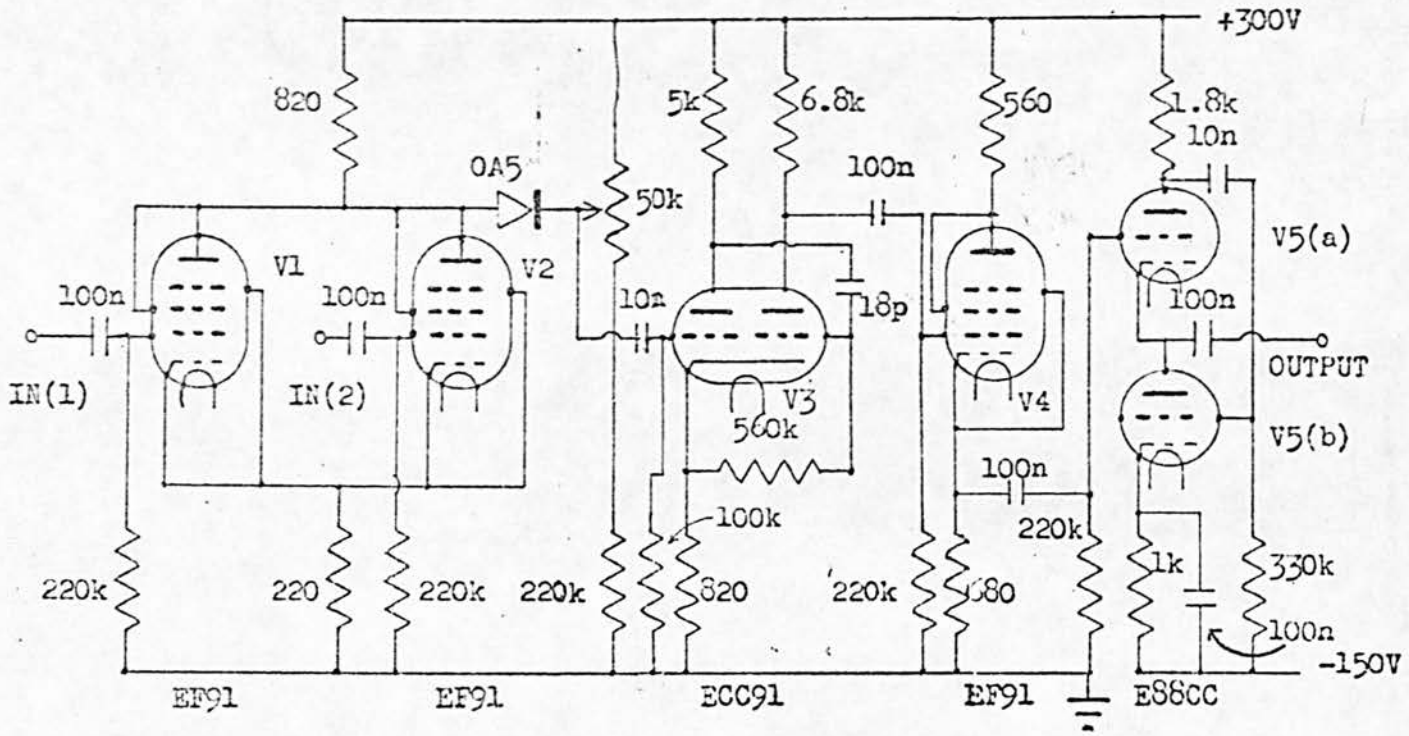

Figure 4.4.(h) Circuit diagram of the coincidence unit.

it off then the anode voltage rose only slightly. However, if both valves were cut off by coincident input signals then the anode voltage rose to + 300 V and a large positive signal resulted. The bias on the OA5 diode was adjusted so that the diode only conducted for coincident input signals. The double triode V_3 was a cathode coupled trigger which produced an output pulse of fixed duration and amplitude (determined by circuit component values) when triggered into operation by a signal from the diode discriminator. Valve V_4 was a phase inverter and V_5 a White cathode follower. The completed unit delivered a 30 V positive pulse of 5 μs duration and 60 ns risetime for coincident input signals. The input sensitivity was better than 5 V.

4.5. THE STANDARD NUCLEAR ELECTRONIC UNITS

The relevant performance specifications quoted for the commercial nuclear electronic units used in the apparatus are given below. All the units, with the exception of Harwell 2000 series equipment and the multichannel analyser were manufactured by Nuclear Enterprises, Edinburgh.

The Ge(Li) detector preamplifier

The charge sensitive preamplifier used with the Ge(Li) semiconductor detector was type NE 5287. This consisted of a charge sensitive stage in cascade with a voltage gain stage (gain X1 or X5). The front end of the preamplifier was incorporated in the Ge(Li) detector cryostat which minimised the effect of stray capacitance at the preamplifier input and enabled the field effect transistor to be operated at a much reduced temperature thus decreasing its noise contribution. The energy and timing signals were obtained from the outputs of the voltage gain and charge sensitive stages respectively, the unit being adapted to provide the latter signal.

Non-linearity	0.1%
Gain stability	0.01% per ^{o}C
Charge sensitivity	305 mV per MeV (Ge detector)
Risetime	20 ns.

The main and time-to-amplitude converter amplifiers

For the work using the unmodified time-to-amplitude converter the two main amplifiers used were both type NE 5259 and the time-to-amplitude converter amplifier was a Harwell 2000 series type number 2044A. The initial part of the work using the modified time-to-amplitude converter made use of one NE 5259 and one NE 4603 as the main amplifiers and a NE 5259 as the time-to-ampliude converter amplifier. The latter part of this work was carried out using two NE 5259 as the main amplifiers and the NE 4603 as the time-to-amplitude converter amplifier.

NE 5259 :-

Shaping	Single or double RC differentiation and integration. Time constants 0.2, 0.5, 1, 2, 5 or 10 μs
Gain	Continuously adjustable in range 8 to 2000
Gain stability	0.05% per °C at full gain
Integral non-linearity	0.1%
Differential non-linearity	1%
Noise	6 μV r.m.s. referred to input for 1 μs single differentiation and integration

NE 4603 -

Shaping	RC shaping with 4 integrations and either 1 or 2 differentiations. Time constants of 0.2 μs to 12.8 μs in binary sequence
Gain	Continuously adjustable in range 8 to 1024
Gain stability	0.005% per ^{o}C
Non-linearity	0.1%
Noise	2.0 μV r.m.s. referred to input for 6.4 μs time constant.

Biased amplifier and stretcher

A type NE 5261A biased amplifier and pulse stretcher was used, the two functions being contained in the same module.

Bias level	Adjustable from 0 to 10 V
Gain	1, 2, 5, 10 or 20 switch selected
Gain stability	0.01% per ^{o}C
Output pulse width	5 μs from stretcher.

The single channel analysers

Two single channel pulse height analysers were used type NE 5159C. The threshold level was continuously variable from 0.2 to 10 V and the window width from 0.1 to 5 V. An output signal accurately timed to the crossover point of the input pulse was available, the signal having a time stability of ± 2 ns for a 0.5 to 10 V input amplitude range using 500 ns double differentiated pulses. This signal could be delayed relative to the crossover point by any time in the range 0.3 to 0.5 μs.

The delay units

Harwell 2000 series units type 2105A and 2046A (both fine delay) and type 2104A (course delay) were used. Various lengths of delay line could be switched in giving delays lying in the approximate range of 4 to 15 ns for the fine delay units and 3 to 56 ns for the course delay unit.

The multichannel analyser

A 100 channel pulse height analyser was used type PHA 3 manufactured by Associated Electrical Industries Ltd. It was a hybrid design using both valves and transistors and was one of the first analysers to make use of ferrite core storage. The memory contents were presented as a linear analogue display

on a cathode ray tube and could be printed out onto a 3" paper tape, each line showing the channel number and the count in that channel. The instrument incorporated a gating circuit which was used for coincidence counting.

Memory capacity	65535 counts per channel
Analysis range	0 - 10 V
Channel width	100 mV
Channel width uniformity	1% except first 4 channels
Channel width stability	± 1 mV.

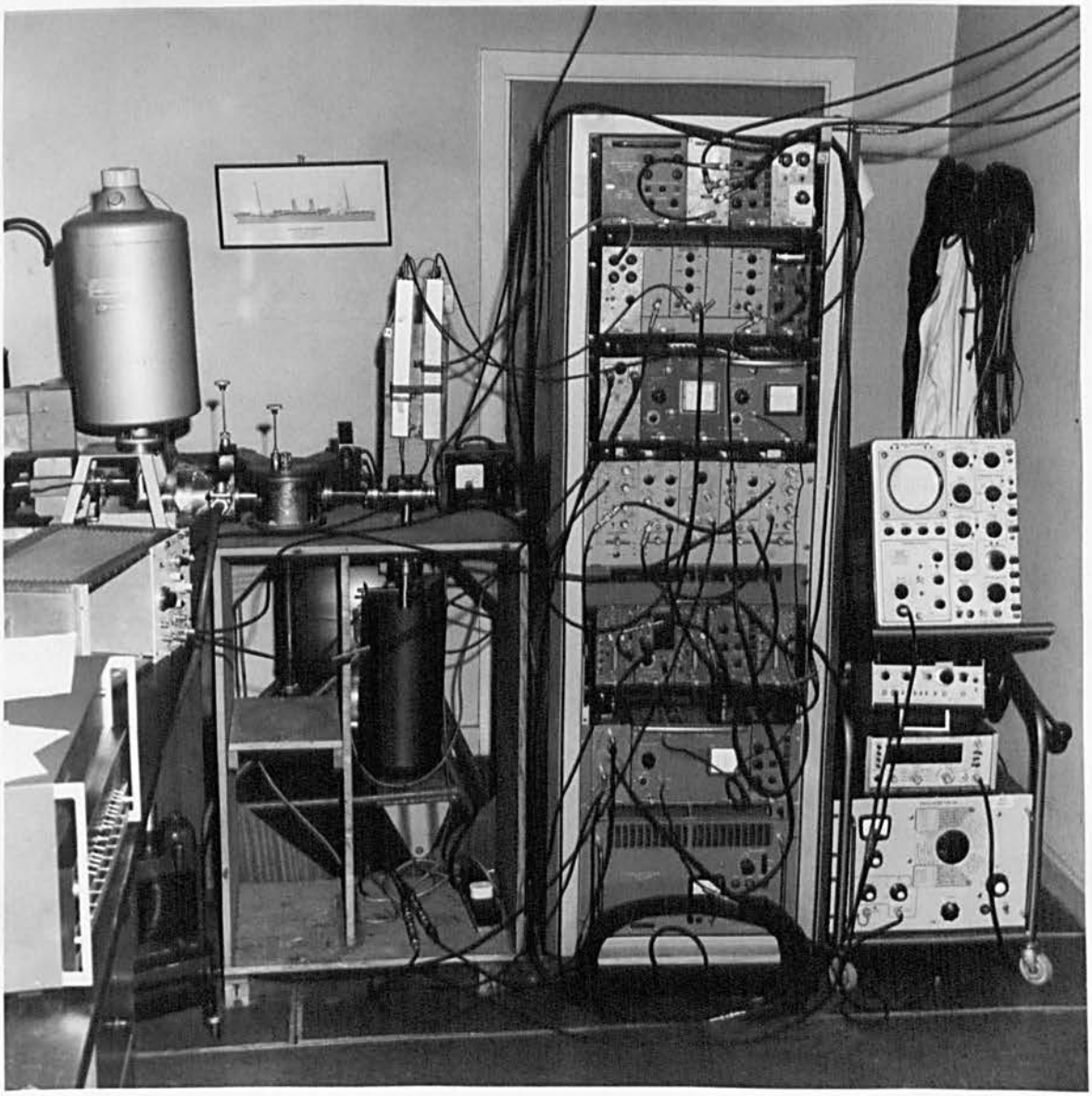

General view of the apparatus excluding the multichannel analyser.

5. MEASUREMENTS AND RESULTS

5.1. CALIBRATION

Two methods of calibrating the time scale of the time-to-amplitude converter were used. The electronic calibration unit described in Section 4.4.5. was used in measurements with the modified (wide range) time-to-amplitude converter, whilst in all other cases calibrated delay cables were used. The use of the electronic calibration unit enabled rapid and accurate calibration to be achieved without the difficulties associated with the measurement of the delay in cables, this delay being pulse shape dependent. Further errors arise from attenuation of the pulses in the cables and many cables are needed to cover the whole conversion range.

The use of these two calibration methods will now be considered.

(a) Electronic calibration unit

For the calibration measurements the calibration unit was coupled to the two fast discriminator inputs, all other connections to these inputs being removed except for 50 Ω terminations. The stop output from the calibrator fed the start discriminator input via a ×50, 50 Ω attenuator(General Radio GR874-G) and the start output fed the stop discriminator input via a ×20, 50 Ω attenuator. This particular arrangement was used as the start discriminator channel was capable of handling a much higher count rate than

the stop channel. The attenuators reduced the calibration unit's output pulse amplitudes from standard TTL logic levels to levels acceptable by the discriminators(no spurious triggering). An RC differentiator (τ = 20 ns) at the calibrator stop output was used to reduce the output pulse width and produce a short duration negative pulse.

Initially the random pulses applied to the calibrator were obtained from the output of the shaping amplifier used with the surface barrier alpha detector but in later work a pulse generator (Nuclear Enterprises NE 6591) was used which simplified the calibration procedure as fewer alterations had to be made to the measurement system when changing from delayed coincidence measurement to calibration. In both cases the input pulse height was adjusted to be about 4 V, a level which assured satisfactory operation of the monostable pulse shaper. A similar adjustment was made to the signals applied at the oscillator input, these signals being obtained from a variable frequency oscillator (Airmec type 304). The oscillator frequency was continuously monitored throughout a calibration run using a six digit digital frequency meter (Philips PM 6620). The manufacturers quoted accuracy of frequency measurement was better than 0.001 % at frequencies above 10 MHz. An internal check frequency of 10 MHz was provided. A check on this accuracy using an eight digit frequency meter (Marconi TF 2410) verified the manufacturers figures.

Before using the calibrator the start output pulses from 16 were monitored on an oscilloscope and the width of the output pulses from the monostable adjusted, if necessary, so that they only overlapped in time with one oscillator pulse (overlapping of more than one oscillator pulse exhibited itself as multiple output pulses as seen on the oscilloscope). Readjustment was normally unnecessary if a narrow range of oscillator frequencies was used.

In changing from delayed coincidence measurement to calibration a small adjustment of the two fast discriminator's tunnel diode bias controls was sometimes necessary in order to restore monostable operation. The settings on the multi-channel analyser, time-to-amplitude converter amplifier and biased amplifier were not touched except for removing the gate input to the analyser and switching from coincidence to anti-coincidence operation.

A check on the linearity of the calibration unit was made using the method of BAKER et al (1968). The oscillator associated with the calibrator was set to 18 MHz and the pulse generator to 10^3 pulses per second. The resulting spectrum was stored and displayed on a 1000 channel analyser (Link Systems 290 series) which was temporarily substituted for the 100 channel device. Figure 5.1.(a) shows the spectrum obtained. The calibrator was then removed and the start discriminator input fed from the pulse generator (10^5 pulses per second, 40 mV pulse amplitude) whilst the stop discriminator was fed with pulses from the fast channel

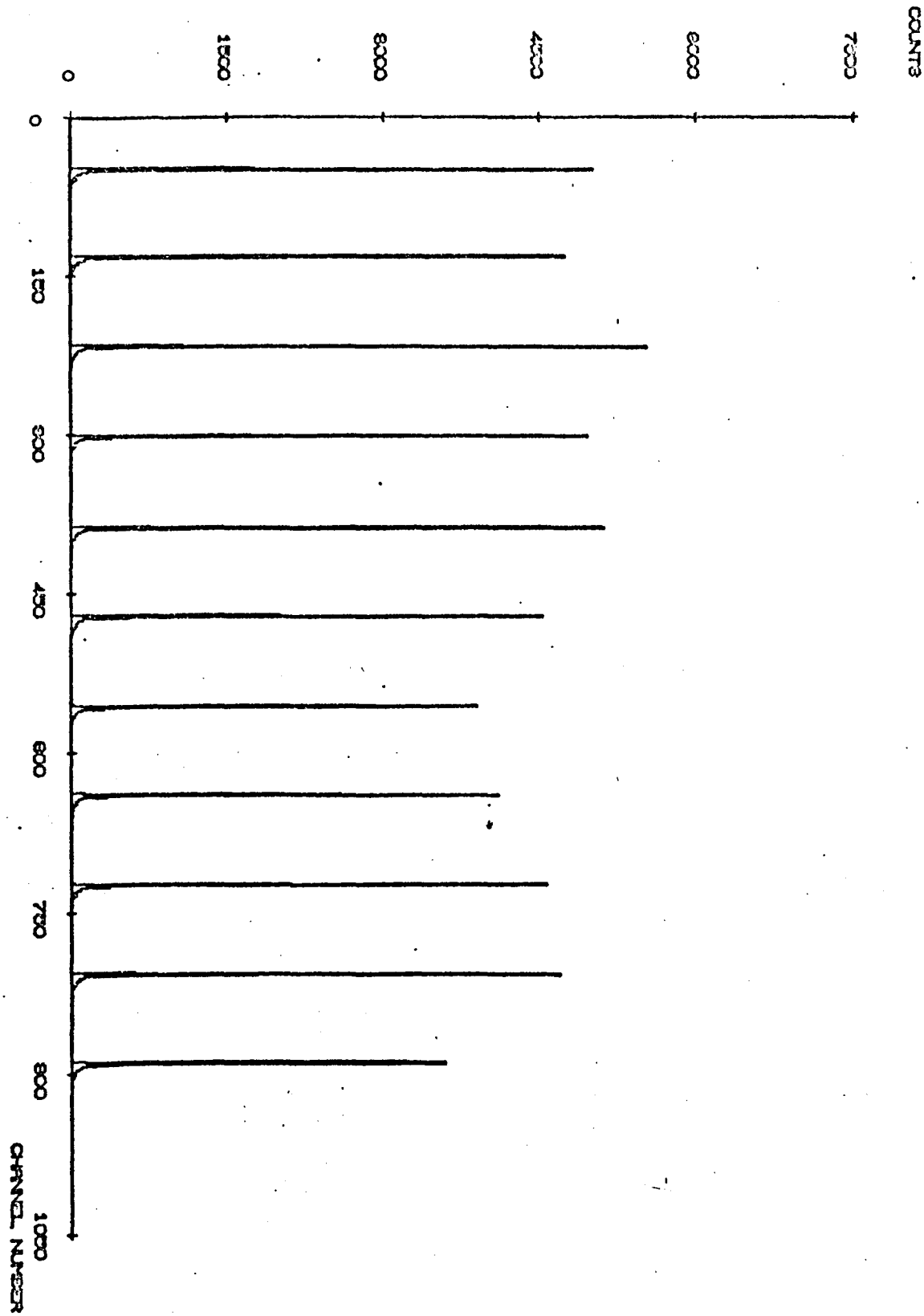

Figure 5.1.(a) Spectrum obtained with the electronic calibration unit.

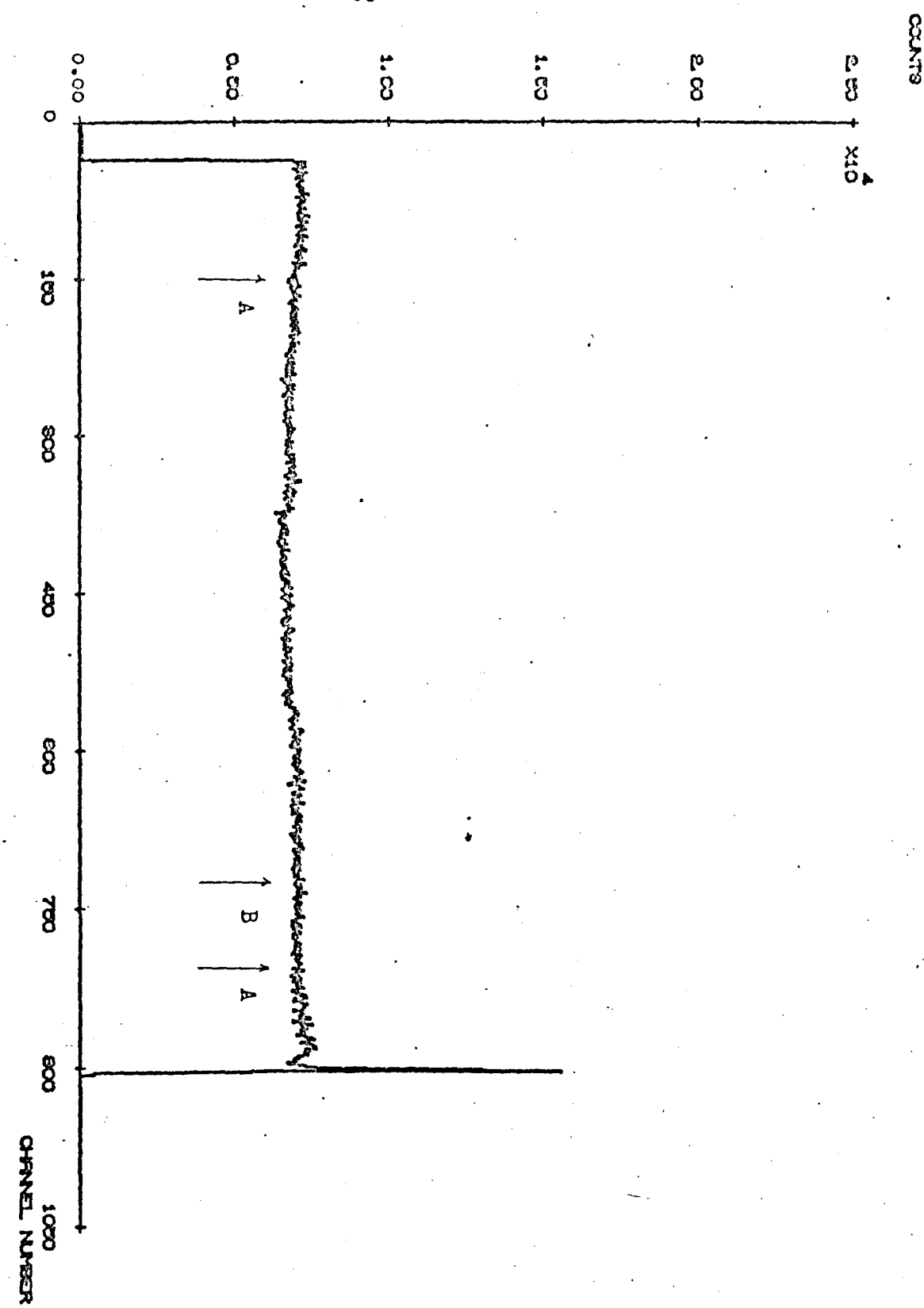

Figure 5.1.(b) Random time spectrum.

incorporating the surface barrier detector (Am-241 alpha source). A random time separation thus existed between the pulse generator and the detector pulses and this enabled the random time spectrum shown in Figure 5.1.(b) to be obtained. The same settings on the multi-channel analyser, time-to-amplitude converter amplifier and biased amplifier were used for both measurements.

If the calibrator produced peaks equally spaced in time then the total counts in the random time spectrum obtained by summing between the positions of any two adjacent peaks in the associated calibration spectrum should have been identical. The set of nine results for the total counts between adjacent peaks obtained here showed a standard deviation of ± 0.32 %. The summation between the last pair of peaks lying between channels 750 and 900 was not used as the final peak fell very close to the end of the range of the time-to-amplitude converter. The uncertainty for each summation was less than ± 0.24 % made up of a statistical uncertainty of ± 0.13 % and an uncertainty in determining the position of the centroid of the peaks in the calibration spectrum of less than ± 0.2 %. Thus the calibration unit produced a set of peaks equally spaced to an accuracy of better than ± 0.5 %. Since the oscillator frequency used could be determined to an accuracy of better than 0.001 %, the basic accuracy of calibration using this calibration unit was taken to be ± 0.5 %.

All the delayed coincidence measurements were performed

using the 100 channel analyser and thus the calibration had to be done on that machine as well. Due to the small number of channels the positions of the calibration peaks could not be determined to the same degree of accuracy as on the 1000 channel device. To overcome this each calibration was carried out at three different oscillator frequencies thus yielding three calibration spectra. The centroid of each peak, in the region of interest (ie. covering the delayed coincidence spectrum), in each spectrum was then determined. A least squares fit (Appendix A, program (i)) was then applied to extract the best straight line from the pairs of data points (centroid position, delay) and from a knowledge of the oscillator frequency the calibration in ns per channel calculated. The accuracy of this figure was taken as ± 0.5 %, unless the three calibration results from the three spectra showed a standard deviation greater than this in which case the latter figure was used.

The time calibration of the time-to-amplitude converter was carried out after each delayed coincidence measurement and where measurements were made in immediate succession the average of the calibration before and after measurement was taken. The standard deviation of these two figures was used for the calibration if greater than the figure calculated in the above paragraph. For much of the work the calibration results were found to be consistent to within ± 0.5 % over periods up to a week.

By expanding a small region of the calibration spectrum using

the biased amplifier the fwhm of the calibration peaks was found to be 0.7 ns.

(b) Calibrated delay cables

Two Harwell 2000 series delay units type 2046A were used for calibrating the time scale of the unmodified (narrow range) time-to-amplitude converter. Each unit consisted of a set of eleven separate pre-calibrated delay cables, the length of cable and hence the delay introduced into the system being switch selected. The positions of the delay units in the measurement systems were as in Figures 3.3.(a) and 3.3.(b).

During calibration the fast amplifier outputs were disconnected from the two fast channels and the inputs to the two channels were then fed from a common pulse generator (NE 6591). The positions of the pulser peaks (in terms of a channel number) were found for a series of inserted delays covering the range of the time-to-amplitude converter. A graph was then plotted of inserted delay against pulser peak channel number and the calibration (ns per channel) obtained from its slope.

The accuracy of delay calibration was checked using a 30 cm rigid air line (General Radio GR874-L30). With the system set up for calibration and the biased amplifier on x10 (thus expanding a selected region of the time scale) a pulser peak was obtained with the delay unit set for least delay (switch position (1)).

On switching to position (2) an additional delay of about 1 ns was introduced producing a second pulser peak at a lower channel number. The separation between these two peaks, in terms of number of channels, was found and from the given calibration figures the calibration over that region of the time scale found. This was repeated for the other adjacent switch positions and the meancalibration over the region covered by the delay unit calculated. The delay unit was again set for least delay and a pulser peak obtained. The 30 cm air line was then introduced into the channel containing the delay unit and a second pulser peak obtained. From a knowledge of the separation between these two peaks and the delay introduced by the air line (1.0036 ± 0.0018 ns) the calibration was found. This was repeated for the other switch positions on the delay unit and the mean calibration determined. The calibration using the delay unit was found to be 5% lower than that using the air line. No figures for the calibration accuracy of the delay unit were given by the manufacturers. Because of this and the fact that more consistent results were obtained for the calibration between the pairs of peaks using the air line than using the delay unit, it was assumed that the air line calibration was the more accurate figure. The air line became available about a year after the work using the unmodified converter had been completed and it could not therefore be used to give direct calibration.

Accordingly the calibration figures previously obtained using the delay unit were increased by 5%. The accuracy of calibration was taken as ± 5%. No attempt was made to improve on this figure as no actual measurements of half-lives were made using the unmodified converter.

5.2. TIME-TO-AMPLITUDE CONVERTER PERFORMANCE

The two most important performance figures of a time-to-amplitude converter are the intrinsic time resolution and the differential non-linearity. The former is usually defined as the width (fwhm) of the time distribution obtained when both start and stop inputs are fed from the same signal source, whilst the latter is a measure of the deviation of the time width of any channel with respect to the mean time width of all the channels. This latter may be determined by using two uncorrelated (in time) signals as the start and stop inputs. A random time spectrum then results, the number of counts in any channel being proportioal to the time width of that channel. In this work the stop signal was obtained from the surface barrier detector (Am-241 alpha source) and the start signal from a pulse generator.

With the present apparatus access was not possible to the time-to-amplitude converter start and stop inputs as the two fast discriminators were permanently connected to them. Instead the

start and stop signals were fed to the appropriate discriminator inputs and thus the following performance figures relate to the time-to-amplitude converter combined with the fast discriminators.

(a) The modified converter

The random time spectrum obtained in Section 5.1 and illustrated in Figure 5.1(b) was used to obtain the differential non-linearity. Over the region A-A the mean time width of the channels (expressed as counts) was 6968 and the maximum deviation of the time width of any of the channels in this range from the mean was 346. Thus the maximum differential non-linearity over this region was ± 5%. Over the region A-B the figure was ± 3.6%. The figure of 0.7 ns quoted in Section 5.1 for the fwhm of the calibration peaks was taken as the intrinsic time resolution of the converter.

(b) The unmodified converter

Figure 5.2.(a) shows the random time spectrum obtained using the unmodified converter (the peak between channels 90 and 95 extended to 17152 counts). Over the region A-A the maximum differential non-linearity was ± 20% whilst in the region B-B it was ± 9%. In the delayed coincidence results obtained with this converter most of the counts fell in the range B-B. The intrinsic time resolution was 100 ps for input pulse amplitudes to the discriminators of greater than 40 mV.

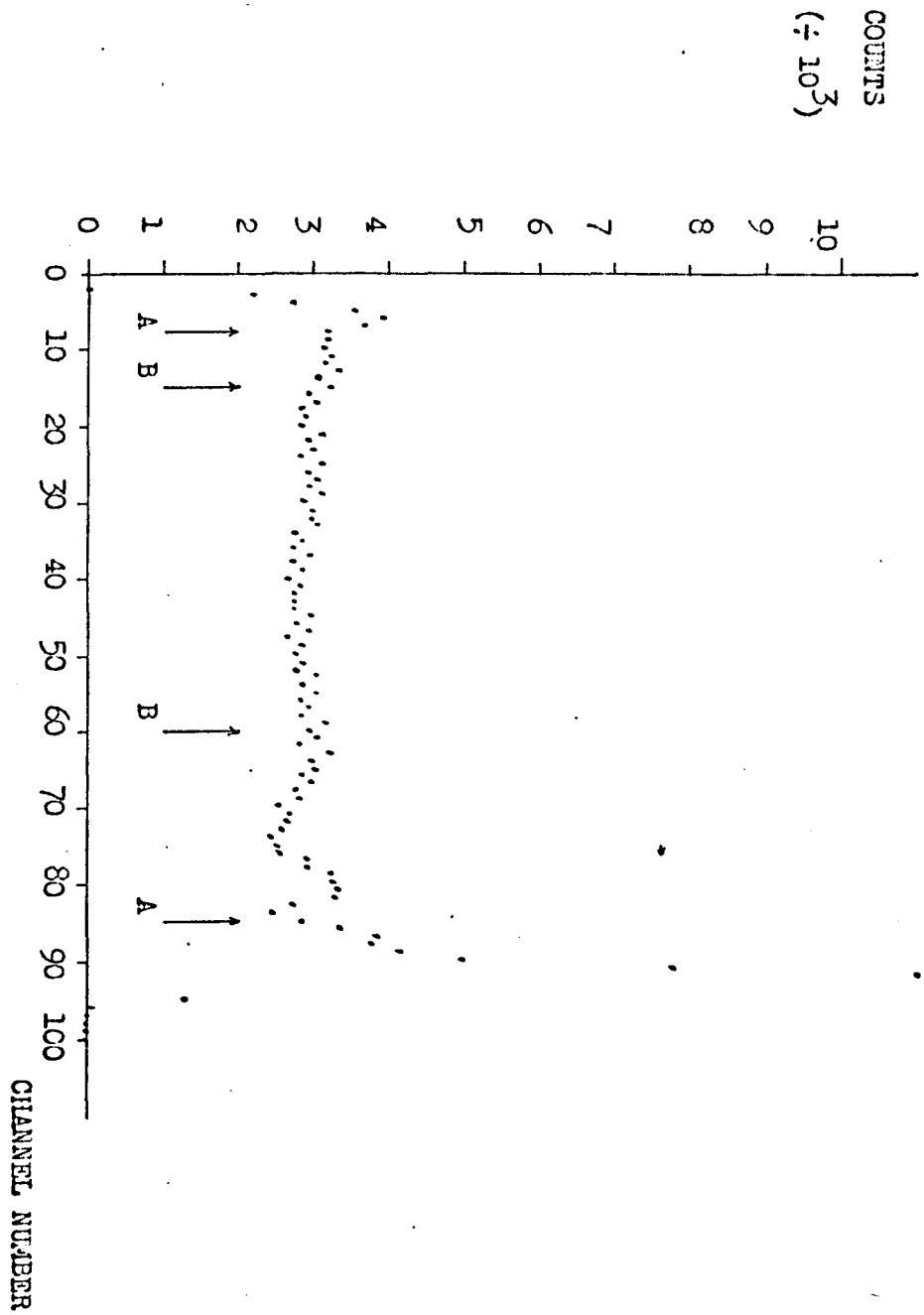

Figure 5.2.(a) Random time spectrum obtained using the unmodified time-to-amplitude converter.

5.3. DELAYED COINCIDENCE MEASUREMENTS USING THE MODIFIED CONVERTER

For all the delayed coincidence measurements using the modified time-to-amplitude converter the measurement system of Figure 3.3.(a) was used. D2 was the surface barrier detector and was housed in the vacuum chamber on detector holder (b) (Figure 4.3.(a)). The front face of the detector was positioned in approximately the same plane as the outer face of the source valve assembly. The Ge(Li) detector D1 was positioned with its front face adjacent to the surface barrier detector. The source under study was sandwiched between these two detectors, the source backing plate being towards D1 to prevent absorption of the alpha particles before they reach D2. The spacings between the front faces of the two detectors and the source were then approximately 2 mm and 7 mm respectively for D2 and D1. The vacuum chamber was here used only as a convenient means of holding detector D2. Only one of the five gain stages of the fast amplifier in the stop channel was used whilst three stages in the start channel fast amplifier were employed. The delay in the start channel was provided by two Harwell 2000 series delay units type 2105A (fine delay) and type 2104A (course delay) together with a 29 m length of coaxial cable (approximate delay 95 ns). The total delay thus introduced, relative to any delay in the stop channel, was approximately 175 ns. This delay was used to

shift the delayed coincidence spectra towards lower channel numbers (0-70 approximately) and enabled the higher channels (75-90 approximately) to be used for storing chance coincidences simultaneously with the delayed coincidence spectra. Such chance coincidences arise due to the possibility of those start and stop signals which are randomly distributed in time producing an output from the time-to-amplitude converter. These coincidences were subtracted, channel by channel, from the observed coincidences in the delayed coincidence spectrum in order to obtain the spectrum due to the wanted coincidence events. A measurement was made to investigate the distribution of chance coincidences over most of the range of the time-to-amplitude converter by inserting a large additional delay (about 300 ns) into the start channel which shifted the delayed coincidence spectrum being studied at that time (59.6 keV level of Np-237, see later) to below about channel 20. The counts recorded in the higher channels were then due to the chance overlapping of start and stop signals. The resulting distribution was found to have a definite slope, the chance coincidences increasing with decrease in channel number. The actual increase was 12% over the 100 channels and could not be accounted for by the non-linearity of the time-to-amplitude converter. A repeated measurement but with a much higher true coincidence rate (about 18 times greater) yielded a slope of 33%.

In determining the chance coincidences under the delayed coincidence spectrum this increase was taken into account (Appendix A, program (ii)), the figure of 12% being used where the true coincidence rate in any channel in the delayed coincidence spectrum did not exceed 8 per minute and the figure of 33% used for true rates above 8 per minute but below 140 per minute. The effect of neglecting this correction altogether would have resulted in a change of not more than 0.5% in the final results obtained for the half-lives studied in this work. The method used here for correcting for chance coincidences was considered to be better than first recording the delayed coincidence spectrum and then inserting a large delay into the start channel and recording the chance coincidences as the experimental conditions and the environment (eg. electrical interference) could change during the time period between taking the two spectra, especially when long run times are considered. A disadvantage of the method used was the small number of channels available to accumulate the chance coincidence data.

The apparatus was switched on and allowed to settle down for a period of at least 24 hours before any measurements were made. Before each measurement the bias currents of the tunnel diodes in the two fast discriminators were adjusted to give monostable operation. This was done with the aid of an

oscilloscope connected to the output of the associated pulse stretcher. The bias levels were set as low as possible consistent with no spurious triggering on noise pulses. To set the single channel analysers to select the energies of interest the following method was used. The outputs from the single channel analysers to the two inputs on the slow coincidence unit were removed and the two inputs on the coincidence unit connected together and to the output of the single channel analyser under adjustment. The signal feeding this analyser was also routed to the biased amplifier and stretcher input, the previous connection to that input being removed. With the gate input to the multi-channel analyser removed and the gate switch on anti-coincidence the energy spectrum was displayed and the biased amplifier used to expand the region of the spectrum to be selected. The gate switch was then set to coincidence and the gate input reconnected. The single channel analyser controls were then adjusted so that the displayed spectrum showed only those energies which were to be selected. Finally the single channel analyser controls were locked in position and the system reconnected as in Figure 3.3.(a).

To extract the half-life of the excited state under measurement from the delayed coincidence spectrum obtained, a least squares fit was made to the pairs of data points (coincidences, channel number) on the positive slope side of the spectra. To determine

the range of data points to be used, a graph was first plotted of $\log_{10}$(coincidences) against channel number for each delayed coincidence spectrum, from which the linear region on the positive slope side was found (scatter in the data points set the limit on the lowest channel to be included). All the data points falling in the linear region of the spectrum, as seen from the graph, were then used, the only exceptions being the data in those channels which occasionally malfunctioned above a certain stored count. This spurious data was easily recognisable as it exhibited itself either as zero stored counts or as a much larger number of counts than would be expected. Channel 54 was the chief offender. The least squares fit calculations were carried out on a computer (Appendix A, program (ii)).

5.3.1. Delayed Coincidence Measurements on the 59.6 keV level in Np-237

From the simplified decay scheme for Am-241 shown in Figure 5.3.1.(a) (Nuclear Data Sheets B, Volume 6, Number 6, 1971) it can be seen that the 59.6 keV excited state of Np-237 is fed mainly by the 5.486 MeV (86%) alpha branch from the decay of Am-241. The state de-excites by E1 transitions of 59.6 keV and 26.4 keV, both being appreciably internally converted.

The Am-241 source used was obtained from the Radio Chemical Centre, Amersham and was code number AMR14. The source consisted of a thin layer of Am-241 deposited by vacuum sublimation on to a lightly oxidized stainless steel disc of thickness 0.5 mm. The diameter of the active area was 7 mm and the quoted activity 3×10^6 disintegrations per minute. Figures 5.3.1.(b) and 5.3.1.(c) respectively show the energy spectra of gamma rays and alpha particles emitted from this source. The former spectrum was analysed using the 1000 channel multi-channel analyser (Link Systems) in order to obtain sufficient energy resolution over a wide energy range whilst in the latter the biased amplifier was used (X20 expansion) in conjunction with the 100 channel analyser to expand the region of the alpha particle spectrum around 5.5 MeV. It should be noted that this alpha energy spectrum was obtained with a source-detector separation of about 4 cm and with the space between source and detector under vacuum. In the

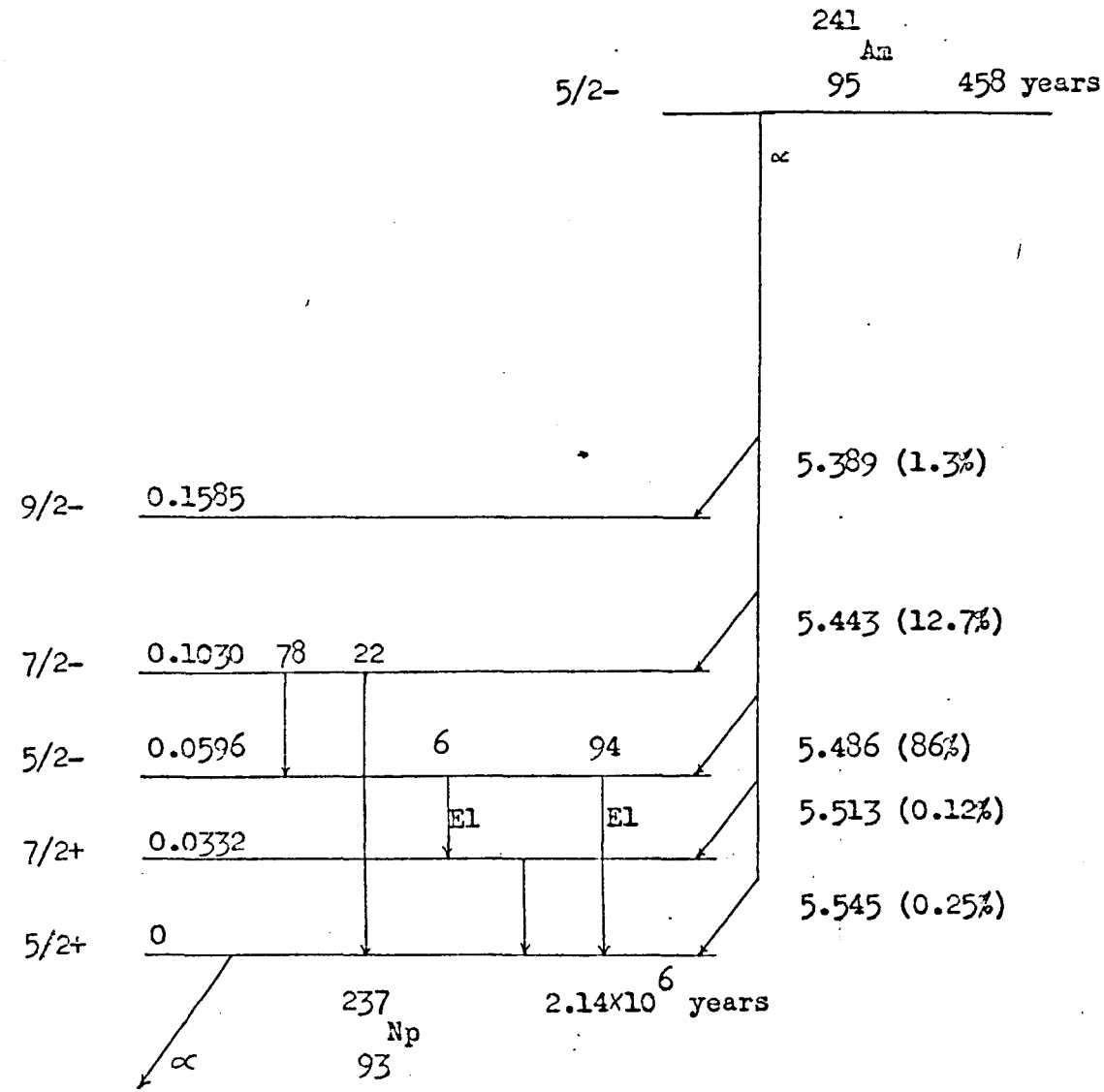

Figure 5.3.1.(e) Simplified decay scheme for Am-241.

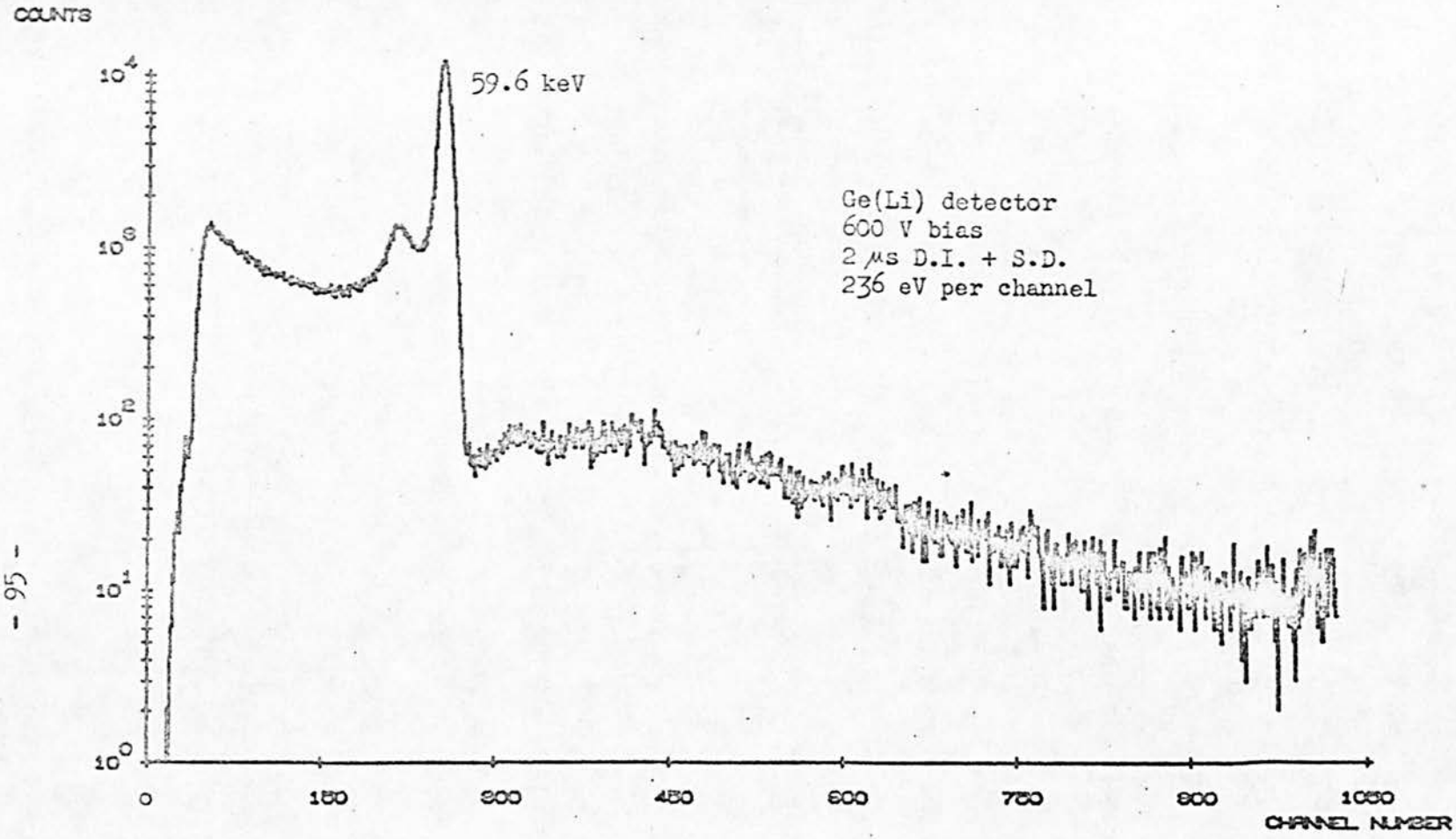

Figure 5.3.1.(b) Part of the gamma ray energy spectrum of Am-241.

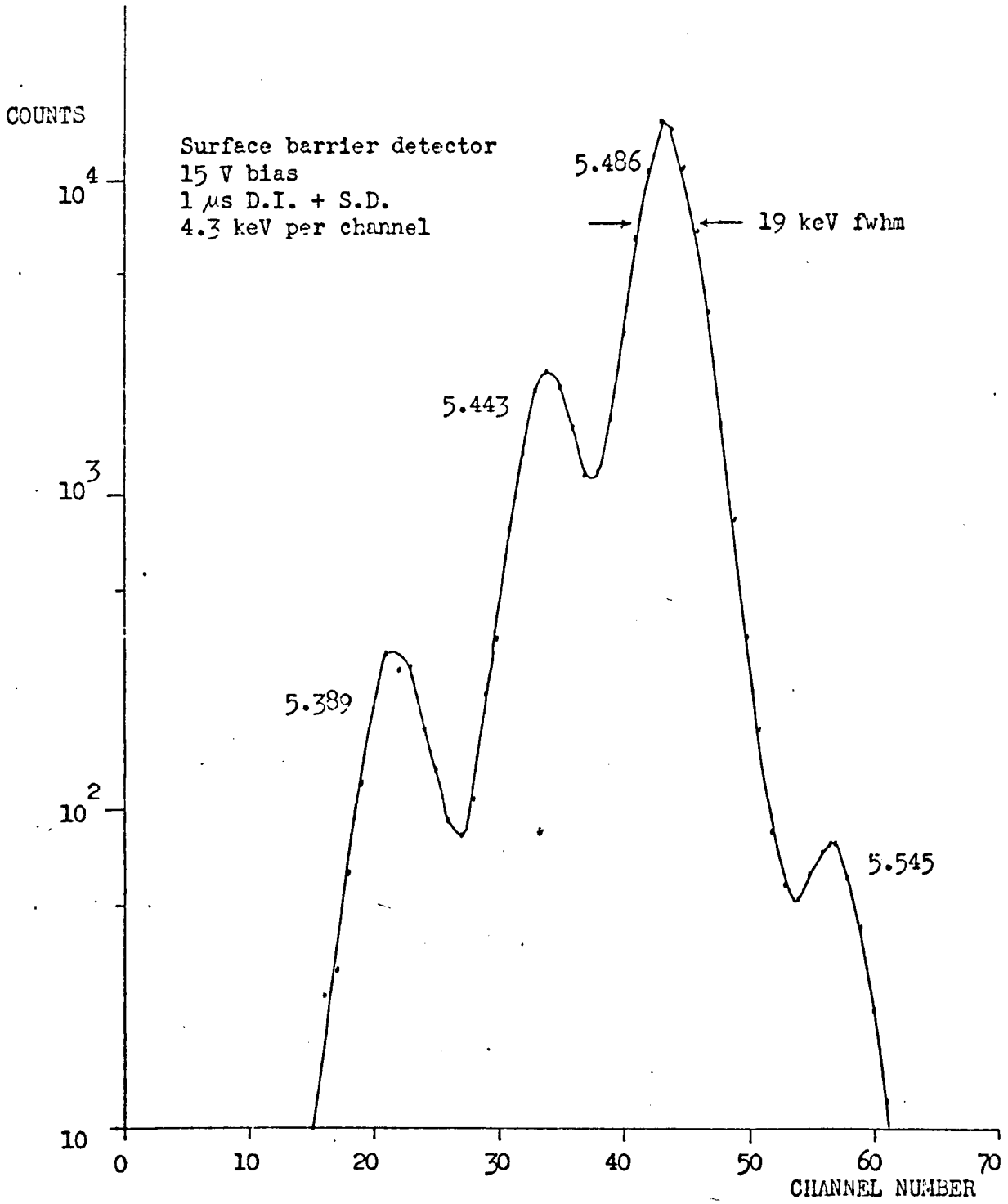

Figure 5.3.1.(c) Part of the alpha particle energy spectrum of Am-241.

following delayed coincidence measurements the source-detector separation was only 2 mm and the system was not evacuated. Consequently the energy resolution was seriously degraded compared with that shown in Figure 5.3.1.(c), the actual figure being about 120 keV fwhm.

For the delayed coincidence measurements on the 59.6 keV level the single channel analyser in the gamma channel was set to accept gammas in the energy range 55 keV to 63 keV whilst the analyser in the alpha channel accepted alphas with energies above 5 MeV. These figures were obtained by feeding the output of the pulser (NE 6591), calibrated in terms of energy, into the test inputs on the preamplifiers when setting up the single channel analysers.

Table 5.3.(a) gives a summary of the results obtained from four measurement runs and Figure 5.3.1.(d) shows an example of one of the delayed coincidence spectra (15.8.72 (5)). The figures for $T_{\frac{1}{2}}$ in terms of channels were determined using a chance slope of 33%. The error in $T_{\frac{1}{2}}$ was found from the error in the associated chance coincidences per channel together with the error in the chance slope (taken to be ± 50%). The calibration frequency figures have an error of 0.001%. The mean of the four figures for $T_{\frac{1}{2}}$ in ns was (68.5 ± 0.4) ns.

In order to establish the overall system time resolution at

Measurement code	Run time (hours)	Chance coincidences $(\text{channel})^{-1}$	$T_{\frac{1}{2}}$ (channels)	Calibration frequencies (MHz)	Calibration (ns ch^{-1})	$T_{\frac{1}{2}}$ (ns)
15.8.72 (1)	1.5	15 ± 2	11.512 ± 0.03	14, 14.5, 15	6.040 ± 0.03	69.53 ± 0.4
15.8.72 (5)	2.8	59 ± 2	11.463 ± 0.04	14, 15, 20	5.942 ± 0.05	68.11 ± 0.7
15.8.72 (6)	1.7	29 ± 2	11.431 ± 0.03	14, 15, 20	5.892 ± 0.03	67.35 ± 0.4
16.8.72 (1)	1.8	18 ± 1	11.779 ± 0.03	14, 15, 20	5.852 ± 0.03	68.93 ± 0.4

Ge(Li) bias 600 V

Surface barrier bias 25 V

Table 5.3.(a) Summary of results obtained when analysing the 59.6 keV excited state of Np-237.

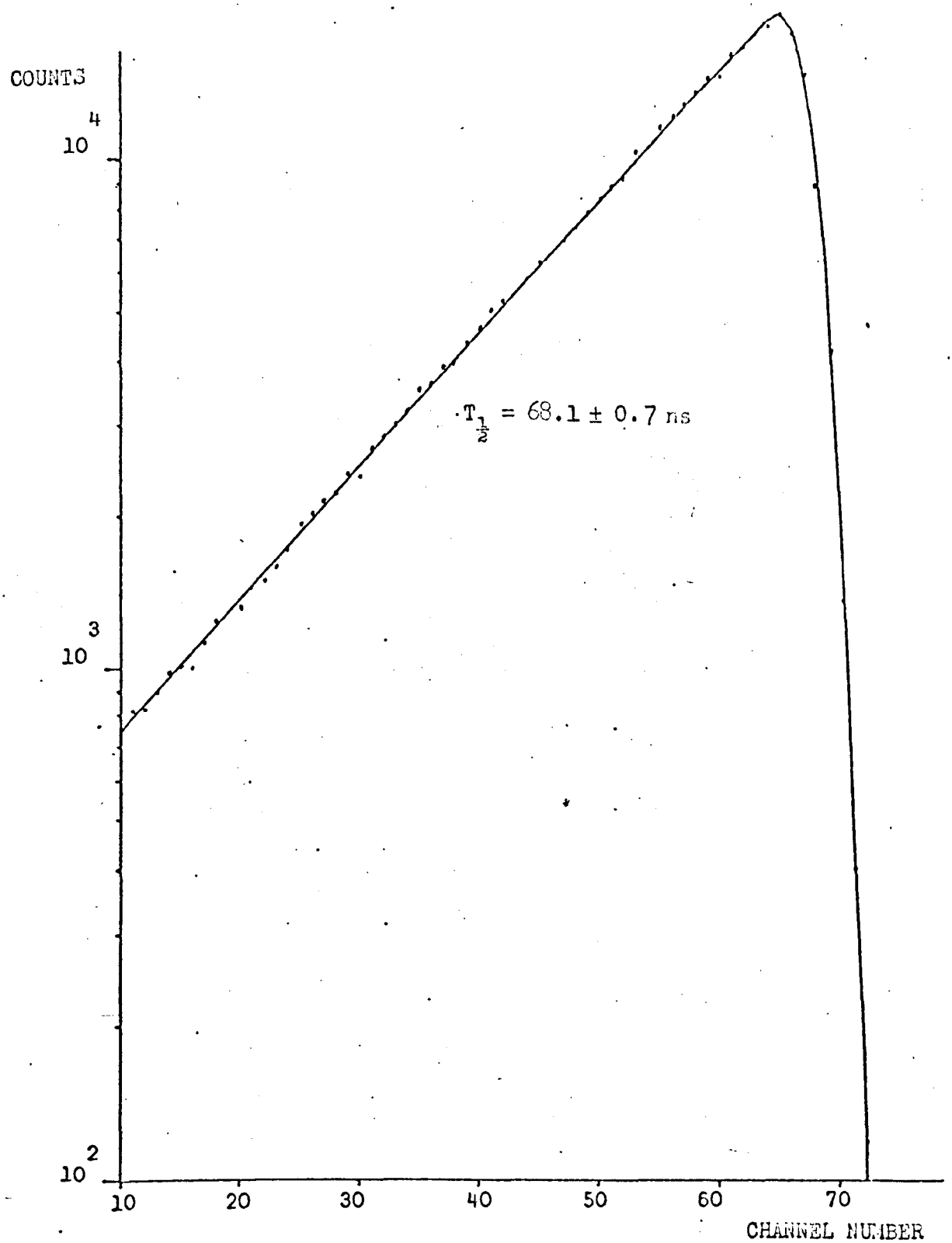

Figure 5.3.1.(d) Delayed coincidence spectrum showing the half-life of the 59.6 keV excited state in Np-237.

energies similar to those selected in the above determination, a prompt spectrum was obtained using a Th-228 source (R.C.C.). Figure 5.3.1.(e) shows the decay scheme of Th-228 (Nuclear Data Sheets B, Volume 1, Number 5, 1971). Coincidences were recorded between the 5.341 MeV alpha particles from Th-228 and the 84.5 keV gamma rays emitted on de-excitation of the 84.5 keV excited state of Ra-224. The half-life of this level has been measured to be 0.75 ns. The source used for this measurement was very inactive (about 10 nCi) and this coupled with the fact that the 84.5 keV transition is highly internally converted ($\alpha = 17$) led to the use of the long measurement period of 67 hours. Inspection of Figure 5.3.1.(f), the gamma ray energy spectrum from the source, shows that no line at 84.5 keV is resolved. The single channel analyser in the gamma channel was therefore set to accept gammas from the region of the spectrum where the 84.5 keV line would be expected. The analyser in the alpha channel accepted all alphas above an energy of 1 MeV. The resulting prompt spectrum is shown in Figure 5.3.1.(g). The time resolution (fwhm) was 8 ns and the apparent system half-life, found from the positive slope side of the spectrum, was 3 ns. For this measurement the biased amplifier was set to X5 expansion and the calibration was 1.24 ns per channel. This measurement also gave some idea of the long term time stability of the system.

The same source (Th-228) was also used to obtain coincidences

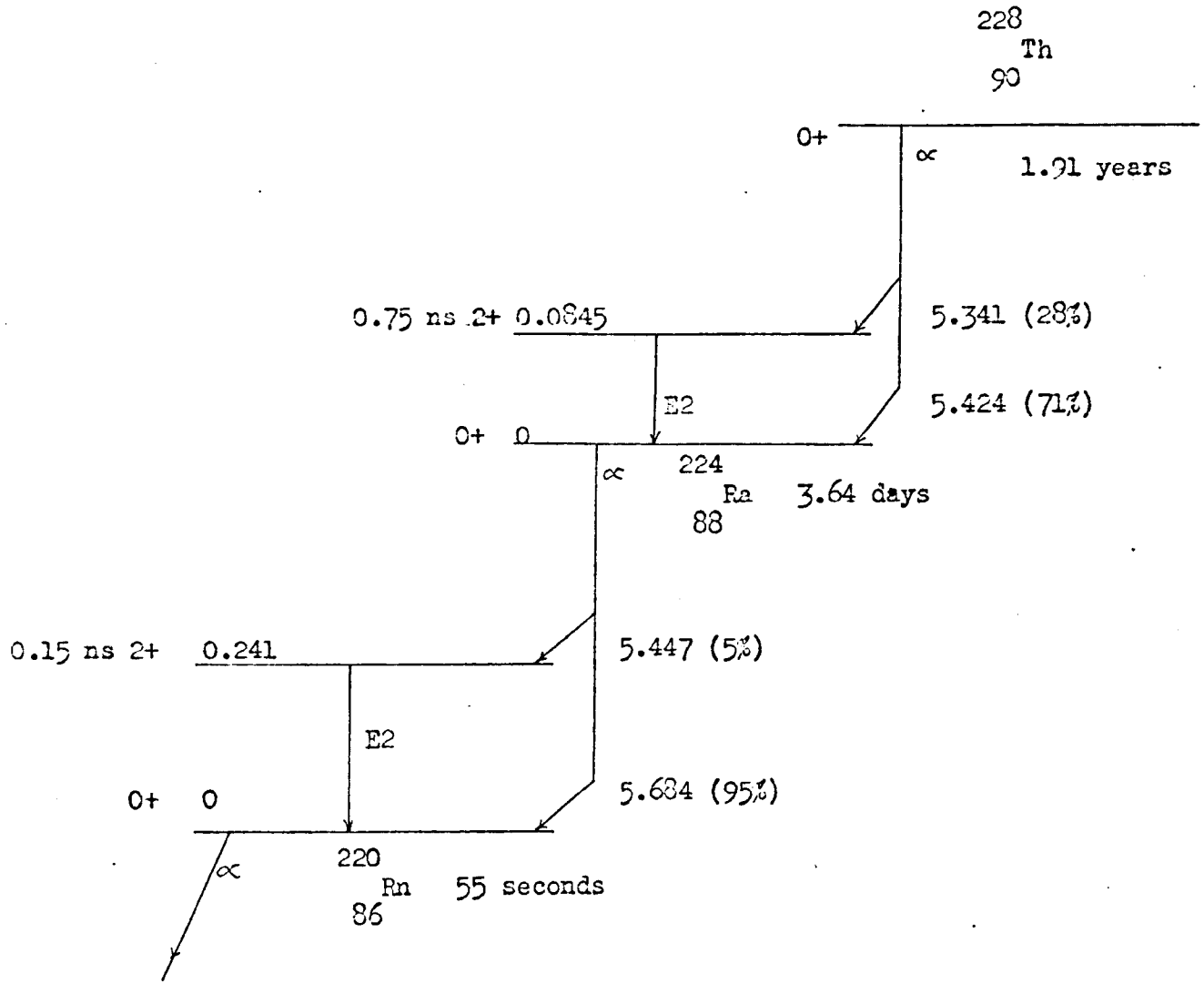

Figure 5.3.1.(e) Simplified decay scheme for Th-228.

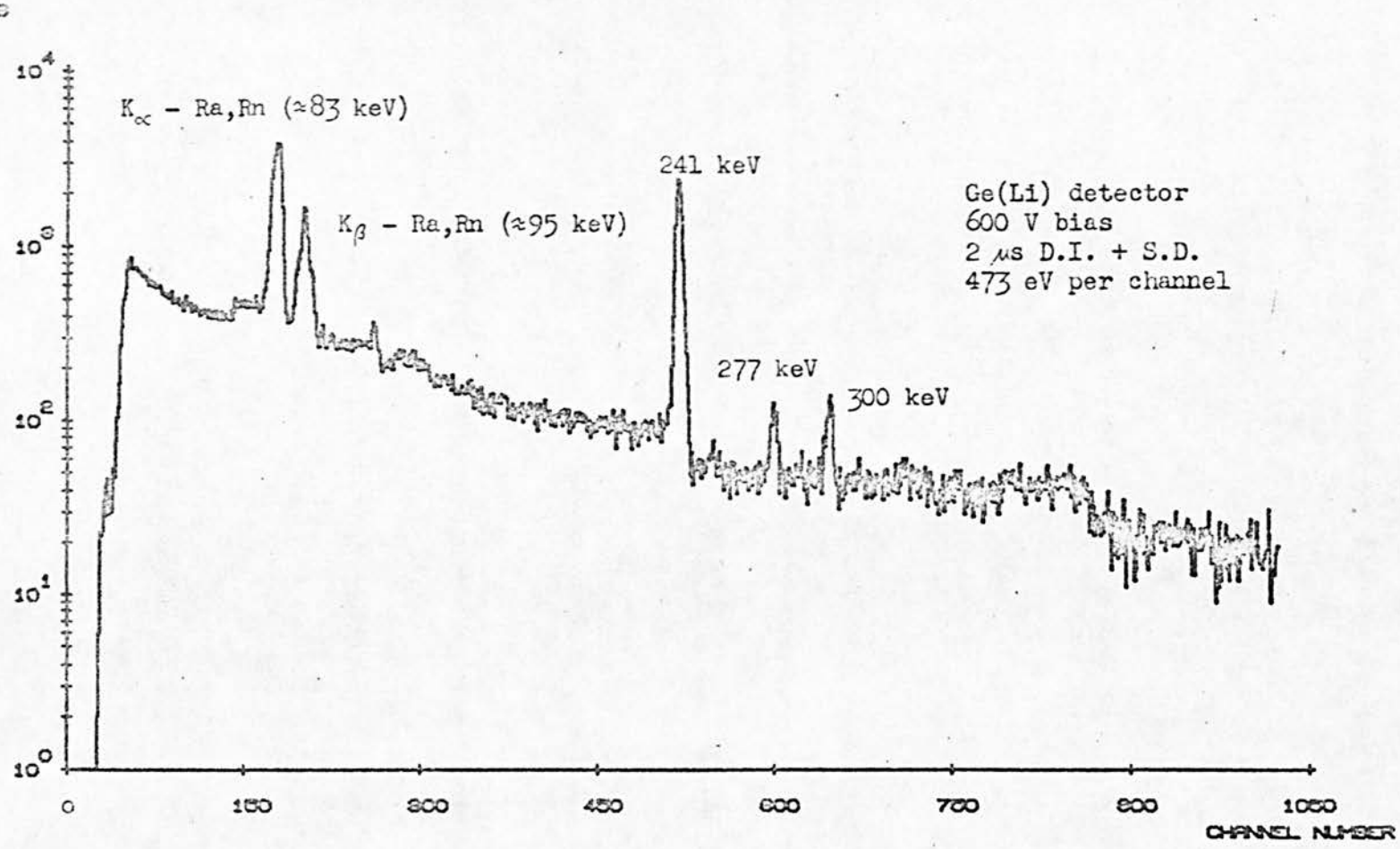

Figure 5.3.1.(f) Part of the X and gamma ray energy spectrum of Th-228.

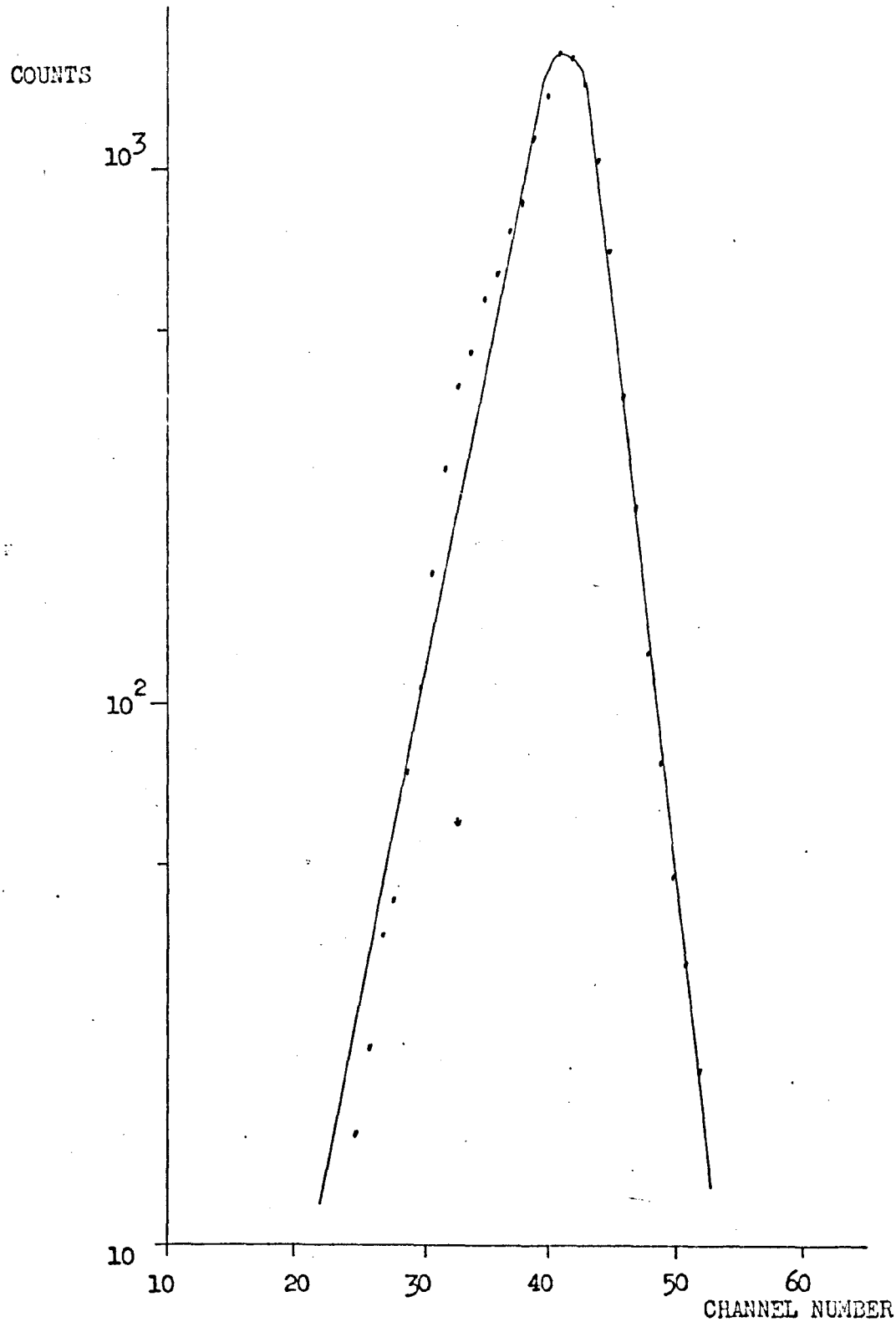

Figure 5.3.1.(g) Prompt coincidence spectrum obtained when analysing the 84.5 keV excited state of Ra-224.

between the 5.447 MeV alpha particles from Ra-224 and the 241 keV gamma rays emitted on de-excitation of the 241 keV level in Rn-220 (Figure 5.3.1.(e)). The prompt spectrum obtained at these energies is shown in Figure 5.3.1.(h). The time resolution (fwhm) was 4 ns and the apparent half-life, obtained from the linear region on the positive slope side of the spectrum, was 1.6 ns. The measurement period was 21 hours.

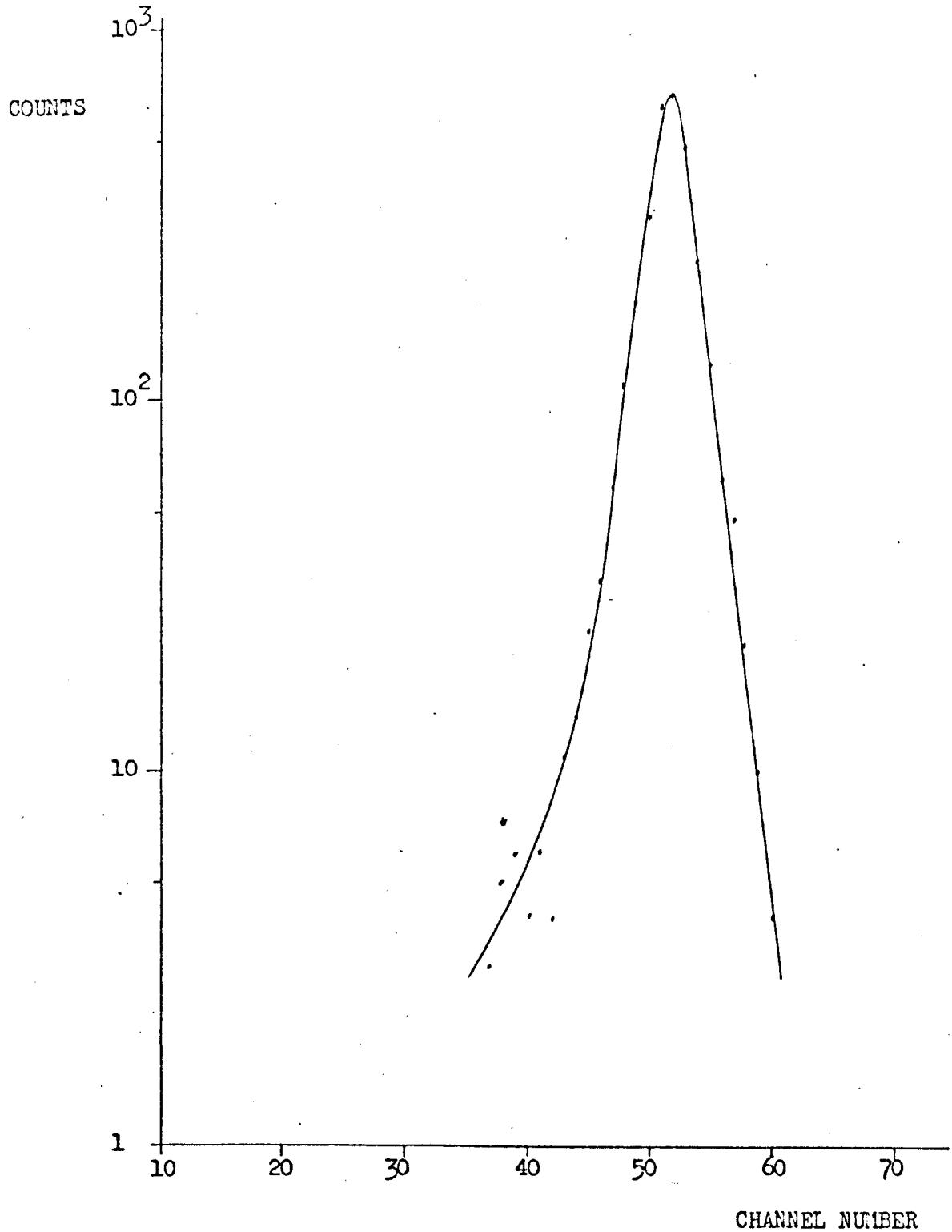

Figure 5.3.1.(h) Prompt coincidence spectrum obtained when analysing the 241 keV excited state of Rn-220.

5.3.2. Delayed Coincidence Measurements on the 86.5 keV level in Pa-233

From the simplified decay scheme for Np-237 shown in Figure 5.3.2.(a) (Nuclear Data Sheets B, Volume 6, Number 3, 1971) it can be seen that the 86.5 keV excited state of Pa-233 is fed partly by the 4.787 MeV (47%) alpha branch from the decay of Np-237 and partly by gamma decay from higher energy levels in Pa-233. The state de-excites by E1 transitions of 86.5 keV and 29.6 keV, both being appreciably internally converted.

The Np-237 source used was prepared from a solution in 3N HNO_3 (R.C.C. code NGS 2). The solution was evaporated and burned in on a 1 mm thick stainless steel backing. The diameter of the active area was 7 mm and the source activity was approximately 1 μCi. Due to the appreciable thickness of the deposited layer the alpha energy spectrum showed strong tailing towards lower energies. The energy spectrum of gamma rays emitted from the source is shown in Figure 5.3.2.(b). The four lines above channel number 750 result from transitions in U-233, the daughter product of Pa-233.

A summary of the results obtained from four measurement runs on the 86.5 keV excited state of Pa-233 is shown in Table 5.3.(b). For measurement 22.11.72 (1) no energy restrictions were imposed other than those set by the two fast discriminators (the alpha

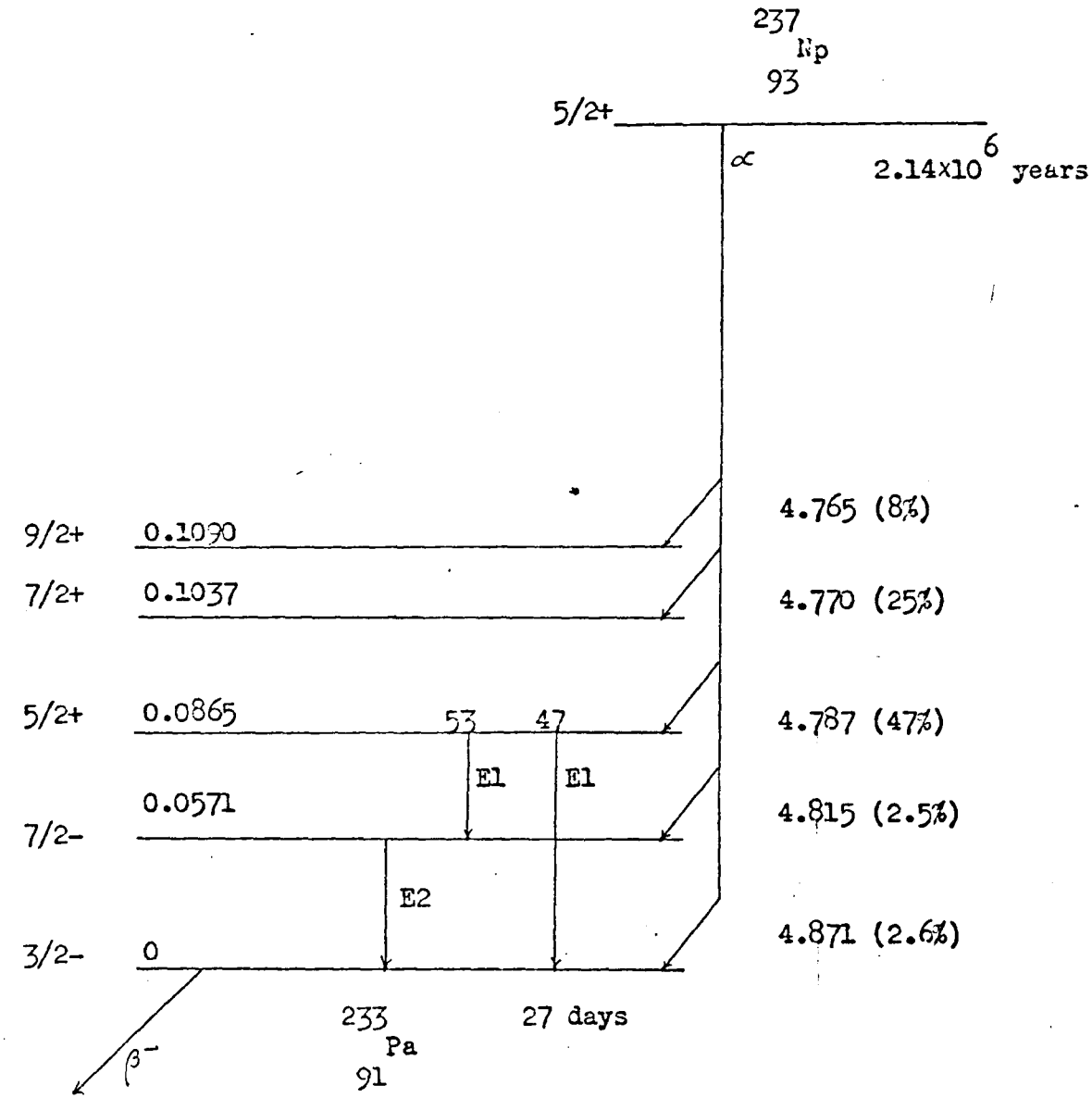

Figure 5.3.2.(a) Simplified decay scheme for Np-237.

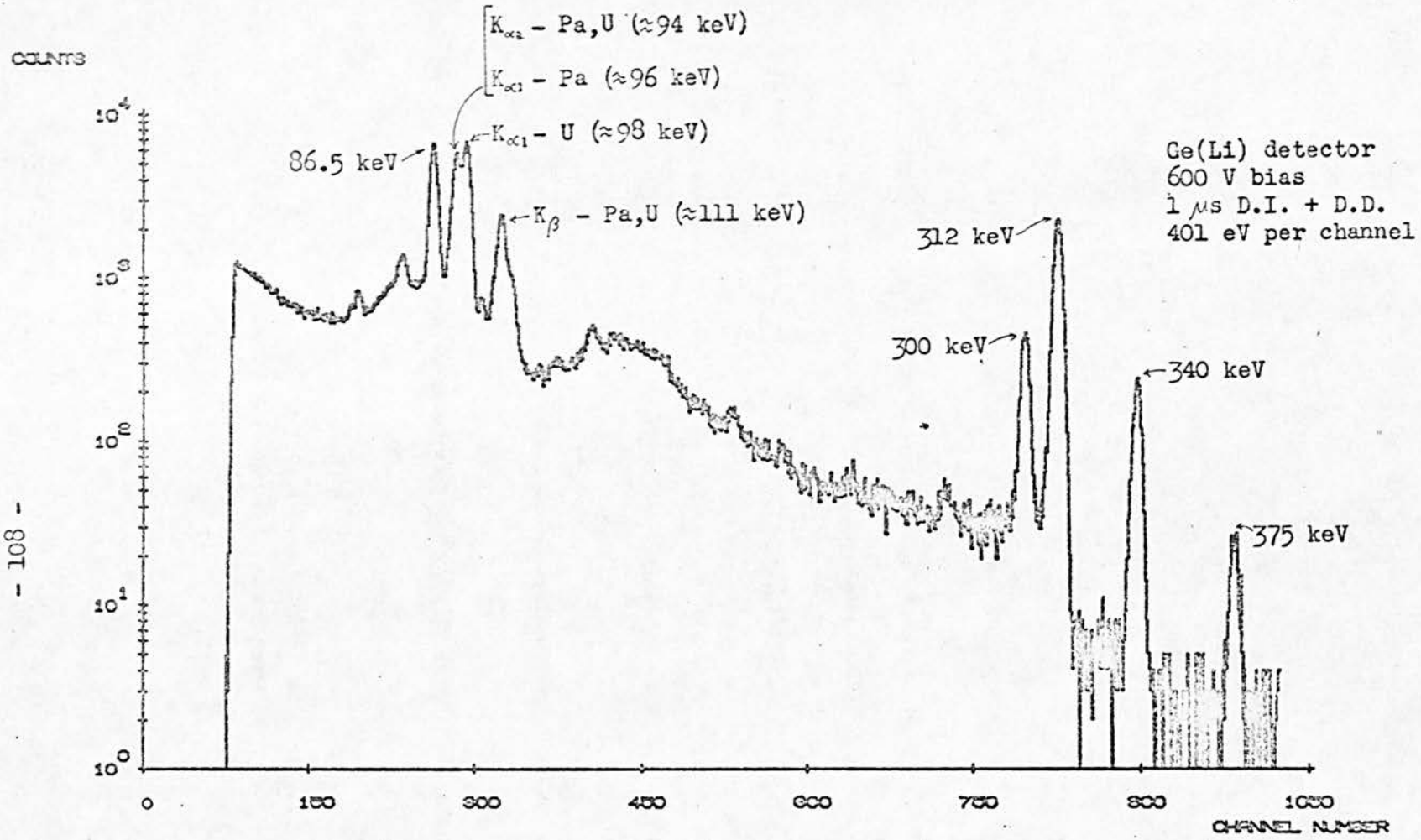

Figure 5.3.2.(b) Part of the X and gamma ray spectrum of Np-237.

Measurement code	Run time (hours)	Chance coincidences $(\text{channel})^{-1}$	$T_{\frac{1}{2}}$ (channels)	Calibration frequencies (MHz)	Calibration (ns ch^{-1})	$T_{\frac{1}{2}}$ (ns)
22.11.72 (1)	12.5	15 ± 3	6.076 ± 0.07	15, 16, 17	6.213 ± 0.03	37.75 ± 0.5
23.11.72 (1)	15.5	2 ± 2	5.997 ± 0.04	15.75, 17, 18	6.275 ± 0.03	37.63 ± 0.3
24.11.72 (1)	11.0	7 ± 3	6.009 ± 0.06	15.75, 17, 18	6.273 ± 0·03	37.69 ± 0.4
29.11.72 (1)	7.0	0.5 ± 0.5	6.053 ± 0.02	17, 18, 19	6.257 ± 0.05	37.87 ± 0.3

Ge(Li) bias 600 V

Surface barrier bias 15 V

Table 5.3.(b) Summary of results obtained when analysing the 86.5 keV excited state of Pa-233.

channel accepted energies above about 100 keV and the gamma channel energies above about 20 keV). The delayed coincidence spectrum obtained from this measurement is shown in Figure 5.3.2.(c) and exhibits prompt and delayed parts. For measurements 23.11.72 (1) and 24.11.72 (1) the single channel analyser in the gamma channel was set on the 86.5 keV gamma line only. Figure 5.3.2.(d) shows the delayed coincidence spectrum resulting from measurement 23.11.72 (1) and as can be seen the prompt part of Figure 5.3.2.(c) is virtually absent. Measurement 29.11.72 (1) was similar to the previous two measurements except that an additional restriction on the alpha particle energies selected was introduced. The single channel analyser in the alpha channel was set to accept alpha particles with energies lying between approximately 3.4 MeV and 5 MeV. The figures for $T_{\frac{1}{2}}$ in terms of channels in Table 5.3.(b) were determined using a chance slope of 12%. Other comments similar to those relating to Table 5.3.(a) can be made. The mean of the four figures for $T_{\frac{1}{2}}$ in ns was (37.7 ± 0.2) ns.

To investigate the origin of the prompt part of the delayed coincidence spectrum shown in Figure 5.3.2.(c) measurements were made with the single channel analyser in the gamma channel set to accept energies corresponding to the K_α X-rays from Pa (90 keV - 102 keV). An example of one of the spectra obtained is shown in Figure 5.3.2.(e). For this measurement the biased amplifier was set for X5 expansion giving a time calibration of

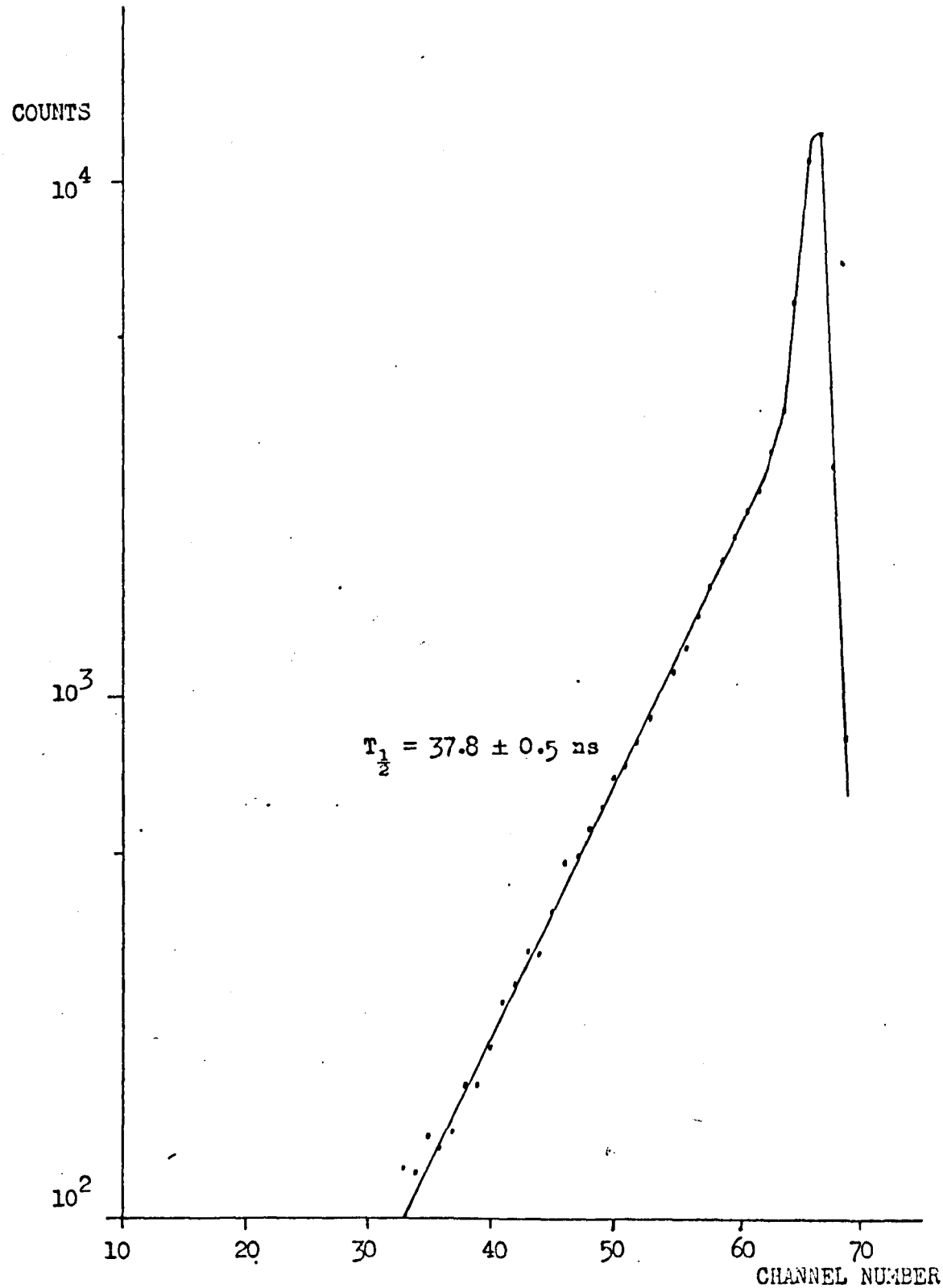

Figure 5.3.2.(c) Delayed coincidence spectrum obtained with no energy restrictions (Np-237 source).

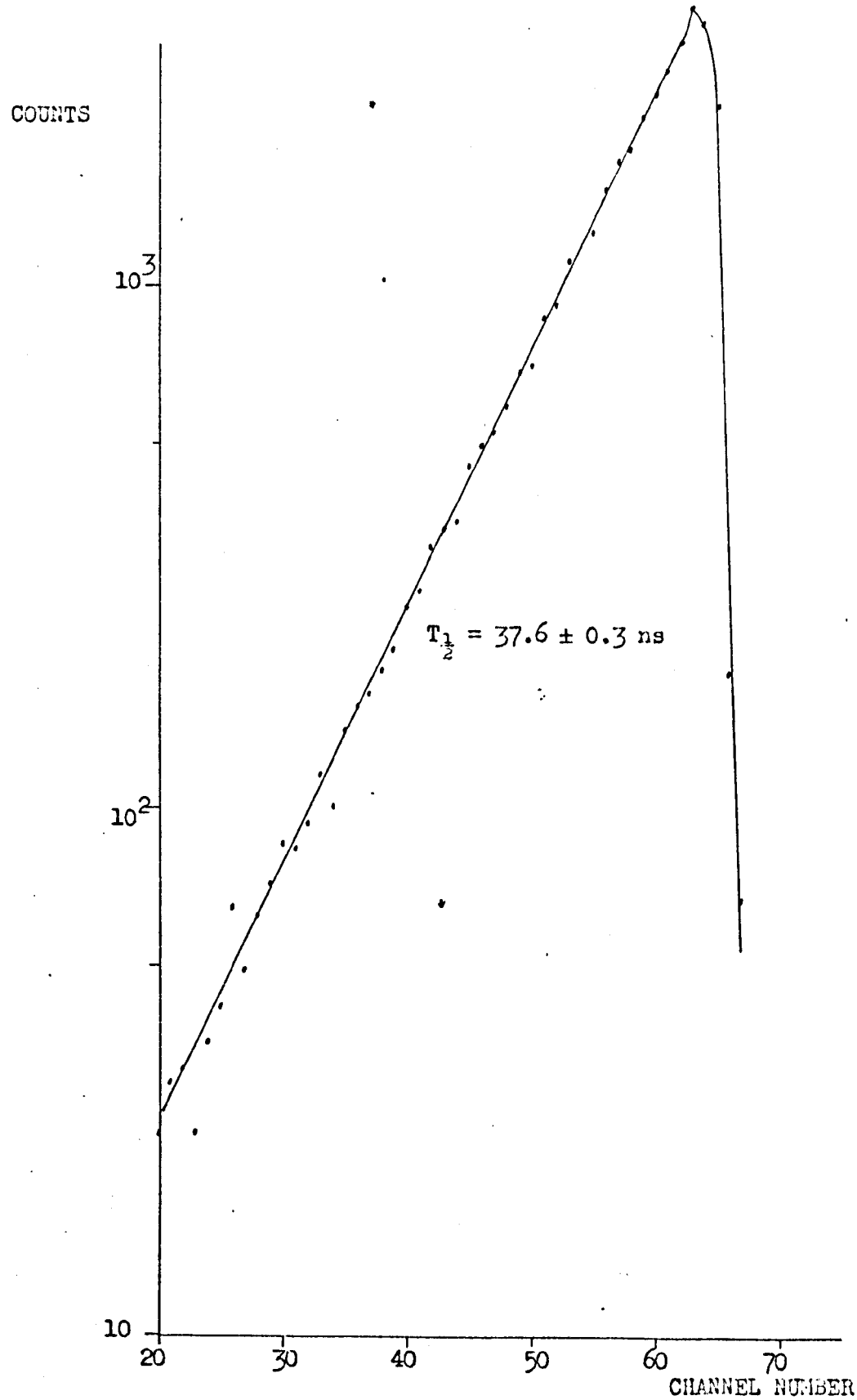

Figure 5.3.2.(d) Delayed coincidence spectrum showing the half-life of the 86.5 keV excited state in Pa-233.

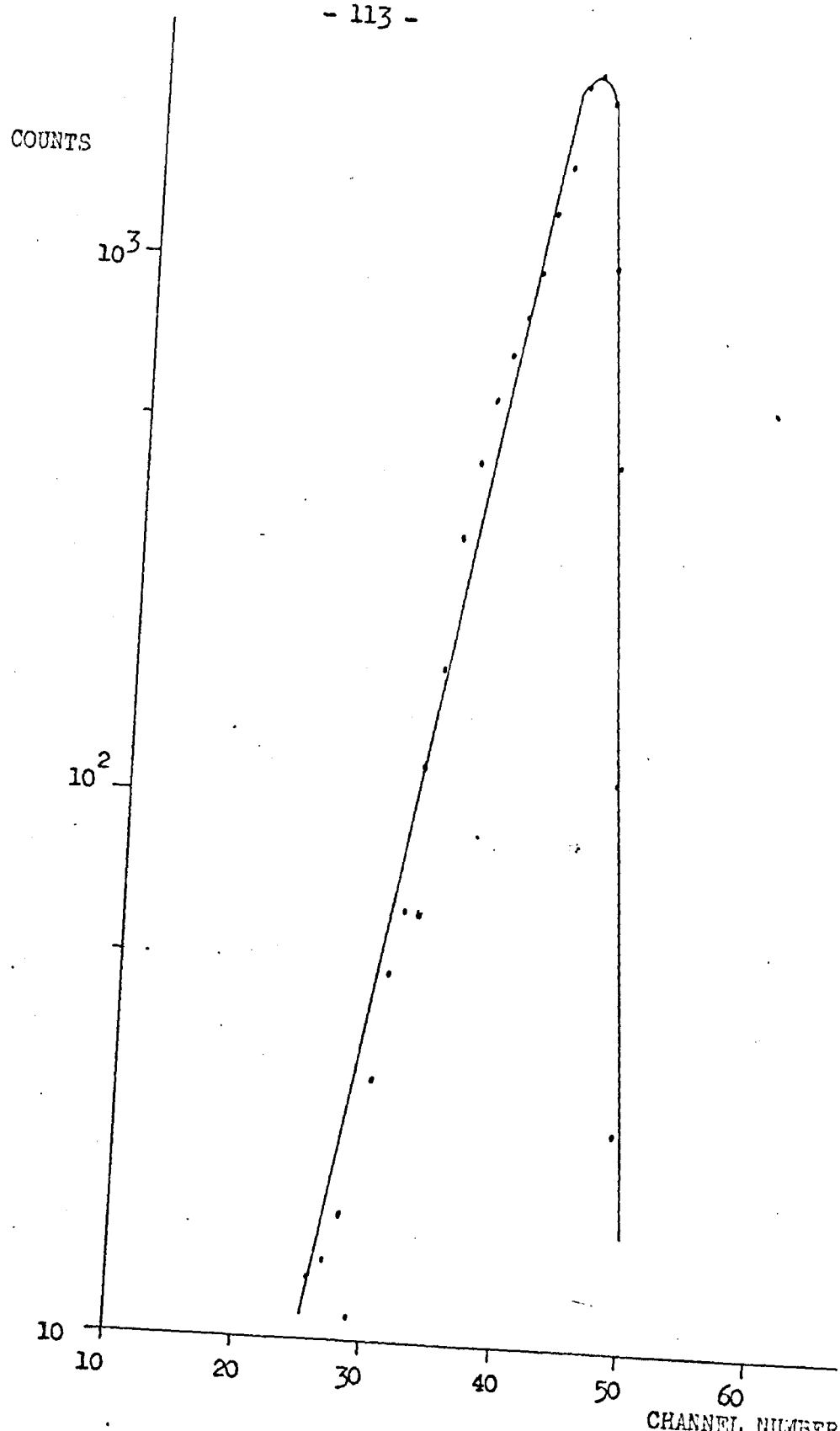

Figure 5.3.2.(e) Coincidence time spectrum of the Pa K_α X-rays measured in coincidence with 3.4-5 MeV alpha particles.

1.24 ns per channel. This spectrum had a fwhm of 6.2 ns and the positive slope side gave an apparent half-life of 3.1 ns. The corresponding figure for the negative slope side was 0.8 ns. These figures were sufficiently close to those obtained when analysing the 84.5 keV excited state of Ra-224 (Section 5.3.1.) to suggest that the shape of the prompt part of the spectrum was here determined by the measurement system. These figures were thus taken to give the time resolution of the system at these energies.

5.3.3. Variation of Prompt Spectrum Shape with Ge(Li) Detector Bias and Discriminator Threshold

Using the Np-237 source and the same apparatus settings as used in the measurement described in the last paragraph of Section 5.3.2., the shape of the prompt spectrum was investigated a) as a function of Ge(Li) detector bias and b) as a function of the gamma channel fast discriminator threshold level, the spectra obtained being presented in Figures 5.3.3.(a) and 5.3.3.(b) respectively. Table 5.3.(c) summarises some of the information obtained from these spectra. In order to quote the discriminator threshold level in terms of equivalent energy deposited in the detector, use was made of a pulser (NE 6591) calibrated in energy. In the table fwl/10m and fwl/100m are the full width of the spectrum at 1/10 and 1/100 of the maximum height respectively, whilst $T_{\frac{1}{2}}(p)$ and $T_{\frac{1}{2}}(n)$ respectively refer to the apparent half-life found from the positive and negative slope sides of the spectra (the regions where the slopes were approximately linear were used). The calibration was 1.24 ns per channel. The pulses delivered to the fast discriminators had approximate risetimes of 10 ns and 30 ns for the alpha and gamma channels respectively. The signal to noise ratio (signal referred to the K X ray lines, noise peak-to-peak as seen on a 100 MHz bandwidth oscilloscope) was about 6:1 in the gamma channel. The figure for the alpha channel was about 100:1.

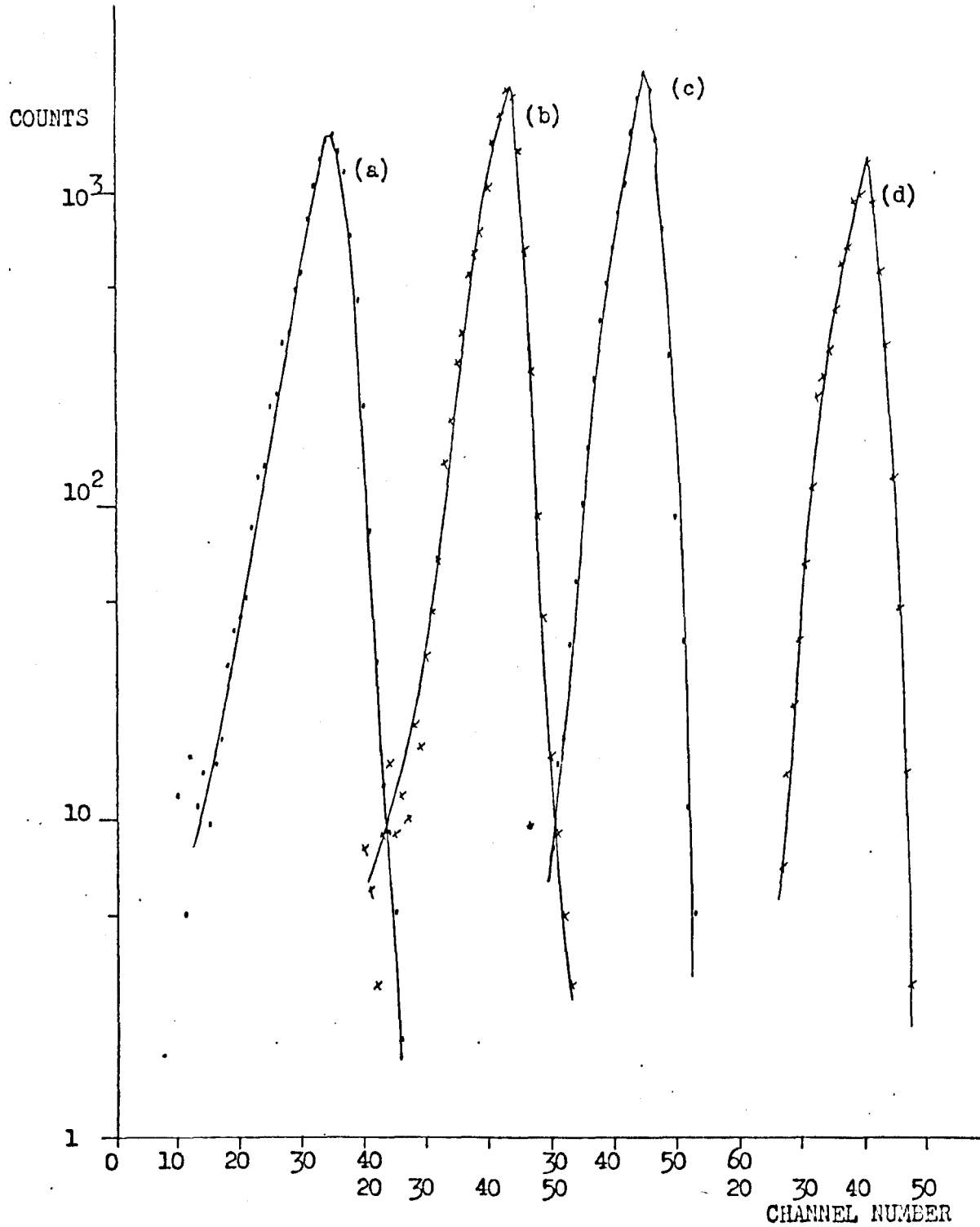

Figure 5.3.3.(a) Variation of prompt spectrum shape with Ge(Li) bias.

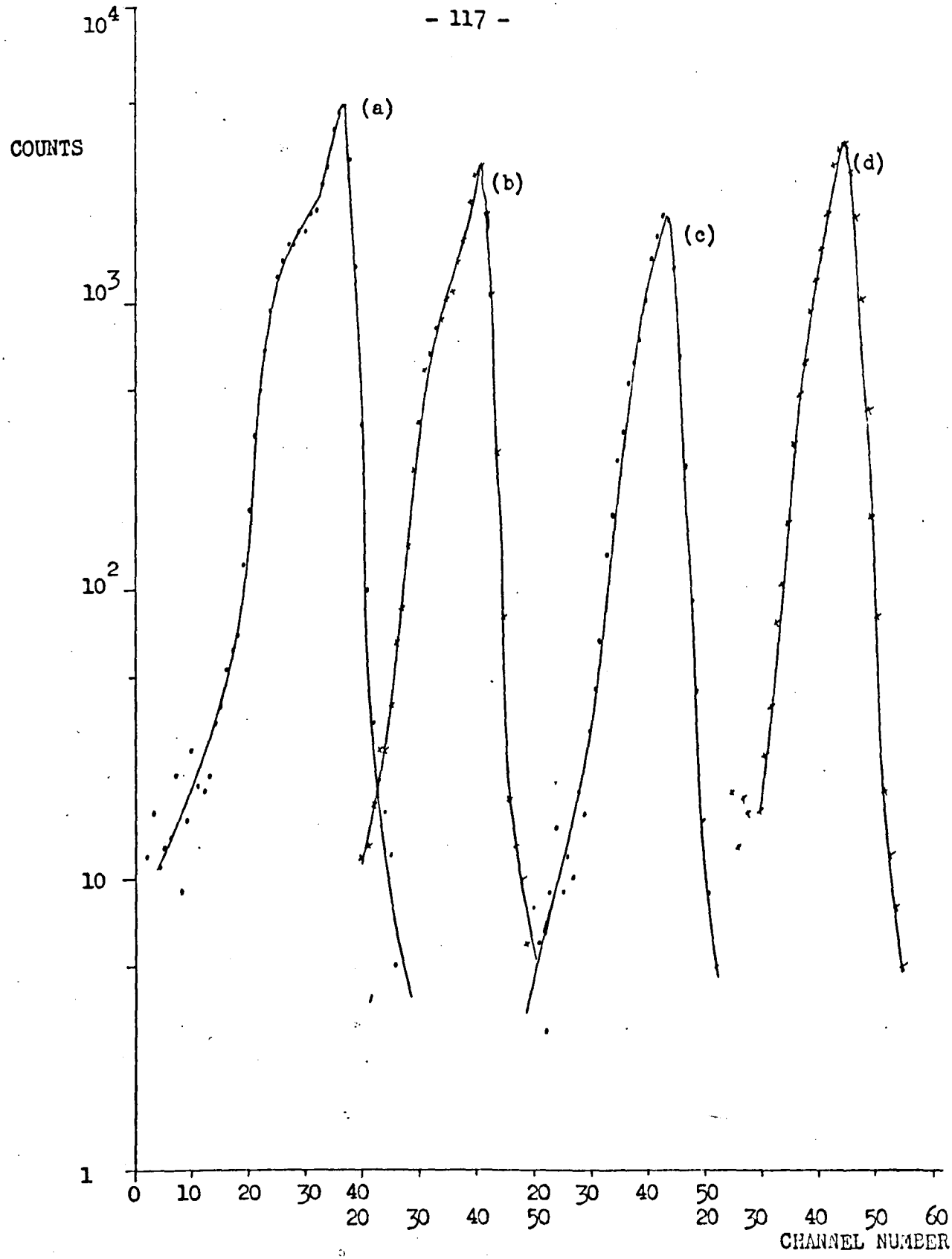

Figure 5.3.3.(b) Variation of prompt spectrum shape with discriminator threshold level.

Measurement	Run time (hours)	Discriminator threshold (keV)	Detector bias (V)	fwhm (ns)	fwl/10m (ns)	fwl/100m (ns)	$T_{\frac{1}{2}}(p)$ (ns)	$T_{\frac{1}{2}}(n)$ (ns)
Figure 5.3.3.(a)								
(a)	16	20	200	7.4	19	33	3.3	1.0
(b)	16	20	500	6.2	15	26	2.1	1.0
(c)	17	20	800	6.2	15	23	2.1	0.8
(d)	11.5	20	1000	6.8	16	23	1.6	1.0
Figure 5.3.3.(b)								
(a)	48	40	600	6.2	22	31	-	1.0
(b)	24	30	600	6.2	19	26	2.1	0.8
(c)	16	20	500	6.2	15	26	2.1	1.0
(d)	23	15	600	6.2	15	24	2.1	1.0

Table 5.3.(c) Summary of information from Figures 5.3.3.(a) and 5.3.3.(b).

5.3.4. Time Stability of the System

In order to measure the time stability of the system the outputs from the two fast amplifiers were uncoupled from the inputs to the start and stop channels and a common pulser (NE 6591) used to feed these channels. This pulser was triggered from a second pulse generator operating at a repetition rate of approximately 1.5 pulses per second. A run time of 13 hours was used and gave a time spectrum with a fwhm of 1.4 ns. The biased amplifier was set for X10 expansion and the amplitude of the pulses at the discriminator inputs was approximately twice the discriminator threshold level.

5.4. DELAYED COINCIDENCE MEASUREMENTS USING THE UNMODIFIED CONVERTER

For the delayed coincidence measurements using the unmodified time-to-amplitude converter both the measurement systems shown in Figures 3.3.(a) and 3.3.(b) were used. D1 and D2 were 0.5 mm and 1.0 mm sensitive depth Si(Li) detectors respectively. These two detectors were mounted in the vacuum chamber on detector holder (a) (Figure 4.3.(a)) and throughout all the measurements were cooled to liquid nitrogen temperature. The source under study was sandwiched between the two detectors, the source-detector separation being about 3 mm. The chamber was evacuated to pressures below 10^{-3} mm Hg. With the measurement system of Figure 3.3.(a) only one of the five gain stages of each of the fast amplifiers was used, whilst with the system of Figure 3.3.(b) all five stages were employed. The delay in the start channel was provided by two Harwell 2000 series delay units type 2046A and enabled the delayed coincidence spectra to be shifted towards the middle of the time scale of the time-to-amplitude converter. The setting up of the apparatus prior to each measurement run was similar to that described in Section 5.3. . A bias voltage of 150 V was used for both detectors.

5.4.1. Delayed Coincidence Measurements on the 279 keV level in Tl-203

The decay scheme for Hg-203 is shown in Figure 5.4.1.(a) (Nuclear Data Sheets B, Volume 5, Number 5, 1971). The 279 keV excited state in Tl-203 is fed by the 212 keV (≈100%) beta branch from the decay of Hg-203. The state de-excites by a transition of energy 279 keV, the K shell conversion coefficient for this transition being 0.16. The half-life of the 279 keV level has been measured to be 0.278 ns.

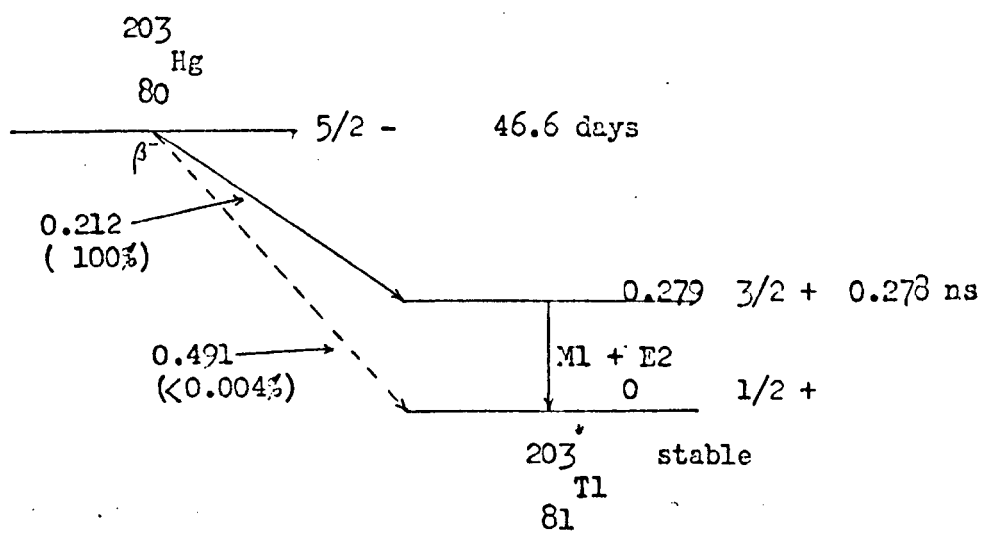

Figure 5.4.1.(a) Decay scheme for Hg-203.

The Hg-203 source used for the delayed coincidence measurements was prepared from mercuric acetate in aqueous solution (R.C.C. code MBS 2). The source, an evaporated deposit on an aluminium foil backing, had an activity of the order of 40 μCi. Figure 5.4.1.(b) shows part of the energy spectrum of beta particles

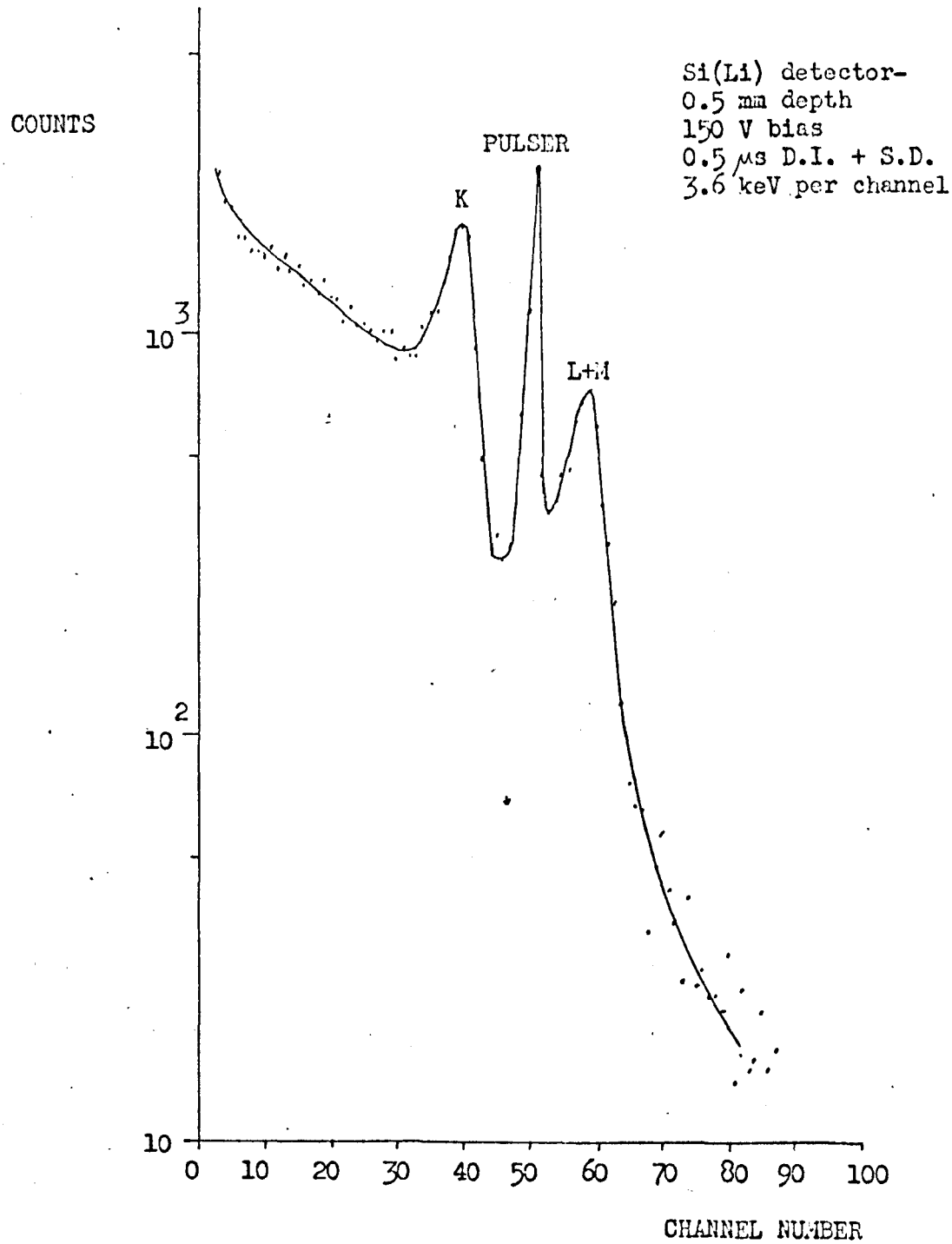

Figure 5.4.1.(b) Part of the energy spectrum of beta particles and conversion electrons emitted from the Hg-203 source.

and conversion electrons emitted from this source. Due to the high activity of the source considerable pulse pile-up in the shaping amplifiers resulted and this together with the fact that the source had an appreciable thickness accounts for the very poor energy resolution exhibited by this spectrum. Another Hg-203 source specially prepared with regard to obtaining high energy resolution gave a resolution (fwhm) of 3 keV at 264 keV.

For the delayed coincidence measurements on the 279 keV level in Tl-203 using the measurement system of Figure 3.3.(a) the single channel analyser in the start channel was set on the K conversion line at 194 keV (ΔE = 22 keV) whilst the analyser in the stop channel viewed the continuous beta spectrum and accepted pulses corresponding to the energy range 155 keV - 165 keV. The discriminator threshold levels were set as close to the baseline as the noise would allow, this level corresponding to an equivalent energy deposited in the detectors of 75 keV and 65 keV for the start and stop channels respectively. The signal (referred to the K conversion line), noise (peak to peak as seen on a 100 MHz bandwidth oscilloscope) and pulse risetimes at the inputs to the start and stop fast discriminators were 30 mV, 7 mV and 7 ns and 30 mV, 6 mV and 10 ns respectively. Figure 5.4.1.(c) shows an example of one of the delayed coincidence spectra obtained. The time resolution was 3.6 ns fwhm and the late and early slopes corresponded to apparent half-lives of 0.69 ns and 0.77 ns

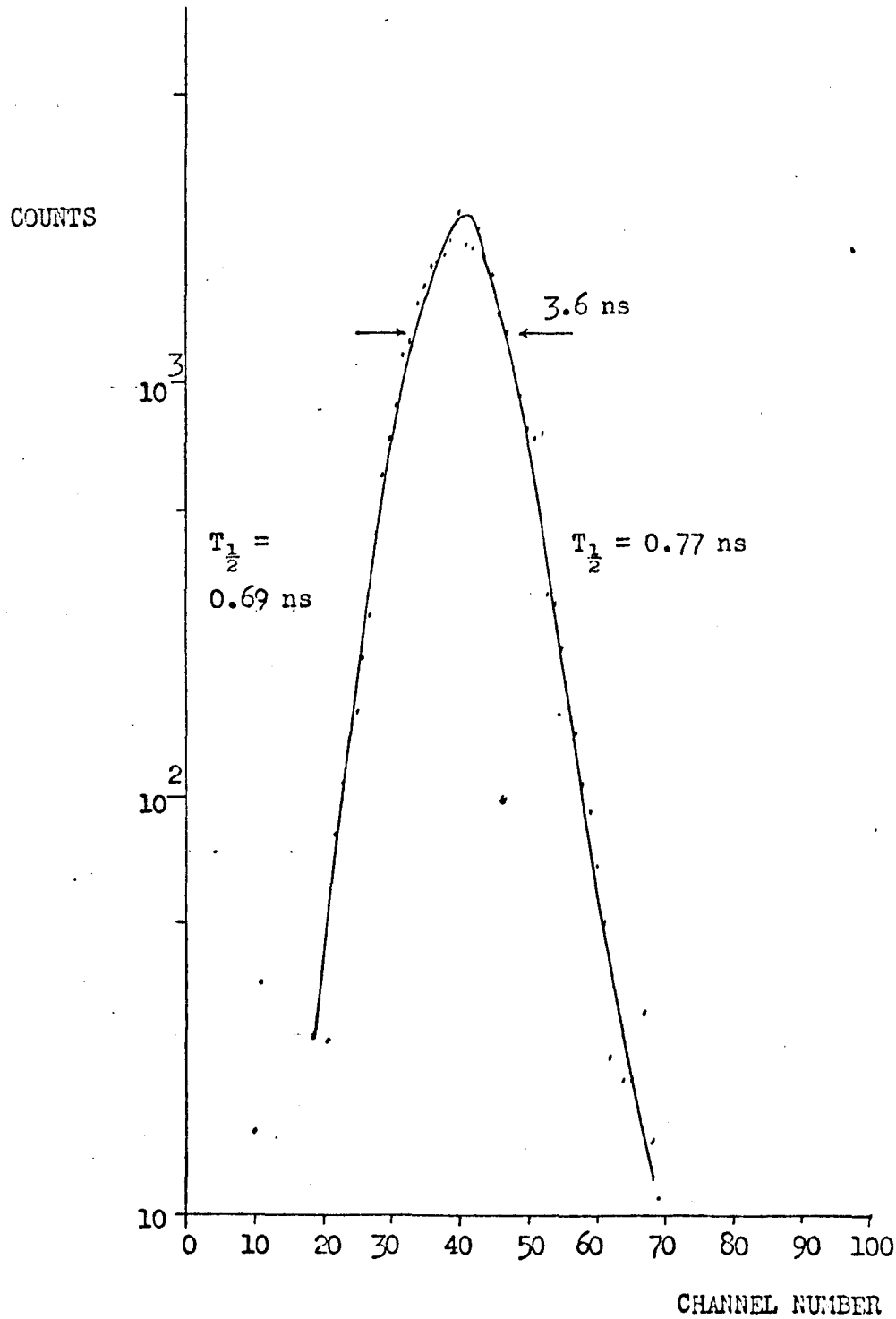

Figure 5.4.1.(c) Delayed coincidence spectrum obtained when analysing the 279 keV excited state in Tl-203.

respectively. The spectrum was corrected for chance coincidences and the measurement period was 255 minutes. The half-life found here from the late slope was over a factor of two greater than the value that would be expected if it corresponded to the half-life of the 279 keV level (ie. 0.278 ns). Thus the spectrum of Figure 5.4.1.(c) gives the intrinsic time resolution of the system at the energies considered here.

It is clear from the above that the slope method of analysis of the delayed coincidence spectrum cannot be used to give a value for the half-life of the 279 keV level using the present measurement system. One possible method that can be used to extract the half-life is the self comparison method (BELL et al 1952). In the work described here this involved first recording a coincidence curve with the start and stop channels accepting energies as for the above paragraph and then recording a second coincidence curve with the start channel accepting energies previously handled by the stop channel and vice-versa. The results of two sets of measurements gave a shift between the centroids of the pairs of coincidence curves of (2.23 ± 0.12) ns (program (iii), Appendix A was used to calculate the positions of the centroids). Part of this shift was due to the electronics, the finite risetimes of the input pulses causing the fast discriminators to trigger either earlier (change to a higher energy) or later (change to a lower energy).

Some idea of this instrumental time shift was obtained by measuring the shift in the position of the coincidence spectrum centroid when the start channel single channel analyser was first set on the K conversion line and then on the L + M lines, the stop channel viewing the continuous beta spectrum (155 keV - 175 keV) during the two measurements. The time shift thus obtained was (2.0 ± 0.2) ns and corresponded to an energy change of about 73 keV.

As it could not be assumed that the time shift per unit energy change was independent of the energy, the energy dependence was investigated by feeding artificial pulses into the system (including the detectors) via the preamplifier test inputs. The pulses were supplied by two pulse generators (NE 6591 and Hewlett Packard model 2138) which were set up to produce pairs of simultaneous pulses. The amplitude of the pulses fed into the stop channel were fixed in magnitude and corresponded to an equivalent energy deposited in the detector of about 155 keV. The amplitude of the start channel pulses was variable. The risetimes of the pulses at the discriminator inputs was 11 ns and 10 ns for the start and stop channels respectively and the discriminator threshold levels corresponded to energies of about 70 keV. The positions of the centroids of the pulser peaks (in terms of channel numbers) was found for five values of equivalent energy deposited in the start detector (expressed as settings of the

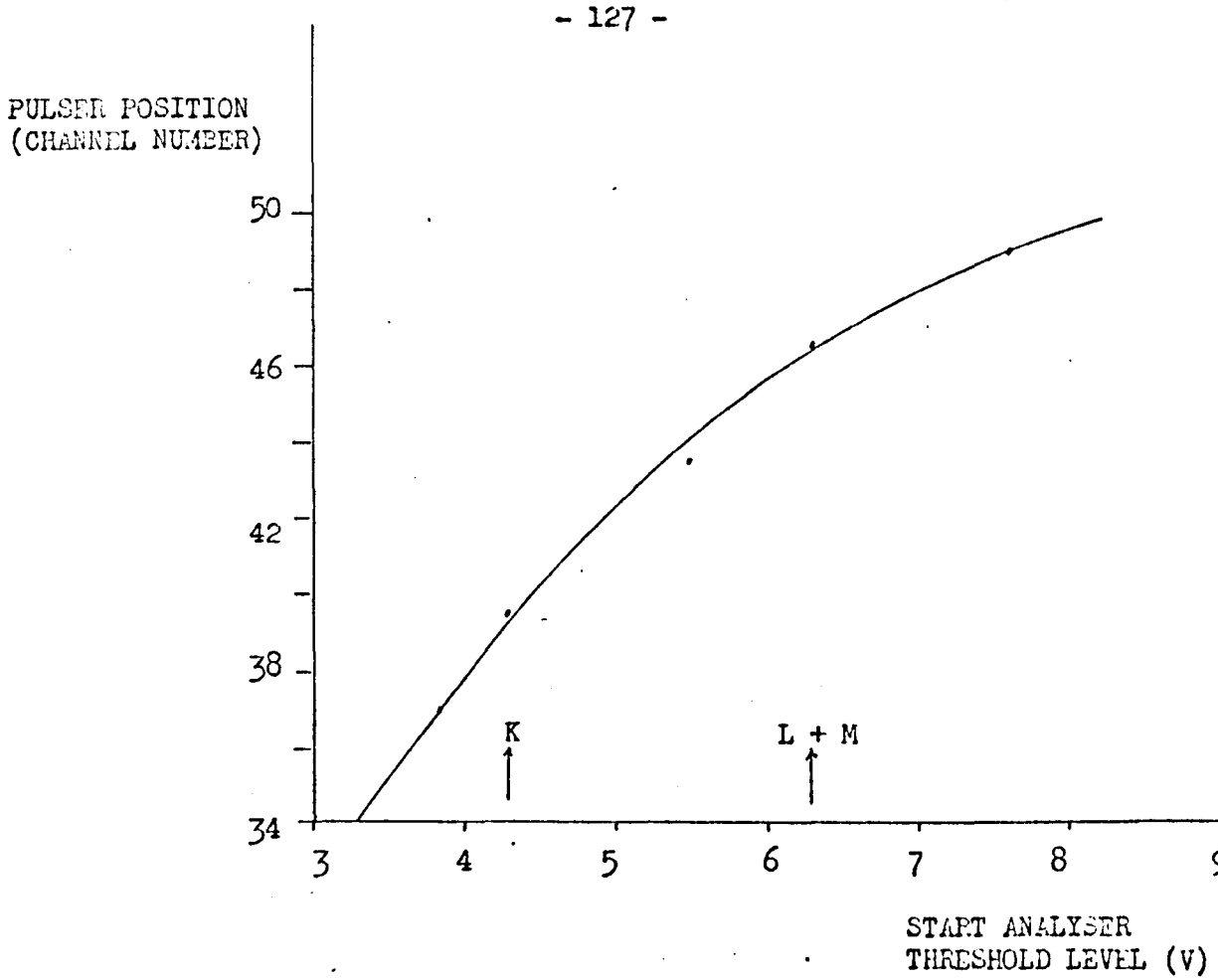

Figure 5.4.1.(d) Instrumental time shift as a function of energy.

start channel single channel analyser, the results being presented in graphical form in Figure 5.4.1.(d). This clearly shows the energy dependence of the time shift. From this graph the time shift corresponding to an energy change from the K conversion line to the L + M lines was 1.8 ns. This may be compared with the figure of 2.0 ns found using the Hg-203 source.

In the above application of the self comparison method the start channel single channel analyser threshold level was changed from 4.3 V to 3.66 V. From Figure 5.4.1.(d) the corresponding

instrumental time shift was 0.90 ns. Assuming the time shift in the stop channel was the same the total instrumental shift was 1.8 ns. The shift in the positions of the centroids, corrected for instrumental shift, was thus 0.43 ns and corresponded to a half-life of 0.15 ns. The estimated error in this figure was at least as large as the figure itself in view of the assumptions made above. Figure 5.4.1.(e) shows the calibration graph used for this work.

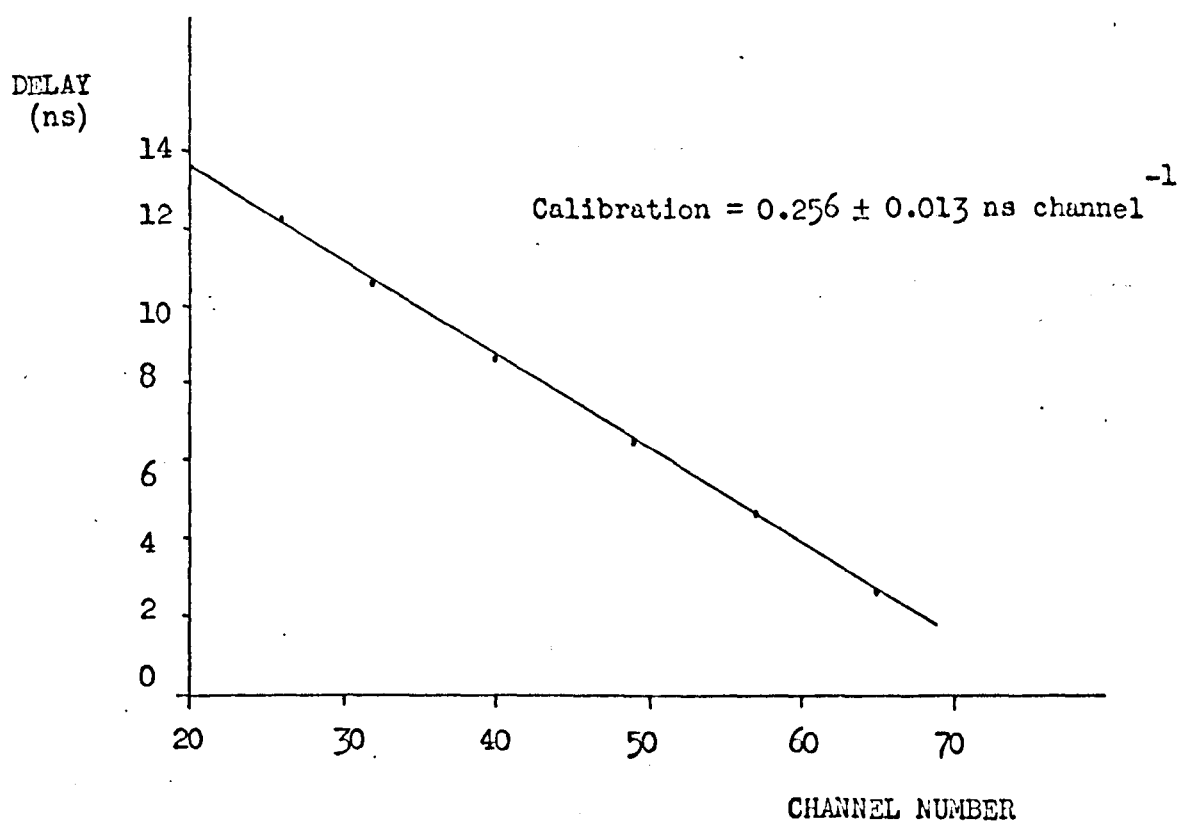

Figure 5.4.1.(e) Calibration graph for the time-to-amplitude converter time scale.

Use of the measurement system of Figure 3.3.(b) resulted in a coincidence time spectrum having a fwhm of 8.4 ns and late and early slopes corresponding to apparent half-lives of 2.2 ns and 1.9 ns respectively. As no recognisable energy spectra were obtained at the outputs of the main amplifiers the single channel analysers in the slow channels were set to approximately half the maximum pulse height seen, with a window width of about 20 % of this maximum. The signal (peak amplitude seen), noise (peak-to-peak) and pulse risetimes at the inputs to the start and stop fast discriminators were 80 mV, 15 mV and 6 ns and 40 mV, 15 mV and 8 ns respectively. The factor of two difference between the peak amplitudes seen in the two channels was due to the stop detector having twice the sensitive depth of the start detector.

5.4.2. Delayed Coincidence Measurements on the 412 keV level in Hg-198

The decay scheme for Au-198 is shown in Figure 5.4.2.(a) (Nuclear Data Sheets B, Volume 6, Number 4, 1971). The 412 keV excited state in Hg-198 is fed mainly by the 962 keV (99%) beta branch from the decay of Au-198. The state de-excites by an E2 transition of energy 412 keV, the K shell conversion coefficient for this transition being 0.03. The half-life of the 412 keV level has been measured to be 0.02 ns.

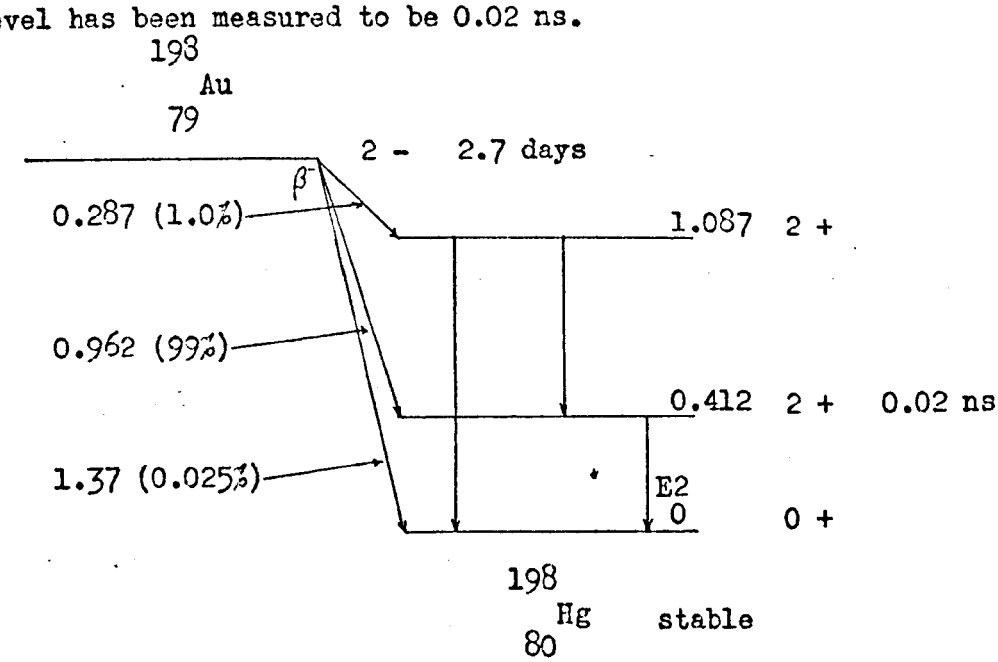

Figure 5.4.2.(a) Decay scheme for Au-198

The Au-198 source used for the delayed coincidence measurements was prepared from auric chloride in 3N HCl (R.C.C. code GCS 3). The source, an evaporated deposit on an aluminium foil backing, had

an activity of the order of 10 μCi. Figure 5.4.2.(b) shows part of the energy spectrum of beta particles and conversion electrons emitted from this source.

For the delayed coincidence measurements on the 412 keV level in Hg-198 using the measurement system of Figure 3.3.(a) the single channel analyser in the start channel was set on the K conversion line at 329 keV (ΔE = 50 keV) whilst the analyser in the stop channel viewed the continuous beta spectrum and accepted pulses corresponding to the energy range 430 keV - 560 keV. Other settings were similar to those used in Section 5.4.1. . Figure 5.4.2.(c) shows an example of one of the delayed coincidence spectra obtained. The time resolution was 3.4 ns fwhm and the late and early slopes corresponded to apparent half-lives of 1.1 ns and 0.7 ns respectively. These latter two figures were obtained from the portion of the spectrum lying between counts of 100 and 500. The spectrum was corrected for chance coincidences and the measurement period was 105 minutes.

Use of the measurement system of Figure 3.3.(b) resulted in a coincidence time spectrum having a fwhm of 4.5 ns and late and early slopes corresponding to apparent half-lives of 1.1 ns and 1.2 ns respectively. The setting of the single channel analysers was similar to that used in Section 5.4.1.

The time calibration for these measurements was (0.241 ± 0.012) ns per channel.

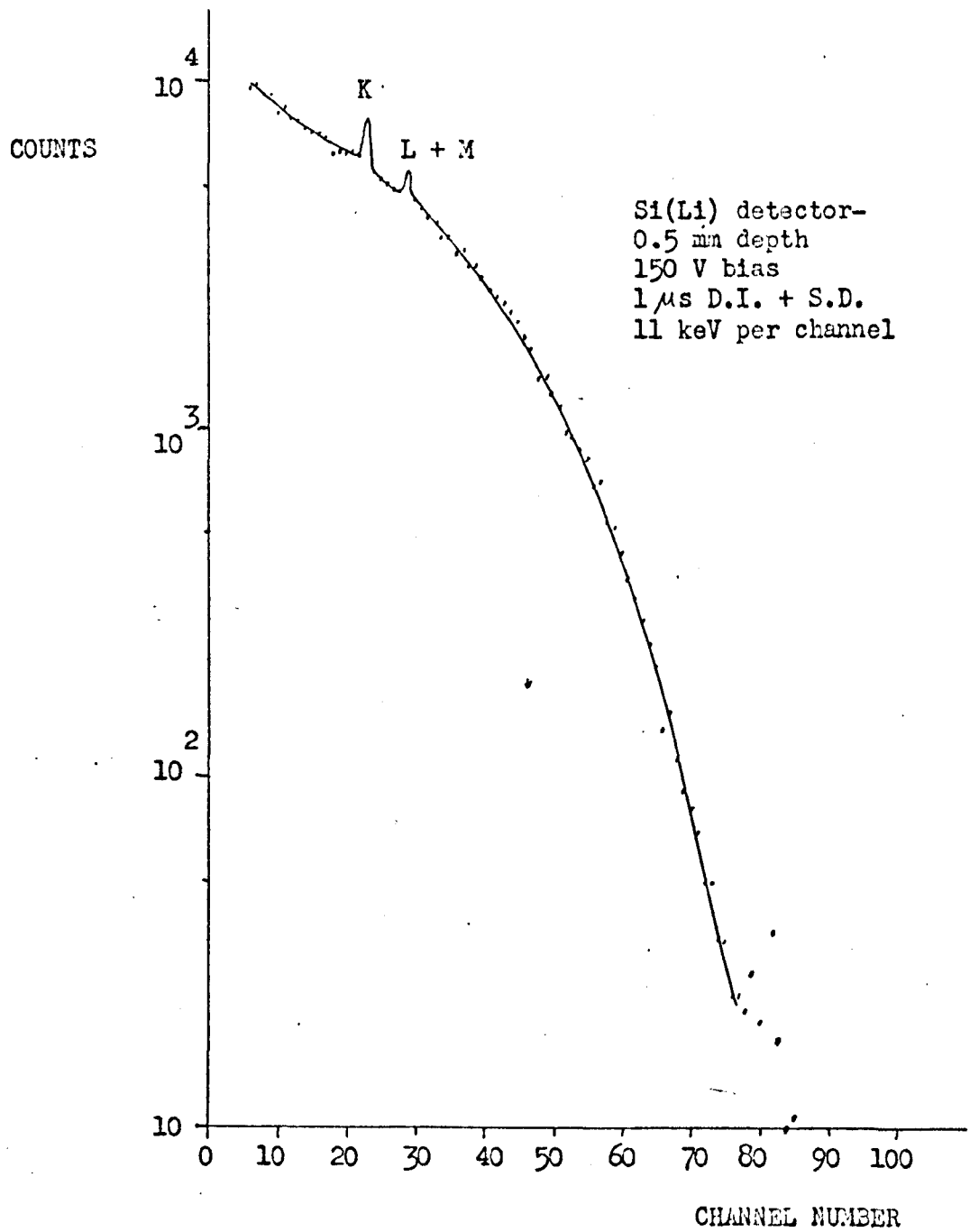

Figure 5.4.2.(b) Part of the energy spectrum of beta particles and conversion electrons emitted from the Au-198 source.

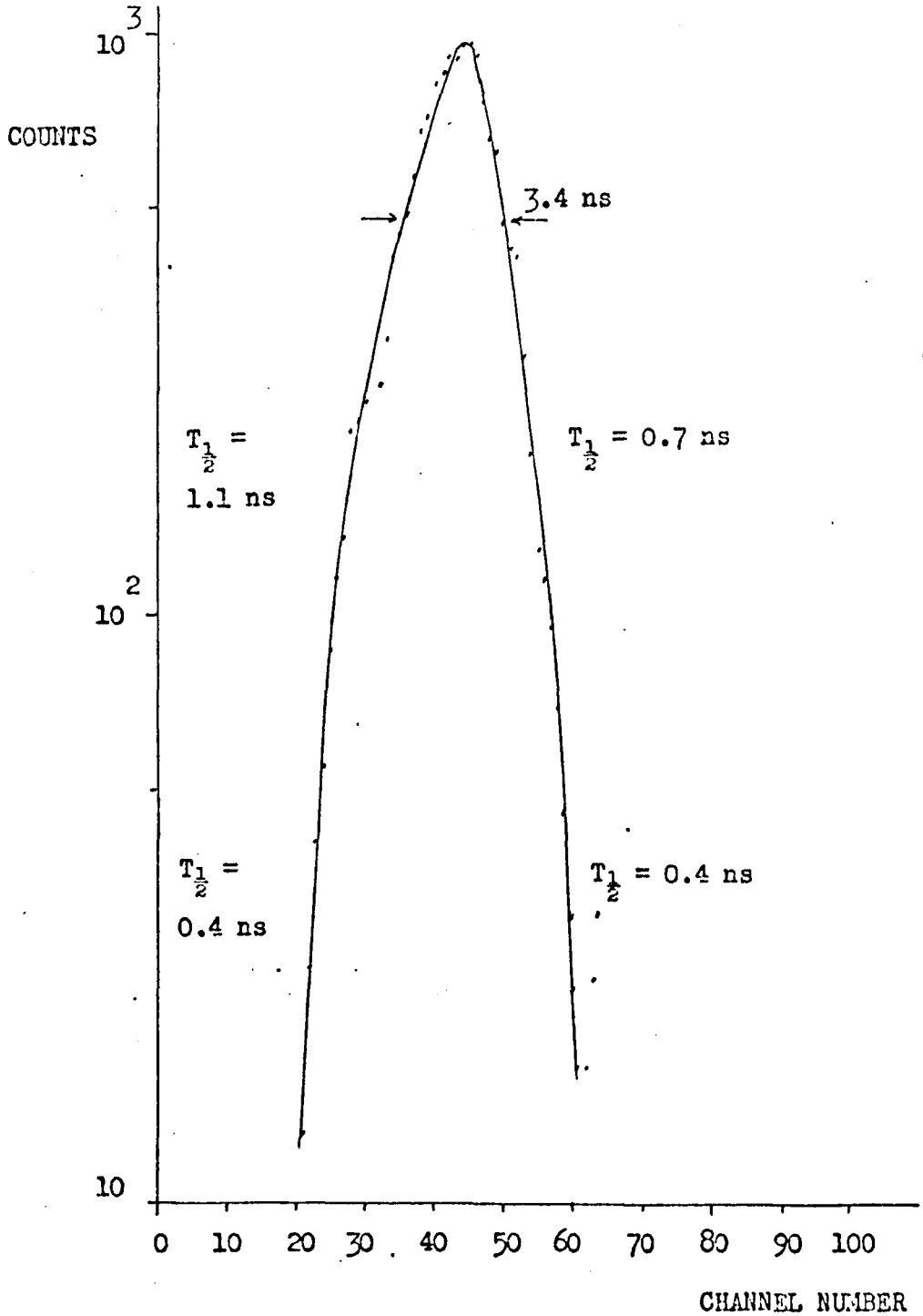

Figure 5.4.2.(c) Delayed coincidence time spectrum obtained when analysing the 412 keV excited state in Hg-198.

5.4.3. Variation of System Time Resolution with Equivalent Energy Deposited in the Detectors and Slow Channel Window Width

The time resolution (fwhm) of the system was measured as a function of equivalent energy deposited in the two detectors by feeding the output of a pulser (NE 6591), calibrated in terms of energy, simultaneously into the test inputs of the preamplifiers. The fast discriminators were adjusted to have equal threshold levels. The results obtained for two discriminator threshold levels are shown in Figure 5.4.3.(a). Curve (a) corresponds to a threshold level

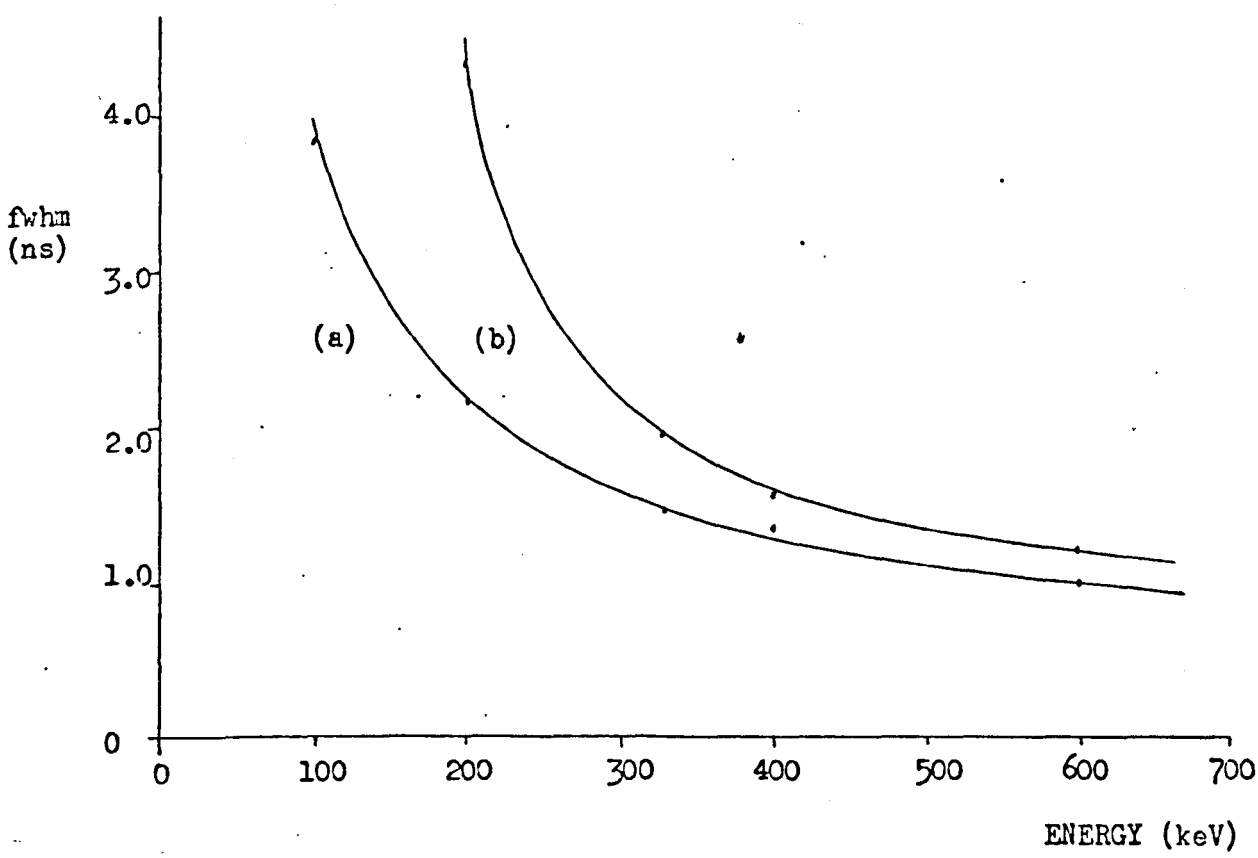

Figure 5.4.3.(a) Time resolution as a function of equivalent energy deposited in the two detectors.

set as low as possible consistent with negligible triggering on noise pulses whilst for curve (b) the threshold level was set well above this minimum value.

Figure 5.4.3.(b) shows the results obtained by feeding the pulser output directly into the input of each discriminator, the charge sensitive preamplifiers having been previously disconnected. The discriminator threshold levels were set at approximately 70 keV. Points x and y resulted when noise was added to the discriminator input signals by connecting the output of the start channel charge sensitive preamplifier in parallel with the pulser output. This noise had a peak amplitude corresponding to an equivalent deposited energy of about 60 keV.

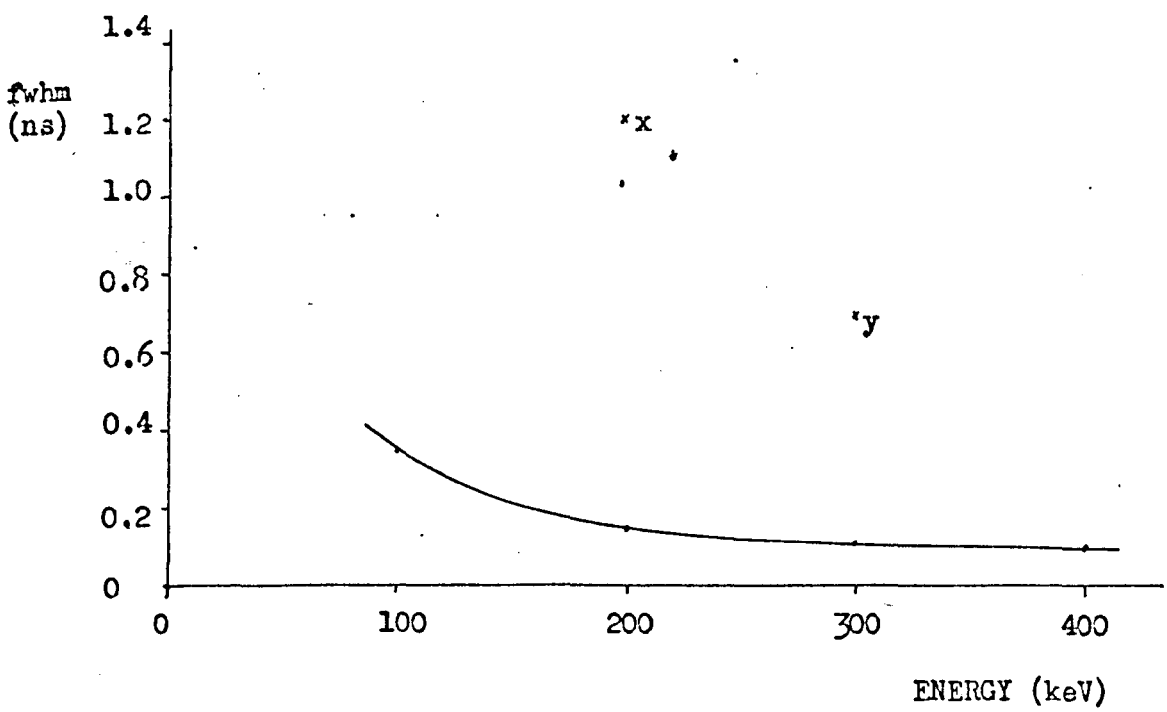

Figure 5.4.3.(b) Time resolution of the system less preamplifiers as a function of equivalent energy deposited in the two detectors.

The effect of the slow channel window width on the time resolution was also investigated. Prompt coincidence time spectra were obtained when analysing the 279 keV level in Tl-203 for three window width settings of the single channel analyser in the stop channel (the analyser viewing the continuous beta spectrum). The window width on the start channel single channel analyser was fixed in value at 12%. For the settings used (33%, 25% and 6%) it was found that very little variation in resolution (fwhm and fwl/10m) occurred with window width . However, the results indicated that there was a small advantage to be gained as far as time resolution was concerned by the use of a narrow window width.

5.4.4. Time Stability of the System

The time stability of the system was checked in a similar manner to that used in Section 5.3.4. except that the pulser output was connected to the test inputs on the preamplifiers. A run time of 11 hours was used and resulted in a time spectrum with a fwhm of 1.3 ns. A similar measurement but with a run time of only 90 seconds gave the same value.

6. DISCUSSION AND CONCLUSION

6.1. DISCUSSION OF RESULTS

The results obtained with the modified and with the unmodified time-to-amplitude converter are discussed separately below.

6.1.1. The Modified Converter

a) Am-241 source

Table 5.3.(a) summarises the results obtained when analysing the 59.6 keV excited state of Np-237. Although the four measurements were taken with identical apparatus settings it can be seen on considering column three of the table that the chance coincidences range from 10 to 21 counts per channel per hour. The reason for this wide variation is not known for certain. A possible explanation is that during measurements 15.8.72 (5) and 15.8.72 (6) electrical interference was picked up by the apparatus producing spurious pulses. The building in which the work was carried out is known to suffer badly from such interference. As a result of this, further measurements were taken overnight, where possible, when electrical activity in the building might be expected to be at a minimum. Column six of Table 5.3.(a) reveals that during this particular series of measurements there was appreciable drift in the calibration of the system. Again the reason for this is not

known as there was no dramatic room temperature changes during the measurements and the apparatus had been running for several days prior to the first of these measurements. The mean of the results from the four measurements of the half-life of the 59.6 keV excited state in Np-237 was (68.5 ± 0.4) ns. Table 6.1.(a) summarises the half-life measurements made on this state. As can be seen the result obtained here is in good agreement with recent previous measurements. Only one of these measurements made use of a semiconductor detector (GARG et al 1971, surface barrier alpha particle detector).

(b) Th-228 source

Figure 5.3.1.(g) shows the prompt coincidence spectrum obtained when analysing the 84.5 keV excited state in Ra-224. The time resolution (fwhm) was 8.0 ns and the late and early slopes corresponded to apparent half-lives of 3.0 ns and 2.1 ns respectively. The comparatively small difference between these $T_{\frac{1}{2}}$ slopes, when compared with those of Figure 5.3.2.(e) can be explained by drift in the conversion gain (ns ch^{-1}) during the long measurement period of 67 hours. This gave the long term time stability of the complete system as about ± 2 ns. The prompt coincidence spectrum of Figure 5.3.1.(h) shows considerably faster late and early slopes of 1.6 ns and 1.4 ns respectively due partly to the higher energy

Table 6.1.(a) Summary of the half-life determinations of the 59.6 keV excited state in Np-237.

Technique	$T_{\frac{1}{2}}$ (ns)	Reference
$\alpha-\gamma$(59.6 keV). Scintillation counters	63 ± 5	BELING et al (1952)
$\alpha-\gamma$(59.6 keV). Scintillation counters	62 ± 3	VARTAPETIAN (1958)
$\alpha-\gamma$(59.6 keV). Surface barrier-NaI(Tl)	66.7 ± 0.7	GARG et al (1971)
$\alpha-\gamma$(59.6 keV). Scintillation counters	66.9 ± 1.0	McBETH and WINYARD (1972)
$\alpha-\gamma$(59.6 keV). Scintillation counters	68.3 ± 0.2	MILLER et al (1972)
$\alpha-\gamma$(59.6 keV). Surface barrier-Ge(Li)	68.5 ± 0.4	Present work (BISHOP)

of the depopulating radiation (241 keV compared with 84.5 keV) but the late slope is linear only for just over one decade. A somewhat faster early slope would be expected when comparison is made with Figure 5.3.2.(e) especially in view of the higher gamma transition energy involved.

(c) Np-237 source

Table 5.3.(b) summarises the results obtained when analysing the 86.5 keV excited state in Pa-233. As might be expected the number of chance coincidences recorded per channel per hour were a function of the side channel restrictions used. These ranged from 1.2 for measurement 22.11.72 (1) (no energy restrictions except as set by the fast discriminators) to 0.07 for measurement 29.11.72 (1) (restrictions on both alpha and gamma energies). Measurements 23.11.72 (1) and 24.11.72 (1) (restriction on gamma energies only) yielded figures of 0.13 and 0.64 respectively although the apparatus settings were identical in the two cases. Advantage is therefore to be gained from using side channel restrictions as for measurement 29.11.72. (1). The mean of the results from the four measurements of the half-life of the 86.5 keV state was (37.7 ± 0.2) ns. Table 6.1.(b) summarises the previous measurements on this state where the depopulating radiation used was the 86.5 keV gamma ray. All these previous measurements used scintillation counters to

Table 6.1.(b) Summary of the half-life determinations of the 86.5 keV excited state in Pa-233.

Technique		$T_{\frac{1}{2}}$ (ns)	Reference
α - e	Scintillation counters	36.9 ± 0.4	ENGELKEMEIR and MAGNUSSON (1954)
α-γ (86.5 keV)	Scintillation counters	36.0 ± 0.5	MARCHAL and YVON (1961)
α-γ (86.5 keV)	Surface barrier-NaI(Tl)	37.4 ± 0.4	GARG et al (1971)
α-γ (86.5 keV)	Scintillation counters	35.7 ± 0.5	WINYARD and McBETH (1972)
α-γ (86.5 keV)	Surface barrier-Ge(Li)	37.7 ± 0.2	Present work (BISHOP)

detect the depopulating radiation and only one of the measurements (GARG et al 1971) made use of a semiconductor detector as the alpha particle detector. The use of scintillation counters with their inherently poor energy resolution made it impossible to solely select the 86.5 keV gamma rays, the Pa K_α X rays (also U K_α X rays) from the internal conversion of high energy gamma rays being accepted also. The shape of the resulting delayed coincidence spectrum in these measurements was then determined by more than one half-life. However, as shown here, the use of semiconductor detectors with their superior energy resolution, automatically overcomes this problem. A further advantage of the semiconductor detectors' high energy resolution is that much narrower side channel windows may be used resulting in a considerable reduction in the chance coincidence rate. This in turn improves the accuracy of measurement of the half-life under consideration.

The origin of the prompt component in Figure 5.3.2.(c) is on consideration of Figure 5.3.2.(e) seen to be due to coincidences between the 3.4 - 5.0 MeV alpha particles from the decay of Np-237 and the K X rays (mainly K_α) from the internal conversion of high energy gamma rays in Pa-233.

The work of Section 5.3.3. shows that there is little advantage to be gained as far as time resolution and slope are concerned by the use of discriminator threshold levels below the equivalent of about 30 keV or Ge(Li) detector bias voltages greater than about

500 V, at the radiation energies considered here. This indicates that above about 500 V the detector carrier saturation velocity is reached. The early (negative) slopes of the prompt spectra show no significant variation with either Ge(Li) detector bias or discriminator threshold. This is to be expected as the early slope is here almost solely determined by noise jitter, the noise originating mainly from the preamplifier used with the Ge(Li) detector. Pulse shape jitter from the surface barrier detector is negligible due to the shallow depletion depth and the large amplitude output signal, this latter also ensuring an excellent signal to noise ratio in the alpha channel. Thus the contribution to the time resolution from the alpha detector compared with that from the Ge(Li) detector can be considered to be negligible.

The output pulses from the 5 mm sensitive depth Ge(Li) detector used here would ideally be expected to have risetimes in the approximate range of 25 ns - 50 ns (Section 2.3.4.). After passing through the detector preamplifier (risetime 20 ns) the pulses would have risetimes in the range of 32 ns - 54 ns. (The minimum pulse risetime seen on a fast oscilloscope connected to the preamplifier was about 30 ns). The effect of this risetime spread can be reduced by use of low discriminator threshold settings. From a simple geometrical consideration, assuming pulses rising linearly with time, the effective time spread for pulses with risetimes in the above range would be

about 5 ns and 9 ns for discriminator threshold levels of 20 keV and 40 keV respectively. But from the results of Section 5.3.3., after allowing for noise jitter, it is clear that a large number of pulses from the Ge(Li) detector must have risetimes lying well outside the above range. The theoretical charge pulse shapes presented in Figure 2.3.4.(a) for an ideal detector thus do not apply here. The shape distribution of pulses generated by gamma rays in planar Ge(Li) detectors has been studied by several workers (MOSZYNSKI and BENGTSON 1972, STRAUSS et al 1967, STRAUSS and LARSEN 1967, BALLAND et al 1968). Their work has shown that substantial regions near one or both electrodes of the detector are often poorly compensated giving rise to regions of low electric field strength. Charge carriers generated by the incident radiation in these dead layers give rise to pulses having long risetimes. The use of presently available risetime compensated discriminators do not by themselves overcome this problem. Pulse shape selection (Section 3.2.) appears the only solution at the present time, but this technique suffers from the large disadvantage that a high percentage (up to 50 %) of otherwise usable events must be rejected to achieve coincidence spectra with fast late slopes over several decades.

6.1.2. The Unmodified Converter

The delayed coincidence spectrum obtained when analysing the 279 keV excited state in Tl-203 (Figure 5.4.1.(c), coincidences recorded between 160 keV betas and 194 keV conversion electrons) gave a resolution (fwhm) of 3.6 ns and late and early slopes of 0.69 ns and 0.77 ns. The corresponding figures obtained for the 412 keV state in Hg-198 (Figure 5.4.2.(c), coincidences recorded between 495 keV betas and 329 keV conversion electrons) were 3.4 ns fwhm and 1.1 ns and 0.7 ns respectively for the late and early $T_{\frac{1}{2}}$ slopes. This last set of figures is little different from the first even though the radiations involved were of higher energies, but on consideration of Figure 5.4.2.(c) it is seen that the late and early $T_{\frac{1}{2}}$ slopes become equal at 0.4 ns in the region of the spectrum lying below a count of about 100. The shape of these spectra is determined mainly by noise generated in the preamplifiers but also, to a much lesser extent, by fluctuations in the pulse shape delivered by the detectors. The strong dependence of the spectrum shape on the signal to noise ratio present at the discriminator inputs is clearly seen from Figure 5.4.3.(a) and shows the advantage to be gained by using as low a discriminator threshold level as possible, this being particularly true for the lower radiation energies. The resolution, fwhm, as seen from the two curves in Figure 5.4.3.(a) shows roughly an $(\text{energy})^{-1}$ dependence at the lower energies, as might be

expected from the relation $\sigma_t = \sigma_v/(dV/dt)$ (Section 3.2.) assuming output pulses rising linearly with time. The fact that the preamplifiers are the main source of noise and hence the main contributors to loss of time resolution can be seen on comparing Figures 5.4.3.(a) and 5.4.3.(b). A reduction in preamplifier noise would decrease time jitter due to noise (Section 3.2.) and would enable lower discriminator threshold levels to be used thus decreasing the effects of both amplitude and risetime dependent walk and may result in a further reduction in noise jitter if the slope of the signal at the trigger point is increased.

Although a very simplified approach was used in the measurement of the half-life of the 279 keV state in Tl-203 using the self comparison method it did serve to illustrate the possibilities of this technique. A much more careful study would be needed if any worthwhile measurements were to be made of excited state half-lives. The instrumental time shift would have to be accurately determined for both the start and stop channels. This should be done using pulses delivered by the detectors rather than, as described here, using artificial pulses fed into the preamplifiers. Such artificial pulses do not have the same shape as those delivered by the detectors and in addition their use excludes the effect of detector energy dependent time shifts. These instrumental time shifts could be considerably reduced if more sophisticated timing discriminators such as the constant fraction types were to

be substituted for the existing leading edge ones.

Considering the results obtained from the measurements using the system of Figure 3.3.(b), the rapid improvement of time resolution with increasing energy suggests that the timing performance of the current preamplifiers would be superior to that of the charge sensitive type at energies higher than those considered here. The good time performance is due to the fact that the current pulses have a constant risetime determined by the time constants of the detector circuit and the bandwidth of the current preamplifiers. As the signal to noise ratio using current preamplifiers is proportional to (detector sensitive depth)$^{-1}$ (Section 2.3.2.) optimum results would be obtained by matching the sensitive depth of the detector to the range of the incident particles, germanium detectors being superior by at least a factor of two compared with silicon ones in this respect due to their higher stopping power. With such an optimised system the time resolution using current preamplifiers would be at least comparable to that obtained with charge preamplifiers at the energies considered here. A serious disadvantage of this apparatus arrangement was the very poor energy resolution obtainable, estimated to be of the order of 50 keV at 200 keV. The lack of energy resolution is mainly due to the amplitude of the current pulses delivered by the detectors being dependent on the position of the initial ionisation relative to the detector collecting electrodes (Section 2.3.2.).

This problem can be overcome if a charge sensitive preamplifier is added to each channel to give the energy signal, as in Figure 3.2.(a) - c), but it has been found here that this seriously degrades the time resolution for reasons given in Section 3.2. and also because the fast discriminators are fed with a range of pulse amplitudes for a given deposited energy selected by the analysers in the slow channels. This latter would necessitate the use of some form of constant fraction discriminator.

6.2. POSSIBLE FUTURE WORK

It is proposed to continue this study of the use of semiconductor detectors for short nuclear half-life measurements in an attempt to decrease the lower limit on half-lives that may be measured using the Ge(Li)-surface barrier system described here. The effect of adding an amplitude and risetime compensated discriminator to the gamma channel will be investigated with regard to timing performance. The use of pulse shape selection will also be considered. A faster and quieter preamplifier could be substituted in the gamma channel. Replacement of the existing surface barrier detector with one of the Si(Li) detectors would extend the capability of the system so that a study of beta-gamma coincidence measurements could be made.

6.3. CONCLUSION

The work reported here is a contribution to a better knowledge of the use of semiconductor detectors for short half-life measurements. The results have shown that pairs of semiconductor detectors operated in coincidence are capable of good time resolution with simultaneous good energy resolution. Their time performance does not, at present, compare favourably with that obtained from organic scintillation counters, although the fwhm values are close to those obtained from NaI(Tl) counters. Advances in the design of low noise preamplifiers and fast discriminators designed specifically with semiconductor detectors in mind will undoubtedly narrow the gap.

With the present Ge(Li)-surface barrier system it appears possible to measure half-lives down to about 5 ns at gamma energies of 90 keV when using the slope method of analysis of the delayed coincidence curve and considerably less than this at higher energies. The results obtained for the half-lives of the two excited states measured illustrates the performance capability of the system and in the case of the measurement of the 86.5 keV state in Pa-233 clearly shows the advantage to be gained from a system with combined good time and energy resolution. However, a serious disadvantage of small volume planar Ge(Li) detectors when used for coincidence measurements is their low full energy peak detection efficiency, especially for gamma energies above

about 100 keV.

The results obtained with the Si(Li)-Si(Li) system indicate that half-lives greater than about 2 ns can be measured at 200 keV using the slope method of analysis, whilst careful use of the self comparison technique should extend measurements towards shorter half-lives by about an order of magnitude at similar energies. These figures are about an order of magnitude higher than those obtainable from using scintillation counters. In addition, scintillation counter-magnetic spectrometer combinations show energy resolutions at least comparable with the semiconductor detector system. Thus there would appear to be little advantage to be gained, apart from a better detection efficiency and smaller size, from the use of this latter system at the present time.

ACKNOWLEDGMENTS

The author would like to take this opportunity to express his gratitude to the following for their help and assistance in the completion of this project:-

To Mr J. Williams and Dr. D. Butt, his supervisors, for their help and guidance.

To my wife, for her unselfish patience, understanding and encouragement during the long hours needed to complete this work, and for her assistance with some of the typing.

To the technical staff in the School of Physics, Kingston Polytechnic, particularly Mr. P. Parsons and Mr. J. Johnson.

To the School of Physics, Kingston Polytechnic for providing the facilities for this research.

REFERENCES

ALKHAZOV, G.D., A.P. KOMAR and A.A. VOROBEV, 1967,
Nucl. Instr. and Meth. 48 1.

BAKER, C.A., C.J. BATTY and L.E. WILLIAMS, 1968,
Nucl. Instr. and Meth. 59 125.

BALLAND, J.C., J. PIGNERET, J.J. SAMUELI and A. SARAZIN, 1968,
IEEE Trans. Nucl. Sci. NS-15 411.

BAY, Z., 1950,
Phys. Rev. 77 419.

BELING, J.K., J.O. NEWTON and B. ROSE, 1952,
Phys. Rev. 87 670.

BELL, R.E., 1965,
Alpha-, Beta- and Gamma-Ray Spectroscopy, Vol.2 p.905.
North-Holland Publishing Company, Amsterdam.

BELL, R.E., R.L. GRAHAM and H.E. PETCH, 1952,
Can. J. Phys. 30 35.

BENGTSON, B. and M. MOSZYNSKI, 1972,
Nucl. Instr. and Meth. 100 293.

BERTOLINI, G. and A. COCHE, 1968,
Semiconductor Detectors.
North-Holland Publishing Company, Amsterdam.

BISHOP, R.J., 1973,
Nucl. Instr. and Meth. 107 9.

BISHOP, R.J., In Press,
Nucl. Instr. and Meth.

CAVALLERI, G., E. GATTI, G. FABRI and V. SVELTO, 1971,
Nucl. Instr. and Meth. 92 137.

CHASE, R.L., 1968,
Rev. Sci. Instr. 39 1318.

CHO, Z.H. and J. LLACER, 1972,
Nucl. Instr. and Meth. 98 461.

DAVIS, W.D., 1958,
J. Appl. Phys. 29 231.

ENGELKEMEIR, D., 1967,
Nucl. Instr. and Meth. 48 335.

ENGELKEMEIR, D. and L.B. MAGNUSSON, 1954,
Phys. Rev. 94 1395.

FANO, U., 1947,
Phys. Rev. 72 26

GARG, R.K., S.D. CHAUHAN, S.L. GUPTA and N.K. SAHA, 1971,
Z. Physik 244 312.

GEDCKE, D.A. and W.J. McDONALD, 1967,
Nucl. Instr. and Meth. 55 377.

GOULDING, F.S. and W.L. HANSEN, 1961,
Nucl. Instr. and Meth. 12 249.

JACOBSEN, J.C., 1934,
Nature 133 565.

JACOBSEN, J.C. and Th. SIGURGEIRSSON, 1943,
Mat.-Fys. Medd. Dan. Vid. Selsk. 20 No. 11.

KERN, H.E. and J.M. McKENZIE, 1970,
IEEE Trans. Nucl. Sci. NS-17 260.

LINDHARD, J. and V. NIELSON, 1962,
Phys. Lett. 2 209.

MACKAY, K.G., 1949,
Phys. Rev. 76 1537.

MACKAY, K.G., 1951,
Phys. Rev. 84 829.

MAIER, M.R. and P. SPERR, 1970,
Nucl. Instr. and Meth. 87 13.

MARCHAL, A. and P. YVON, 1961,
Compt. Rend. 252 3774.

MAYER, J.W., 1959,
J. Appl. Phys. 30 1937.

MAYER, J.W. and B. GOSSICK, 1956,
Rev. Sci. Instr. 27 407.

McBETH, G.W. and R.A. WINYARD, 1972,
Nucl. Instr. and Meth. 100 413.

McKENZIE, J.M. and D.A. BROMLEY, 1959,
Proc. IRE 106 731.

MIEHE, J.A. and P. SIFFERT, 1970,
IEEE Trans. Nucl. Sci. NS-17 8.

MILLER, G.H., P. DILLARD, M. ECKHAUSE and R.E. WELSH, 1972,
Nucl. Instr. and Meth. 104 11.

MOSZYNSKI, M. and B. BENGTSON, 1970,
Nucl. Instr. and Meth. 80 233.

MOSZYNSKI, M. and B. BENGTSON, 1972,
Nucl. Instr. and Meth. 100 285.

NEWTON, T.D., 1950,
Phys. Rev. 78 490.

ORMAN, C., H.Y. FAN, G.J. GOLDSMITH and K. LARK-HOROWITZ, 1950,
Phys. Rev. 78 646.

PELL, E.M., 1960,
J. Appl. Phys. 31 291.

QUARANTA, A.A., M. MARTINI and G. OTTAVIANI, 1969,
IEEE Trans. Nucl. Sci. NS-16 35.

RAMO, S., 1939,
Proc. IRE 27 584.

RUSH, C.J., 1964,
Rev. Sci. Instr. 35 149.

RYGE, P. and R.R. BORCHERS, 1971,
Nucl. Instr. and Meth. 95 137.

SCHWARZSCHILD, A.Z. and E.K. WARBURTON, 1968,
Annual Review Of Nuclear Science, p. 265.

SHERMAN, I.S. and R.G. RODDICK, 1970,
IEEE Trans. Nucl. Sci. NS-17 252.

SHERMAN, I.S., R.G. RODDICK and A.J. METZ, 1968,
IEEE Trans. Nucl. Sci. NS-15 500.

STRAUSS, M.G. and R.N. LARSEN, 1967,
Nucl. Instr. and Meth. 56 80.

STRAUSS, M.G., R.N. LARSEN and L.L. SIFTER, 1967,
Nucl. Instr. and Meth. 46 45.

VAN ROOSEBROECK, W., 1965,
Phys. Rev. 139A 1702.

VARTAPETIAN, H., 1958,
Ann. Phys. 3 569.

WEAVER, R.S. and R.E. BELL, 1960,
Nucl. Instr. and Meth. 9 149.

WEDDIGEN, C. and E.L. HAASE, 1965,
Nucl. Instr. and Meth. 33 157.

WEISBERG, H., 1965,
Nucl. Instr. and Meth. 32 133.

WILLIAMS, C.W., W.E. KIKER and H.W. SCHMITT, 1964,
Rev. Sci. Instr. 35 1116.

WINYARD, R.A. and G.W. McBETH, 1972,
Nucl Instr. and Meth. 100 125.

Program (1)

```
200 PRINT "LEAST SQUARES FIT PROGRAM"
205 DIM E(100),D(100)
207 LET X1,X2,X3,Y1,Y2=0
210 PRINT
220 PRINT "HOW MANY PAIRS OF READINGS HAVE YOU -";
230 INPUT P
240 PRINT "ENTER -Y- VALUE FOLLOWED BY  -X- VALUE ONE PAIR TO A LINE"
241 PRINT "WITH  A COMMA BETWEEN."
250 FOR L = 1 TO P
260 INPUT E(L),D(L)
460 LET Y1 = Y1 + E(L)
465 LET Y2 = Y2 + E(L)**2
470 LET X1 = X1 + D(L)
480 LET X2 = X2 + D(L)**2
490 LET X3 = X3 + D(L)*E(L)
500 NEXT L
700 LET A1 = (P*X3 - X1*Y1)/(P*X2 - X1**2)
710 LET A0 =Y1/P -A1*X1/P
800 PRINT
810 PRINT "YOUR BEST STRAIGHT LINE (LEAST SQUARES FIT) IS -"
820 PRINT
830 PRINT "          Y     =     ";A1;"X     +     ";A0
840 PRINT "          ....................................."
850 LET S2 = (Y2 - A0*Y1 - A1*X3)/(P - 2)
860 LET S3 = X2 - X1**2/P
870 LET E1 = S2/S3
880 LET E0 = S2*(1 + X1**2/(S3*P))/P
885 PRINT
890 PRINT "ERROR IN SLOPE (STANDARD DEVIATION) =";SQR(E1)
891 PRINT
895 PRINT "ERROR IN INTERCEPT (STANDARD DEVIATION) =";SQR(E0)
897 PRINT
990 STOP
995 END
```

```
200 PRINT "EXCITED STATE LIFETIME PROGRAM"
  205 DIM E(100),D(100),C(100)
207 LET X1,X2,X3,Y1,Y2=0
  210 PRINT
211 PRINT "WHAT ARE CHANCE COINCIDENCES";
212 INPUT B
220 PRINT "HOW MANY READINGS DID YOU MAKE";
  230 INPUT P
232 PRINT
234 PRINT "WHAT IS LOWEST DATA CHANNEL USED"
236 INPUT F
237 PRINT "WHAT IS CHANCE SLOPE"
238 INPUT H
240 PRINT "ENTER COUNTS FOLLOWED BY TIME WITH A COMMA BETWEEN"
241 PRINT
  250 FOR L = 1 TO P
  260 INPUT E(L),D(L)
265 LET  E(L) = E(L) -(B+H*B*(83-(L+F)))
  270 LET E(L) = LOG(E(L))
  460 LET Y1 = Y1 + E(L)
  465 LET Y2 = Y2 + E(L)**2
  470 LET X1 = X1 + D(L)
  480 LET X2 = X2 + D(L)**2
  490 LET X3 = X3 + D(L)*E(L)
  500 NEXT L
  700 LET A1 = (P*X3 - X1*Y1)/(P*X2 - X1**2)
  710 LET A0 =Y1/P -A1*X1/P
  800 PRINT
  810 PRINT "THE BEST STRAIGHT LINE (LEAST SQUARES FIT) IS -"
  820 PRINT
830 PRINT "      LOG(COUNTS)  =  ";A1;" T      +      ";A0
  840 PRINT
841 PRINT  "HALF LIFE (IN CHANNELS) OF EXCITED STATE =";0.693/A1
  850 LET S2 = (Y2 - A0*Y1 - A1*X3)/(P - 2)
  860 LET S3 = X2 - X1**2/P
  870 LET E1 = S2/S3
  885 PRINT
886 PRINT  "STANDARD ERROR IN HALF LIFE  =";SQR(E1)/0.693
897 PRINT
  990 STOP
  995 END
```

Program (11)

Program (111)

```
5 PRINT "CENTROID PROGRAM"
6 PRINT
7 PRINT
60 PRINT"NAME DATA FILE"
65 INPUT N1
70 OPEN N1 TO 1,INPUT
75 DIM X(1000),Y(1000)
80 LET I=0
85 LET I=I+1
90 INPUT :1,X(I),Y(I)
 95 IF X(I) >< 1E11 THEN 85
100 LET E=I-1
105 PRINT "NUMBER OF OBSERVATIONS IS ";E
107 PRINT "WHAT ARE CHANCE COINCIDENCES"
109 INPUT B
115 LET I=0
120 LET F=0
125 LET I=I+1
127 LET Y(I) =Y(I) - B
130 LET F=(Y(I) +Y(I+1))/2 +F
135 IF I >< E THEN 125
140 PRINT "AREA UNDER THE DISTRIBUTION IS";F
150 LET I=0
155 LET H=0
160 LET I=I+1
165 LET H = (X(I)*Y(I))/F +H
170 IF I >< E THEN 160
175 PRINT "POSITION OF X CO-ORDINATE OF CENTROID IS";H
180 PRINT
190 END
```

APPENDIX B

POSTGRADUATE STUDIES

Two year part time M.Sc. in nuclear physics (University of London), 1968-1970, North East London Polytechnic.

One week full time course Electronics for Nuclear Particle Analysis, U.K.A.E.A., Harwell, July 1970.

One month full time as visiting scientist at CERN, Geneva, 1970, combined lecture and experimental research program.

Nucleonic Instrumentation Conference, IEEE, University of Reading, 1968.

Various colloquia and symposia held at the National Physical Laboratory and other research establishments.

APPENDIX C

PUBLICATIONS

NUCLEAR INSTRUMENTS AND METHODS 96 (1971) 331–332; © NORTH-HOLLAND PUBLISHING CO.

LETTERS TO THE EDITOR

TIMING WITH Si(Li) SEMICONDUCTOR DETECTORS

R. J. BISHOP

School of Physics, Kingston Polytechnic, Kingston upon Thames, England

Received 12 May 1971

Experimental results are reported of the time resolution obtainable from a pair of Si(Li) semiconductor detectors operated in coincidence.

The inherently good timing characteristics and energy resolution of narrow depletion depth semiconductor detectors make them attractive for use in many types of coincidence experiments. This report describes the results of an experimental investigation into the timing performance obtainable from a pair of Si(Li) semiconductor detectors operated in coincidence.

The delayed coincidence circuit used for the measurements employed a 1 mm depletion depth Si(Li) detector in one channel (the "start" channel) and a similar detector but of 0.5 mm depth in the other. Both detectors were of 50 mm^2 area and were cooled to liquid nitrogen temperature. The problem of extracting the timing signal without degradation of the system energy resolution was overcome by the use of fast charge sensitive preamplifiers ($t_r = 6$ ns) similar to those described in ref. 1. Leading edge triggering was used with no compensation for amplitude dependent walk. The discriminator threshold level was set as close to the baseline as the noise would allow, this level corresponding to an equivalent energy deposited in the detectors of about 90 keV.

The prompt coincidence curve obtained when analysing the 279 keV excited state of ^{203}Tl is shown in fig. 1. The measured fwhm is 4.5 ns and the slope corresponds to a half-life of 1.2 ns. For this measurement one of the slow channels was set on the K internal conversion line at 194 keV, the other channel viewing the continuous beta spectrum and accepting pulses corresponding to the energy range 160 keV–180 keV. The energy resolution obtainable was 3 keV at 194 keV. A similar measurement on the 412 keV excited state of ^{198}Hg yielded a fwhm of 3.3 ns and a slope of 0.8 ns. The slow channel settings used were 329 keV (K conversion line) and 430 keV (continuous beta spectrum) with an acceptance window of 130 keV. Fig. 2 shows the time resolution of the system measured as a function of equivalent energy deposited in the two detectors. The data for curve (a) was taken by simultaneously feeding the output of a pulser ($t_r = 8$ ns) into the test input of each preamplifier and that for curve (b) by feeding the pulser output directly into the input of each discriminator, the charge sensitive preamplifiers having been previously disconnected. The main contribution to the fwhm of the prompt curves obtained can be attributed to preamplifier noise. This can be seen on comparing

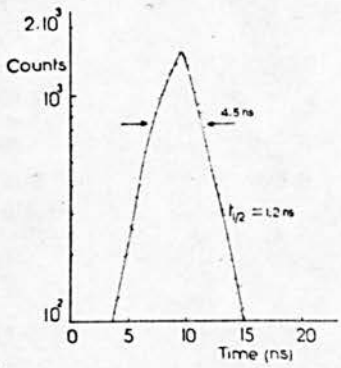

Fig. 1. Prompt coincidence curve obtained when analysing the 279 keV excited state of ^{203}Tl.

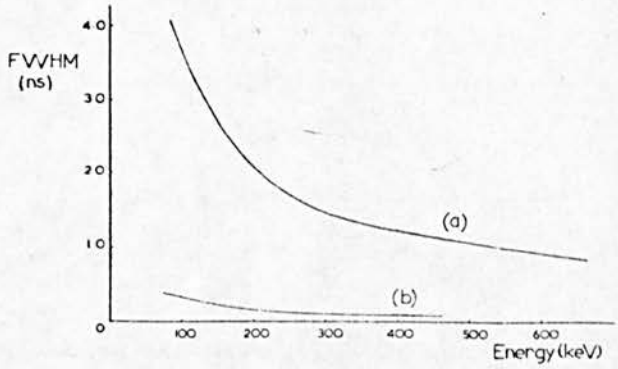

Fig. 2. Time resolution as a function of equivalent energy deposited in the two detectors: (a) whole system, (b) whole system less preamplifiers.

curves (a) and (b) of fig. 2. A reduction in noise would enable lower discriminator threshold levels to be used thus decreasing both amplitude and rise-time dependent walk.

The use of fast current preamplifiers ($t_r = 3$ ns) in place of the charge sensitive ones was also examined. In this case the slow channel signal was derived by feeding the fast output pulses from the preamplifier through a pulse stretcher. Analysis of the same two excited states yielded prompt curves with fwhm of 8.1 ns and 4.3 ns respectively for ^{203}Tl and ^{198}Hg. This rapid improvement in time resolution with increasing energy suggests that the timing performance of the current amplifier would be superior to that of the charge sensitive type at energies higher than those considered here. The energy resolution obtained with this arrangement was poor being about 50 keV. At least an order of magnitude improvement can be achieved by adding a charge sensitive preamplifier to each channel to give the energy signal [2]) but this, depending on the design (rise-time, cold input capacitance) of the charge amplifier, can cause a significant worsening of the time resolution.

The results of these measurements show that fast timing is possible with a pair of Si(Li) detectors used in conjunction with charge sensitive preamplifiers at energies of 200 keV and above with simultaneous good energy resolution. An application of this system which is currently being investigated is that of excited nuclear state lifetime measurement. The determination of lifetimes greater than about 2 ns at 200 keV and considerably less than that at higher energies appears to be possible.

References

[1]) I. S. Sherman and R. G. Roddick, IEEE Trans. Nucl. Sci. NS-17, no. 1 (1970) 252.

[2]) L. Papadopoulos, Nucl. Instr. and Meth. 41 (1966) 241.

NUCLEAR INSTRUMENTS AND METHODS 107 (1973) 9-11; © NORTH-HOLLAND PUBLISHING CO.

SHORT HALF-LIFE MEASUREMENTS USING A PAIR OF SEMICONDUCTOR DETECTORS

R. J. BISHOP

School of Physics, Kingston Polytechnic, Kingston upon Thames, Surrey, England

Received 2 October 1972

A Ge(Li) detector and a surface barrier detector have been operated in coincidence to measure the half-life of the 59.6 keV excited state of ^{237}Np, yielding a result of 70 ± 3 ns.

1. Introduction

As part of a programme involved with the experimental investigation of the timing performance of semiconductor detectors[1]) it was decided to examine the possibility of using a Ge(Li) detector and a surface barrier detector in coincidence to determine short nuclear half-lives. Several papers[2-5]) have already appeared reporting the results of similar measurements but using a semiconductor detector in coincidence with a scintillation counter. This article describes the re-measurement of the half-life of the 59.6 keV excited state of ^{237}Np.

2. Measurement system

A block diagram of the apparatus used for the measurements is shown in fig. 1. The 3 cm^3 planar Ge(Li) gamma detector had a sensitive depth of 5 mm and was operated at 600 V. The alpha particles were detected with a 25 mm^2 active area and 0.1 mm depletion depth surface barrier detector which was biased at 25 V and operated at room temperature. The timing output signals from the charge sensitive amplifiers had approximate rise times of 30 ns and 10 ns for the gamma and alpha channels respectively. Leading edge triggering was used with no compensation for rise time and amplitude dependent walk. Discriminator threshold levels were set just above the noise. Weisberg's circuit[6]) was used as the basis for the time-to-amplitude converter, the small range of the original converter being extended to about 600 ns by use of a 60 m long delay line. To handle the longer pulse widths in the circuit larger decoupling capacitors were used where appropriate and the integrator was modified to prevent overloading. The measured differential non-linearity of the modified converter was better than ±4% over most of its range.

3. Calibration

A simple electronic unit was constructed using TTL integrated circuits enabling rapid calibration of the time scale of the time-to-amplitude converter. The principle of operation of the unit is similar to that used

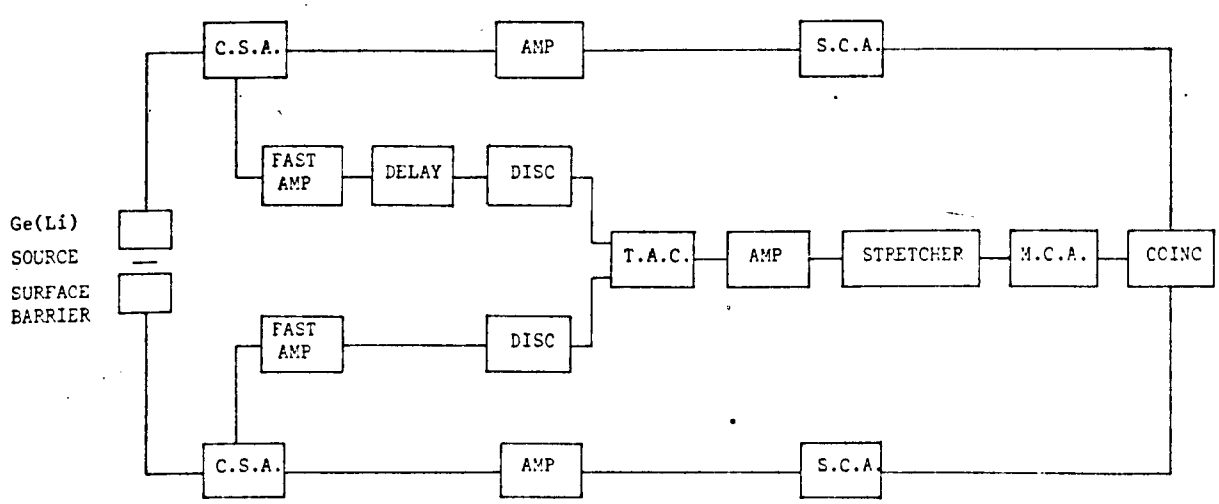

Fig. 1. Block diagram of the measurement system.

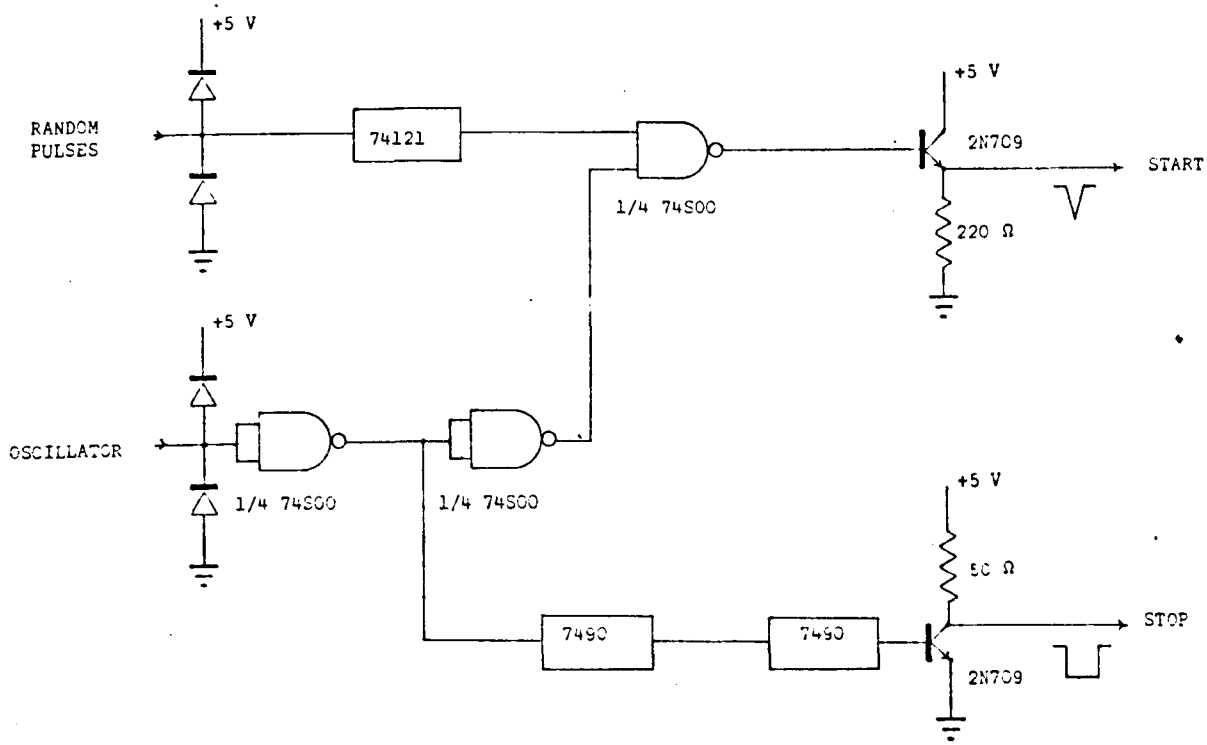

Fig. 2. Schematic diagram of the time-to-amplitude converter calibration unit.

in the design of Baker et al.[7]). Fig. 2 shows the schematic circuit diagram of the device. Pulses randomly distributed in time were obtained from the alpha detector and, after suitable amplification, shaped by the 74121 monostable before being applied to the 74S00 coincidence gate. The monostable was set to produce pulses having a width approximately 20% less than the oscillator period. Oscillator pulses shaped by the two 74S00 gates were applied to the other input of the coincidence gate. The output from this gate provided the start pulses. Stop pulses were obtained by scaling down the oscillator frequency by a factor of 100. Speed limitations in the discriminators associated with the time-to-amplitude converter forced the use of such a large scaling factor. The resulting calibration spectrum consists of up to 100 peaks (depending on the converter range) separated in time by the oscillator period. Oscillator frequencies in the range 13 MHz to 20 MHz have been used and gave results consistent to within better than $\pm 0.5\%$.

4. Results

For the measurement of the half-life of the 59.6 keV level of ^{237}Np the single channel analyser in the gamma channel was set to accept gammas in the energy range 55 keV to 63 keV, whilst the analyzer in the alpha channel accepted alphas with energies above 5 MeV.

An example of one of a set of delayed coincidence spectra obtained with this isotope is shown in fig. 3. The curve has been corrected for chance coincidences and the time calibration is 6.05 ± 0.06 ns per channel. The measured half-life is 70 ± 3 ns, in agreement with the latest accurate measurement[3]). Also shown in fig. 3 is the prompt curve obtained when analysing the 84 keV excited state of ^{224}Ra which has a half-life of 0.75 ns[8]). This gave the system resolution at these energies as 36 ns fwhm. The energy resolution capability of the system at these energies was 0.8 keV and 15 keV for the gamma and alpha channels respectively.

The electronics used in these experiments was relatively unsophisticated but, nevertheless, the work showed the feasability of using a pair of semiconductor detectors, with their inherent excellent energy resolution, for short half-life measurements. With the present system it appears possible to measure half-lives down to about 15 ns at gamma energies of 60 keV when using the slope method of analysis of the delayed coincidence curve.

References

1) R. J. Bishop, Nucl. Instr. and. Meth. 96 (1971) 331.

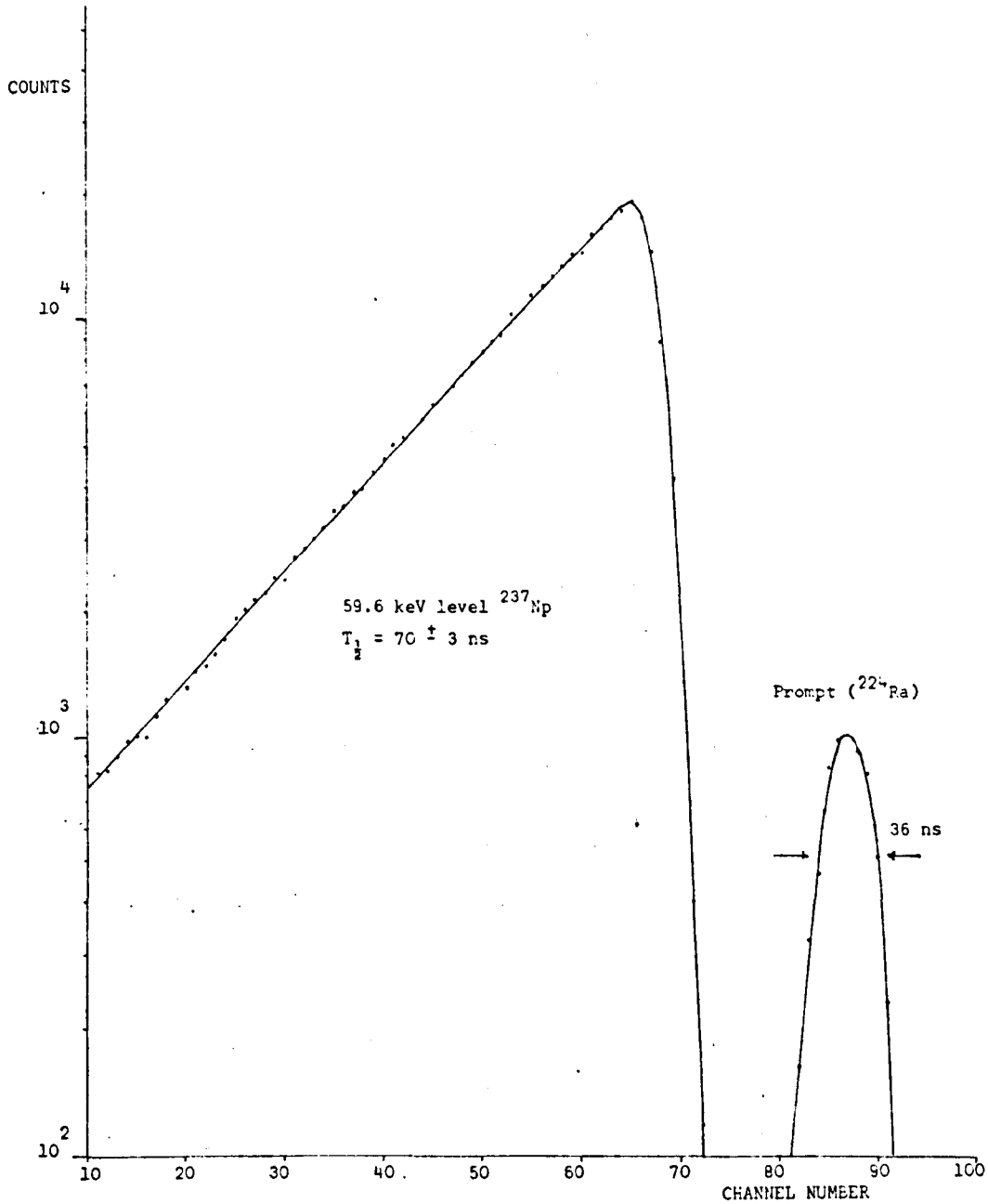

Fig. 3. Delayed coincidence time spectrum showing the half-life of the 59.6 keV excited state of ^{237}Np.

2) B. Bengtson and M. Moszyński, Nucl. Instr. and Meth. **100** (1972) 293.
3) R. K. Garg, S. D. Chauhan, S. L. Gupta and N. K. Saha, Z. Physik **244** (1971) 312.
4) I. Ahmad, A. M. Friedman and J. P. Unik, Nucl. Phys. **A 119** (1968) 27.
5) J. A. Miehe and P. Siffert, IEEE Trans. Nucl. Sci. NS-**17**, no. 5 (1970) 8.
6) H. Weisberg, Nucl. Instr. and Meth. **32** (1965) 133.
7) C. A. Baker, C. J. Batty and L. E. Williams, Nucl. Instr. and Meth. **59** (1968) 125.
8) C. M. Lederer, J. M. Hollander and I. Perlman, *Table of isotopes*, 5th ed. (Wiley, New York, 1967).

Nuclear Instruments and Methods In Press.

1.

DELAYED COINCIDENCE MEASUREMENTS USING SEMICONDUCTOR DETECTORS

R.J.BISHOP

School of Physics, Kingston Polytechnic, Kingston upon Thames, Surrey, England

The use of semiconductor detectors in delayed coincidence measurements of short nuclear half-lives is considered. Their use is illustrated by an accurate measurement of the half-life of the 86.5 keV excited state in ^{233}Pa. A result of (37.7 ± 0.2) ns was obtained. The result of a measurement of the half-life of the 59.6 keV level in ^{237}Np is also reported. The value obtained was (68.5 ± 0.4) ns. Both these results are in good agreement with previous recent determinations.

1. Introduction

The excellent energy resolution and good timing characteristics of semiconductor detectors have recently led to their widespread use in coincidence experiments. To illustrate the application of these detectors to short nuclear half-life measurements, the measurement of the half-life of the 86.5 keV level in ^{233}Pa by the delayed coincidence technique is considered below. This level is fed partly by the 4.787 MeV (47%) alpha branch from the decay of ^{237}Np and partly by gamma decay from higher energy levels in ^{233}Pa. The state de-excites by E1 transitions of 86.5 keV and 29.6 keV, both being appreciably internally converted.

In previous determinations of the half-life of this level [1-4]) the depopulating radiation was detected by scintillation counters but such

detectors suffer from a poor intrinsic energy resolution. Thus, in those measurements where delayed coincidences where recorded between the alpha particles from ^{237}Np and the 86.5 keV gamma rays depopulating the 86.5 keV level it was impossible to solely select the 86.5 keV gamma rays, the Pa K_α X-rays (~92 - 96 keV) from the internal conversion of high energy gamma rays being accepted also. The shape of the resulting delayed coincidence spectrum was then determined by more than one half-life. However, use of semiconductor detectors in such measurements, with their superior energy resolution, automatically overcomes this problem.

2. Experimental details

The ^{237}Np source used was prepared from a solution in 3N HNO_3 (Radiochemical Centre, Amersham). The solution was evaporated and burned in on a 1 mm thick stainless steel backing and produced a source with an activity of approximately 1 μCi. The part of the energy spectrum of X and gamma rays emitted from the source relevant to this work is shown in fig. 1. This was taken with a 3 cm^3 Ge(Li) detector.

The previously described delayed coincidence system [5]) was used for the measurements. The gamma rays were detected by a 3 cm^3, 5 mm sensitive depth planar Ge(Li) detector whilst a surface barrier detector having an active area of 25 mm^2 and 0.1 mm depletion depth was used to detect the alpha particles. Calibration of the time scale of the time-to-amplitude converter was carried out for each delayed coincidence measurement using the electronic calibration unit described previously [5]). The accuracy of calibration using this method was better than ± 1%.

3.

The intrinsic time resolution of the system was determined by recording coincidences between the 5.341 MeV alpha particles from ^{228}Th and the 84.5 keV gamma rays emitted on de-excitation of the 84.5 keV excited state in ^{224}Ra. The half-life of this level has been previously measured to be 0.75 ns [6]. After careful optimisation of the system for the best time resolution the resulting prompt coincidence spectrum exhibited a resolution (fwhm) of 8 ns and an apparent system half-life found from the late slope side of 3 ns.

3. Measurements and results

The delayed coincidence time spectrum shown in fig. 2 (time calibration 6.21 ± 0.03 ns per channel) was obtained with no energy restrictions imposed other than those set by the two discriminators in the fast channels. The alpha channel accepted energies above about 100 keV and the gamma channel energies above about 20 keV. This spectrum exhibites prompt and delayed components, the half-life found from the delayed component being (37.7 ± 0.5) ns. For the spectrum of fig. 3 (time calibration 6.27 ± 0.03 ns per channel) the single channel analyser in the gamma channel was set on the 86.5 keV gamma line only (fig. 1). As can be seen the prompt component of fig. 2 is virtually absent and the exponential decay yields a half-life of (37.6 ± 0.3) ns. With the gamma channel single channel analyser set to accept energies corresponding to the K_α X-rays from Pa and the analyser in the alpha channel accepting energies in the range 3.4 MeV - 5.0 MeV the spectrum of fig. 4 resulted. For this measurement the biased amplifier associated with the time-to-amplitude converter was set to X5 expansion, giving a time calibration of 1.24 ns per channel. The spectrum of fig. 4 yields a fwhm of 6.2 ns and the late and early slopes correspond to half-lives of 3.1 ns and 0.8 ns respectively. These figures were sufficiently close to those obtained when analysing the 84.5 keV excited state in ^{224}Ra to suggest that the shape of this spectrum was here determined by the measurement system. Thus these figures can also be taken to give the time resolution of the system for the radiation energies considered.

5.

The results from four sets of measurements of delayed coincidences between the alpha particles from ^{237}Np and the 86.5 keV gamma rays depopulating the 86.5 keV excited state in ^{233}Pa yielded a half-life of (37.7 ± 0.2) ns for that level. All data was analysed by the method of least squares after correcting for chance coincidences. The present measurement is in agreement with most of the earlier measurements as shown in table 1.

A redetermination of the half-life of the 59.6 keV level in ^{237}Np has also been made. Preliminary results from this have been previously reported [5]. The results obtained from the analysis of four sets of measurements was (68.5 ± 0.4) ns, in good agreement with previous recent results as shown in table 2.

4. Conclusion

Semiconductor detectors offer distinct advantages for short nuclear half-life measurements using the delayed coincidence technique. Using the slope method of analysis of the delayed coincidence spectrum half-lives as short as 5 ns should be measureable at energies similar to those considered here.

6.

Table 1

Summary of the half-life determinations of the 86.5 keV excited state in ^{233}Pa.

Technique		$T_{\frac{1}{2}}$ (ns)	Reference
α - e	Scintillation counters	36.9 ± 0.4	1
α-γ (86.5 keV)	Scintillation counters	36.0 ± 0.5	2
α-γ (86.5 keV)	Surface barrier-NaI(Tl)	37.4 ± 0.4	3
α-γ (86.5 keV)	Scintillation counters	35.7 ± 0.5	4
α-γ (86.5 keV)	Surface barrier-Ge(Li)	37.7 ± 0.2	present work

Table 2

Summary of the recent half-life determinations of the 59.6 keV excited state in ^{237}Np.

Technique		$T_{\frac{1}{2}}$(ns)	Reference
α-γ(59.6 keV)	Surface barrier-NaI(Tl)	66.7 ± 0.7	3
α-γ(59.6 keV)	Scintillation counters	66.9 ± 1.0	7
α-γ(59.6 keV)	Scintillation counters	68.3 ± 0.2	8
α-γ(59.6 keV)	Surface barrier-Ge(Li)	68.5 ± 0.4	present work

7.

References

1) D.Engelkemeir and L.B.Magnusson, Phys. Rev. 94 (1954) 1395

2) A.Marchal and P.Yvon, Compt. Rend. 252 (1961) 3774.

3) R.K.Garg, S.D.Chauhan, S.L.Gupta and N.K.Saha, Z. Physik 244 (1971) 312.

4) R.A.Winyard and G.W.McBeth, Nucl. Instr. and Meth. 100 (1972) 125.

5) R.J.Bishop, Nucl. Instr. and Meth. 107 (1973) 9.

6) C.M.Lederer, J.M.Hollander and I.Perlman, Table of isotopes, 5th ed. (Wiley, New York, 1967).

7) G.W.McBeth and R.A.Winyard, Nucl.Instr. and Meth. 100 (1972) 413.

8) G.H.Miller, P.Dillard, M.Eckhause and R.E.Welsh, Nucl. Instr. and Meth. 104 (1972) 11.

8.

FIGURE CAPTIONS

Fig. 1. Part of the ^{237}Np X and gamma ray energy spectrum taken with a 3 cm^3 Ge(Li) detector.

Fig. 2. Delayed coincidence time spectrum obtained with no energy restrictions (^{237}Np source).

Fig. 3. Delayed coincidence time spectrum showing the half-life of the 86.5 keV excited state in ^{233}Pa.

Fig. 4. Delayed coincidence time spectrum of the Pa K_α X rays measured in coincidence with 3.4 MeV - 5.0 MeV alpha particles.

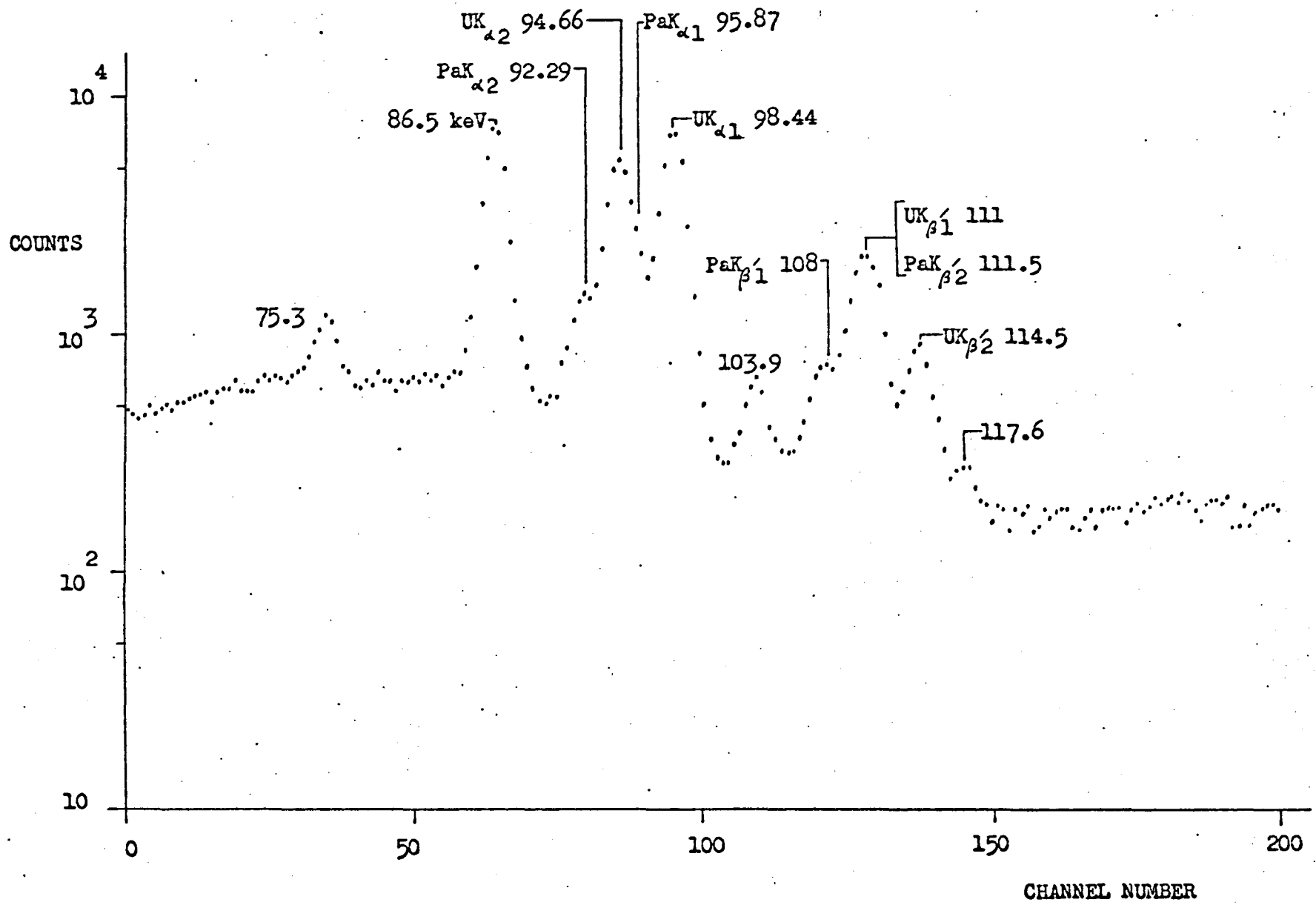
UK$_{\alpha 2}$ 94.66
PaK$_{\alpha 1}$ 95.87
PaK$_{\alpha 2}$ 92.29
86.5 keV
UK$_{\alpha 1}$ 98.44
UK$_{\beta 1}'$ 111
PaK$_{\beta 1}'$ 108
PaK$_{\beta 2}'$ 111.5
75.3
UK$_{\beta 2}'$ 114.5
103.9
117.6
COUNTS
10^4
10^3
10^2
10
0
50
100
150
200
CHANNEL NUMBER

FIG. 1

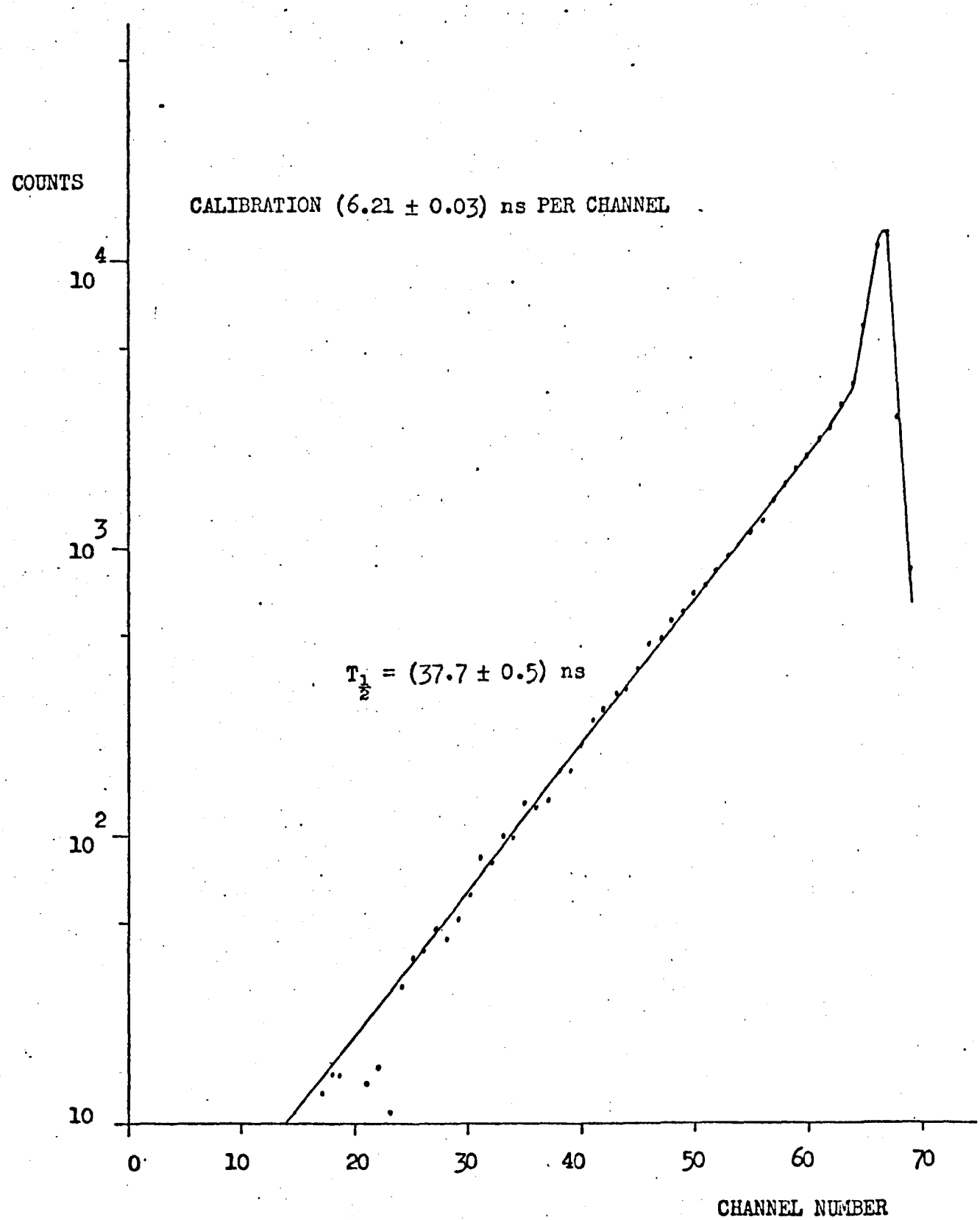
COUNTS
CALIBRATION (6.21 ± 0.03) ns PER CHANNEL
10^4
10^3
10^2
10
$T_{\frac{1}{2}}$ = (37.7 ± 0.5) ns
0
10
20
30
40
50
60
70
CHANNEL NUMBER

FIG. 2

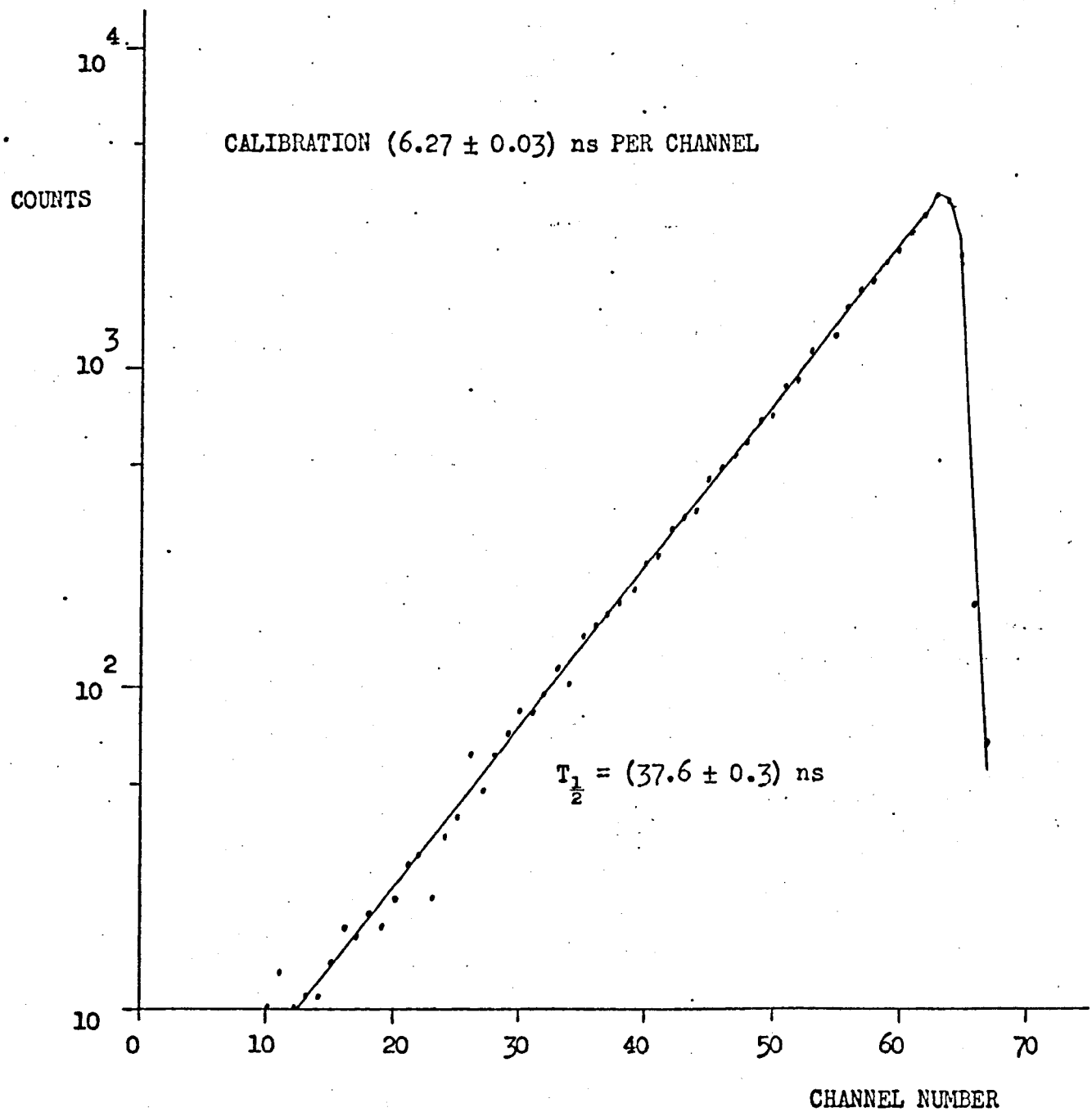
CALIBRATION (6.27 ± 0.03) ns PER CHANNEL
COUNTS
10^4
10^3
10^2
10
$T_{\frac{1}{2}}$ = (37.6 ± 0.3) ns
0
10
20
30
40
50
60
70
CHANNEL NUMBER

FIG. 3

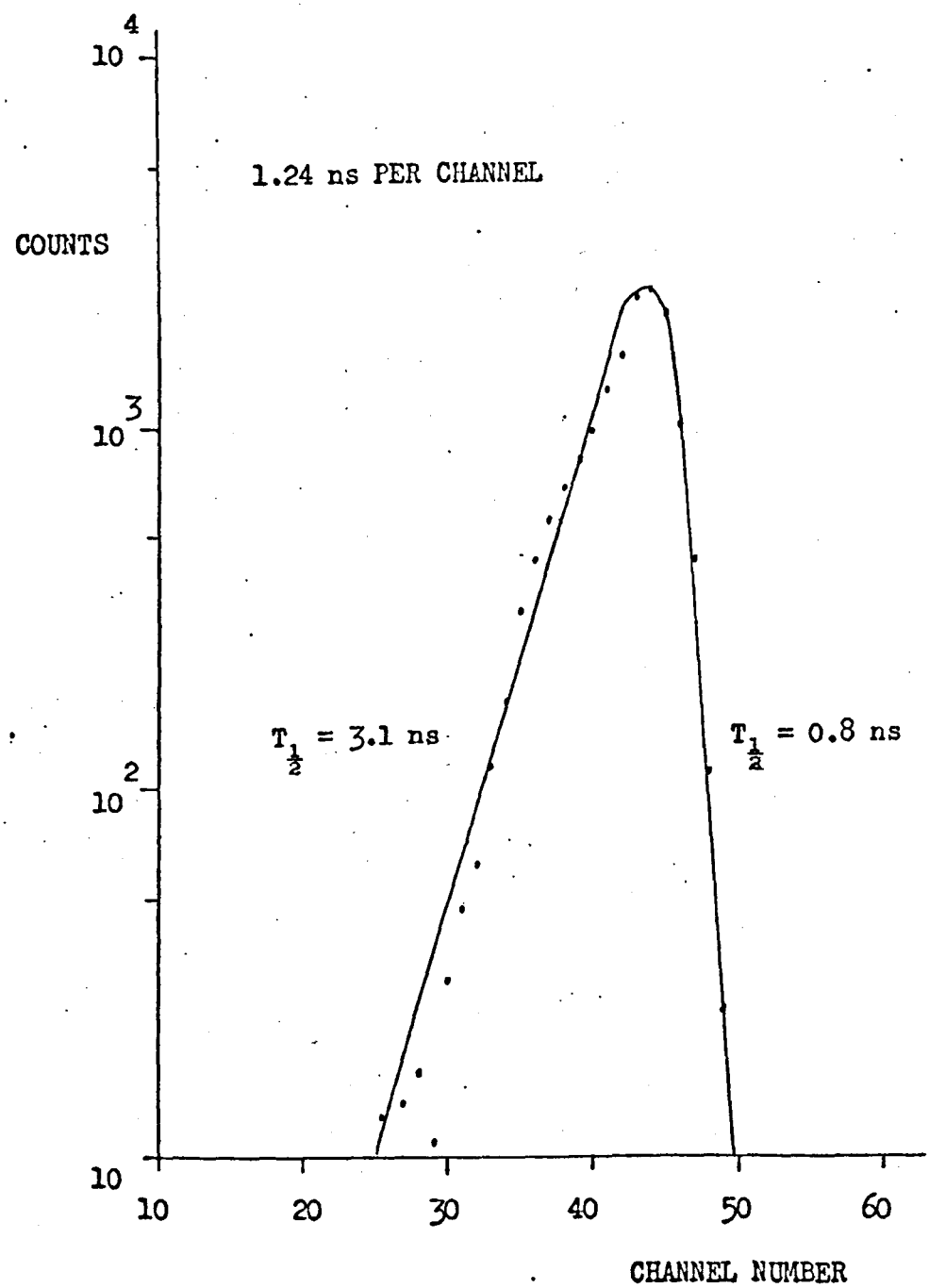
1.24 ns PER CHANNEL
COUNTS
10^4
10^3
10^2
10
$T_{\frac{1}{2}}$ = 3.1 ns
$T_{\frac{1}{2}}$ = 0.8 ns
10
20
30
40
50
60
CHANNEL NUMBER

FIG. 4